

NON-LINEAR BEHAVIOR OF STEEL FRAMES

by

JOHN ADAMS
AB, Harvard University
(1963)
BS, Tufts University
(1964)
MS, Tufts University
(1966)

Submitted in partial fulfillment
of the requirements for the degree of
Doctor of Philosophy

at the
Massachusetts Institute of Technology
June, 1973

Signature of Author

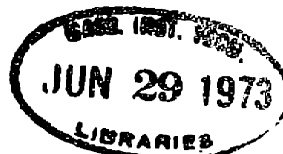
Department of Civil Engineering

Certified by

Thesis Supervisor

Accepted by

Chairman, Departmental Committee on Graduate
Students of the Department of Civil Engineering



ABSTRACT

NON-LINEAR BEHAVIOR OF STEEL FRAMES

by

JOHN ADAMS

Submitted to the Department of Civil Engineering on May 15, 1973, in partial fulfillment of the requirements for the degree of Doctor of Philosophy.

Four analytical models for non-linear frame analysis are analyzed at the member and frame levels for static loading. Three of the models are linear models which have been modified to include the P-Delta effect, the effect of change in geometry at the joints, and the effect of yielding. The fourth model is an exact solution that requires no modification to account for non-linearities. Two of the models are simple models that use a force criterion to determine whether yielding has occurred. The other two models are complicated models that use a technique of monitoring fiber stresses and strains at control cross-sections throughout a member. The accuracy of the exact model, and the importance of the three non-linear effects is examined at the member level for both the elastic and inelastic case. The predictions of all four models are compared at both the member level and the frame level, and the effect of yielding is found to be very significant, causing major differences between the predictions of the simple and complicated models under cyclic loading.

Thesis Supervisor:

Jose M. Roesset

Title:

Associate Professor of Civil Engineering

TABLE OF CONTENTS

	<u>Page</u>
I. Title Page	1
II. Abstract	2
III. Table of Contents	3
Chapter 1: INTRODUCTION	5
1.1 Review of Recent Work	6
1.2 Purpose and Scope	8
Chapter 2: THEORETICAL DESCRIPTIONS OF MODELS	10
2.1 Derivation of the Stiffness Matrix	11
2.2 The P- Δ Effect	20
2.3 The Change in Geometry	25
2.4 The Bending Model	25
2.5 The Interaction Model	30
2.6 The Latona Model	31
2.7 The Complex Model	33
Chapter 3: MEMBER STUDY - ELASTIC	50
3.1 Behavior of the Complex Model	51
3.2 The Elastic Non-Linear Effects	66
3.3 Summary	71
Chapter 4: MEMBER STUDY - INELASTIC	73
4.1 Inelastic Behavior - Without Axial Load	73
4.2 Inelastic Behavior - With Axial Load	89
4.3 Summary	106
Chapter 5: FRAME STUDY - INELASTIC	107
5.1 Parametric Study	108
5.2 Latona Frame Study	137
Chapter 6: CONCLUSION	160
IV. Bibliography	163

V. Biography	165
VI. Appendix	166
A. List of Figures	

1.0 INTRODUCTION

In this thesis, four different mathematical models for the non-linear elastic analysis of rigid frames are developed and investigated. Each of the models includes the three major non-linear effects, the P-Delta effect, the effect of change in geometry, and the effect of yielding, although they may do so in different ways. The four models can be divided into two basic categories, simple models and complicated models. In the simple models, the criterion for yielding is a function of the member forces, in the complicated models it is a function of the member strains. In this study there are two simple models, the Bending Model and the Interaction Model. As their names imply, the Bending Model considers only the magnitude of the moment when determining whether or not yielding has occurred, while the Interaction Model considers the magnitude of both the axial load and the bending moment. The remaining two models are complicated models, the first used by Raymond W. Latona in 1970, and the second developed in this thesis. Both complicated models keep track of the member stresses and strains and are capable of reproducing local yielding, but the Latona Model is in other respects similar to the simple models, in that it assumes that a member is a straight line between joints, while the Complex Model represents an exact solution that includes member deformations. A detailed discussion of all the models, and the assumptions made in them, appears in chapter two.

This thesis is divided into four major parts, a theoretical discussion of each of the models, an elastic member study, an inelastic member study, and an inelastic frame study. In each study, the results of the models are compared, and any differences discussed. In the elastic range, all the models, with the exception of the Complex Model, are linear models which have been modified to account for the two elastic non-linear effects. The success of this modification, and the relative importance of each effect, is considered in chapter three. In chapter four, the predictions of the various failure criteria are examined, and in chapter five, the importance of these differences in the study of a single bay single story frame subjected to a cyclic displacement, is discussed.

1.1 Review of Recent Work

This thesis is directly based on a thesis done at the Massachusetts Institute of Technology by Raymond W. Latona in 1970 (1). In that thesis, he developed a complex mathematical model which monitored member stresses and strains at a number of control cross-sections and fibers along the member. This model, which he calls the Complex Model in his thesis, but which will be referred to as the Latona Model in this work, can thus reproduce the reduction in member stiffness caused by local yielding as well as axial bending coupling. Latona showed that one flange fiber was sufficient to model a wide flange shape correctly, and that the number of web fibers had

little effect on the initial and final values of member stiffness but did affect the transition region. He concluded that the maximum number of web fibers needed was six, but in this thesis four web fibers are used, since there is little distinguishable difference in the M-P- ϕ curves for four and six web fibers. He also concluded that thirteen control cross-sections were sufficient to correctly reproduce member stresses and strains, and this is the number of control cross-sections used in this thesis. After developing this complex model, Latona compared its predictions with those of two simple models, the Bending Model and the Interaction Model, mentioned at the beginning of this chapter. In the cases he studied, a single bay single story and a single bay three story frame subjected to the El Centro Earthquake, Latona found significant differences between the predictions of the various models. Since his thesis contained no real comparison of the three models under static loading, there was no way to tell whether these differences were caused by dynamic effects only, or whether differences would appear under static loading as well.

Many mathematical frame models have been developed, ranging from simple models similar to the Bending and Interaction Models (3, 6, 9, 14), to complicated models that monitor stresses and strains (1, 7). In addition, models have been developed that use some specified moment curvature relationship (8, 12) such as a Ramberg Osgood Function (4), to

relate the moment, the curvature, and the axial load. In all these models, the primary concern is an accurate prediction of the initial collapse load, and the behavior of the models under cyclic loading is not examined. Although some experimental results (2, 13) show that frame resistance increases significantly on the second cycle of a cyclic loading cycle, there has been little concern about the ability of the various mathematical models to predict this behavior. Thus the models examined in this thesis represent the two extremes, the simple models being quite unsophisticated, and the complicated models being as, or more sophisticated than any yet developed to study non-linearities in rigid frames.

1.2 Purpose and Scope

The objective of this thesis is to compare the behavior of the three models in Latona's thesis with a fourth, which represents the exact solution, and determine whether there are any significant differences between these models under static loading. Because the two complicated models, the Latona Model and the Complex Model, are expensive to use, it is desirable to develop a simple inexpensive model that is capable of accurately reproducing frame behavior. Clearly the first step in this procedure is to discover what differences can be found between the predictions of the simple and complicated models, and if possible, what variables these differences depend upon. To some extent that has been accomplished in

this thesis, in that the one major difference between the simple and complicated models appears to be a function of axial load and strain hardening. The precise nature of this relationship is not yet clear, however, and further study will be required before it can be determined.

Because the major goal of this thesis is to examine differences between the models, the Euler Method, rather than a higher order integration method, is used in the solution procedure. Clearly any formulation that uses the Euler Method for the incremental solution of linear differential equations, is going to be very sensitive to the size of the load increment. The results in this thesis reflect this problem, but since this solution procedure is used for all models, the comparative results are not greatly affected.

There appears to be little difference between the results given by the Latona Model, and those given by the Complex Model for a single story single bay frame. In the case of the single story frame studied by Latona, the predictions of the two models are practically identical, both giving an increase in frame resistance that the simple models fail to show. Thus there is a major difference between the Latona Model and the simple models in the static case, that would account for the differences observed by Latona in a dynamic analysis under base motion.

2.0 THEORETICAL DESCRIPTION OF MODELS

All the models in this study use a tangent formulation, which means that incremental loads are applied to a structure, the incremental displacements and forces are calculated, and then added to the previous displacements and forces to get the new displacements and forces. In all cases, the stiffness method is used to calculate the incremental displacements from the applied incremental loads, and the incremental reactions are then computed from these displacements. The first three models described in this chapter use a linear formulation which has been modified to include various non-linear effects, while the fourth model uses a more complicated formulation which includes all the non-linear effects and hence needs no modification.

There are three major non-linear effects, the P-Delta effect, the effect of change in geometry, and the effect of a change in Young's Modulus. Since this thesis is concerned only with steel structures, the latter effect is relatively easy to account for. In this chapter the linear stiffness formulation is treated first, and then the modifications to account for the P-Delta effect and the change in geometry are described, since they apply to all the linear models. The method used to account for yielding varies for each model, and hence is treated along with the basic description of the model.

2.1 Derivation of the Stiffness Matrix

To obtain the incremental force-displacement relationship consider a member loaded only at its ends, with the forces and displacements assumed to be as shown below.

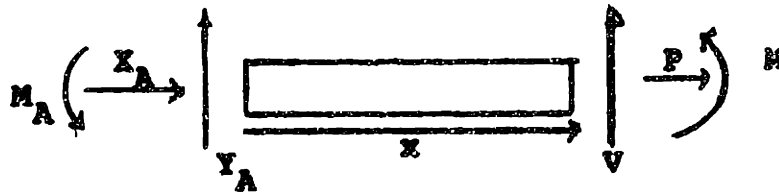
Forces



Displacements



If the forces in the member are assumed to act as shown below,



then equilibrium gives the following equations.

$$P = -X_A$$

$$M = -M_A + Y_A x$$

If the assumption is made that small changes in strain can be related linearly to small changes in the member forces, the following relationship holds

$$\Delta P = a_{11} \Delta u' + a_{12} \Delta v''$$

$$\Delta M = a_{21} \Delta u' + a_{22} \Delta v''$$

where

ΔP = increment in axial force

- ΔM = increment in moment
 $\Delta \epsilon'$ = increment in axial strain
 $\Delta \nu''$ = increment in rotational strain
 if y = distance from the centroidal axis to a point
 in the cross-section
 y_t = distance from the centroidal axis to the top
 of the cross-section
 y_b = distance from the centroidal axis to the
 bottom of the cross-section
 $b(y)$ = width function for the cross-section
 $E(y)$ = Tangent Modulus function for the cross-
 section

With these definitions the stiffness coefficients a_{11} , a_{12} , a_{21} and a_{22} become

$$a_{11} = \int_{y_b}^{y_t} E(y) b(y) dy$$

$$a_{12} = a_{21} = \int_{y_b}^{y_t} E(y) b(y) y dy$$

$$a_{22} = \int_{y_b}^{y_t} E(y) b(y) y^2 dy$$

If $E(y) = E$ (Young's Modulus), then in the elastic case

$$a_{11} = AE, \quad A = \text{area of the member}$$

$$a_{12} = a_{21} = 0$$

$$a_{22} = EI, \quad I = \text{Moment of Inertia of the member}$$

Inversion of the incremental force-strain equations gives the strain-force equations shown on the next page.

$$\Delta u' = b_{11}\Delta P + b_{12}\Delta M$$

$$\Delta v'' = b_{21}\Delta P + b_{22}\Delta M$$

where by Cramers Rule

$$b_{11} = \frac{a_{22}}{D}$$

$$b_{12} = -\frac{a_{12}}{D}$$

$$b_{21} = -\frac{a_{21}}{D}$$

$$b_{22} = \frac{a_{11}}{D}$$

and

$$D = \begin{vmatrix} a_{11} & a_{12} \\ a_{21} & a_{22} \end{vmatrix}$$

since

$$\Delta P = -\Delta X_A$$

$$\Delta M = -\Delta M_A + \Delta Y_A x$$

substitution gives

$$\Delta u' = -b_{11}\Delta X_A + b_{12}\Delta Y_A x - b_{12}\Delta M_A$$

$$\Delta v'' = -b_{21}\Delta X_A + b_{22}\Delta Y_A x - b_{22}\Delta M_A$$

Integrating, $\Delta u'$ once and $\Delta v''$ twice, over the length of the member gives the following displacement-force relationships.

$$\Delta u_B = \Delta u_A - \Delta X_A \int_0^L b_{11} dx + \Delta Y_A \int_0^L b_{12} \Delta Y_A x dx - \Delta M_A \int_0^L b_{12} dx$$

$$\Delta v_B' = \Delta \phi_B = \Delta \phi_A - \Delta X_A \int_0^L b_{21} dx + \Delta Y_A \int_0^L b_{22} x dx - \Delta M_A \int_0^L b_{22} dx$$

$$\Delta v_B = \Delta v_A + \Delta \phi_A L - \Delta X_A \int_0^L \int_0^L (b_{21} dx) dx + \Delta Y_A \int_0^L \int_0^L (b_{22} x dx) dx$$

$$- \Delta M_A \int_0^L \int_0^L (b_{22} dx) dx$$

thus

$$\Delta u_A - \Delta u_B = \Delta X_A \int_0^L b_{11} dx - \Delta Y_A \int_0^L b_{12} x dx + \Delta M_A \int_0^L b_{12} dx$$

$$\Delta \phi_A - \Delta \phi_B = \Delta X_A \int_0^L b_{21} dx - \Delta Y_A \int_0^L b_{22} x dx + \Delta M_A \int_0^L b_{22} dx$$

$$\Delta v_A - \Delta v_B + L \Delta \phi_A = \Delta X_A \int_0^L (L-x) b_{21} dx - \Delta Y_A \int_0^L x(L-x) b_{22} dx$$

$$+ \Delta M_A \int_0^L (L-x) b_{22} dx$$

let

$$\Delta U^* = \begin{bmatrix} \Delta u_A - \Delta u_B \\ \Delta v_A - \Delta v_B + L\Delta\phi_A \\ \Delta\phi_A - \Delta\phi_B \end{bmatrix}$$

$$f_{11} = \int_0^L b_{11} dx$$

$$f_{12} = -\int_0^L b_{12} x dx$$

$$f_{13} = \int_0^L b_{12} dx$$

$$f_{21} = \int_0^L (L-x) b_{21} dx$$

$$f_{22} = -\int_0^L x(L-x) b_{22} dx$$

$$f_{23} = \int_0^L (L-x) b_{22} dx$$

$$f_{31} = \int_0^L b_{21} dx$$

$$f_{32} = \int_0^L x b_{22} dx$$

$$f_{33} = \int_0^L b_{22} dx$$

$$\Delta F_A = \begin{bmatrix} \Delta X_A \\ \Delta Y_A \\ \Delta M_A \end{bmatrix}$$

With this notation the displacement-force relationship becomes

$$\begin{bmatrix} \Delta u \\ \Delta v \\ \Delta \phi \end{bmatrix} = \begin{bmatrix} f_{11} & f_{12} & f_{13} \\ f_{21} & f_{22} & f_{23} \\ f_{31} & f_{32} & f_{33} \end{bmatrix} \begin{bmatrix} \Delta X_A \\ \Delta Y_A \\ \Delta M_A \end{bmatrix}$$

or in matrix notation

$$\Delta U^* = f \Delta F_A$$

Multiplying both sides by f^{-1} gives

$$\Delta F_A = f^{-1} \Delta U^* = K \Delta U^*$$

The equilibrium equations for the member are

$$\Delta X_B = -\Delta X_A$$

$$\Delta Y_B = -\Delta Y_A$$

$$\Delta M_B = \Delta Y_A L - \Delta M_A$$

which can be written

$$\begin{bmatrix} \Delta X_B \\ \Delta Y_B \\ \Delta M_B \end{bmatrix} = \begin{bmatrix} -1 & 0 & 0 \\ 0 & -1 & 0 \\ 0 & L & -1 \end{bmatrix} \begin{bmatrix} \Delta X_A \\ \Delta Y_A \\ \Delta M_A \end{bmatrix}$$

in matrix notation these equations become

$$\Delta F_B = T_2 \Delta F_A$$

now

$$\Delta U^* = \begin{bmatrix} 1 & 0 & 0 \\ 0 & 1 & 0 \\ 0 & L & 1 \end{bmatrix} \begin{bmatrix} \Delta u_A \\ \Delta v_A \\ \Delta \phi_A \end{bmatrix} - \begin{bmatrix} \Delta u_B \\ \Delta v_B \\ \Delta \phi_B \end{bmatrix}$$

which can be written in matrix notation as

$$\Delta U^* = T_1 \Delta U_A - \Delta U_B$$

substituting this into the force-displacement equation gives

$$\Delta F_A = KT_1 \Delta U_A - K \Delta U_B$$

and since

$$\Delta F_B = T_2 \Delta F_A$$

$$\Delta F_B = T_2 KT_1 \Delta U_A - T_2 K \Delta U_B$$

the final incremental force-deformation relationship looks like this

$$\begin{bmatrix} \Delta F_A \\ \Delta F_B \end{bmatrix} = \begin{bmatrix} KT_1 & -K \\ T_2 KT_1 & -T_2 K \end{bmatrix} \begin{bmatrix} \Delta U_A \\ \Delta U_B \end{bmatrix}$$

or

$$\Delta F = KAU$$

where K is the member stiffness matrix. For the elastic case K can be derived as follows

$$b_{11} = \frac{1}{AE}$$

$$b_{22} = \frac{1}{EI}$$

$$b_{12} = b_{21} = 0$$

The non zero flexibility coefficients are

$$f_{11} = \int_0^L b_{11} dx = \frac{L}{AE}$$

$$f_{22} = -\int_0^L x(L-x)b_{22}dx = -\left(\frac{L^3}{2EI} - \frac{L^3}{3EI}\right) = \frac{-L^3}{6EI}$$

$$f_{23} = \int_0^L (L-x)b_{22}dx = \frac{L^2}{EI} - \frac{L^2}{2EI} = \frac{L^2}{2EI}$$

$$f_{32} = \int_0^L xb_{22}dx = \frac{-L^2}{2EI}$$

$$f_{33} = \int_0^L b_{22}dx = \frac{L}{EI}$$

$$f = \begin{bmatrix} \frac{L}{AE} & 0 & 0 \\ 0 & \frac{-L^3}{6EI} & \frac{L^2}{2EI} \\ 0 & \frac{-L^2}{2EI} & \frac{L}{EI} \end{bmatrix}$$

$$K = f^{-1} \phi \begin{bmatrix} \frac{EA}{L} & 0 & 0 \\ 0 & \frac{12EI}{L^3} & \frac{-6EI}{L^2} \\ 0 & \frac{6EI}{L^2} & \frac{-2EI}{L} \end{bmatrix}$$

$$K_{AA} = K T_1 = \begin{bmatrix} \frac{EA}{L} & 0 & 0 \\ 0 & \frac{12EI}{L^3} & \frac{6EI}{L^2} \\ 0 & \frac{6EI}{L^2} & \frac{4EI}{L} \end{bmatrix} \quad K_{AB} = -K = \begin{bmatrix} \frac{-EA}{L} & 0 & 0 \\ 0 & \frac{-12EI}{L^3} & \frac{6EI}{L^2} \\ 0 & \frac{-6EI}{L^2} & \frac{2EI}{L} \end{bmatrix}$$

$$K_{BA} = -T_2 K T_1 = \begin{bmatrix} \frac{-EA}{L} & 0 & 0 \\ 0 & \frac{-12EI}{L^3} & \frac{-6EI}{L^2} \\ 0 & \frac{6EI}{L^2} & \frac{2EI}{L} \end{bmatrix} \quad K_{BB} = -T_2 K = \begin{bmatrix} \frac{EA}{L} & 0 & 0 \\ 0 & \frac{12EI}{L^3} & \frac{-6EI}{L^2} \\ 0 & \frac{-6EI}{L^2} & \frac{4EI}{L} \end{bmatrix}$$

The final incremental force-deformation equations for the elastic case are shown on the next page.

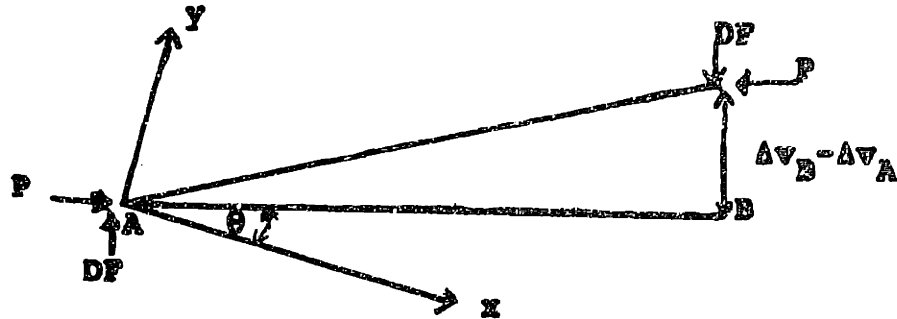
$$\begin{bmatrix} \Delta X_A \\ \Delta Y_A \\ \Delta M_A \\ \Delta X_B \\ \Delta Y_B \\ \Delta M_B \end{bmatrix} = \begin{bmatrix} \frac{EA}{L} & 0 & 0 & -\frac{EA}{L} & 0 & 0 \\ 0 & \frac{12EI}{L^3} & \frac{6EI}{L^2} & 0 & -\frac{12EI}{L^3} & \frac{6EI}{L^2} \\ 0 & \frac{6EI}{L^2} & \frac{4EI}{L} & 0 & -\frac{6EI}{L^2} & \frac{2EI}{L} \\ -\frac{EA}{L} & 0 & 0 & \frac{EA}{L} & 0 & 0 \\ 0 & -\frac{12EI}{L^3} & -\frac{6EI}{L^2} & 0 & \frac{12EI}{L^3} & -\frac{6EI}{L^2} \\ 0 & \frac{6EI}{L^2} & \frac{2EI}{L} & 0 & -\frac{6EI}{L^2} & \frac{4EI}{L} \end{bmatrix} \begin{bmatrix} \Delta U_A \\ \Delta V_A \\ \Delta \phi_A \\ \Delta U_B \\ \Delta V_B \\ \Delta \phi_B \end{bmatrix}$$

The assembly of the structure joint stiffness matrix is accomplished by looping through all the members, rotating each member stiffness matrix into global coordinates and then placing K_{AA} in row A column A, K_{AB} in row A column B, K_{BA} in row B column A, and K_{BB} in row B column B.

2.2 The P-Δ Effect

The P-Delta effect, as defined in this thesis, is the necessity for satisfying member equilibrium in the deformed position, since the linear stiffness matrix is assembled in the initial position, the additional forces caused by the axial load moving as the structure moves, are not considered in a linear model unless the P-Delta effect is included. The procedure used in this thesis consists of the following. Assume that the member shown below was initially oriented

along A B, and that the axial force P is the member force obtained from an analysis in the previous position. The vertical joint displacements at A and B are Δv_A and Δv_B respectively.



In order to satisfy moment equilibrium about A the following equation must hold true.

$$P \cdot (\Delta v_B - \Delta v_A) = DF \cdot (L)$$

where L = the length of the member

$$DF = \frac{\Delta v_B - \Delta v_A}{L} P$$

Thus the global fixed end forces obtained in the undeformed position, need to be altered by the corrective forces DFX and DFY shown below,

$$DFX = \frac{v_B - v_A}{L} P \sin \theta$$

$$DFY = \frac{v_B - v_A}{L} P \cos \theta$$

where θ is the angle between the initial member axis and the X axis in the global coordinate system. Hence if the global fixed end forces at A and B are F_x^A , F_y^A , F_x^B , and F_y^B , they will be modified as follows.

$$F_x^A = F_x^A - DF_x$$

$$F_y^A = F_y^A + DF_y$$

$$F_x^B = F_x^B + DF_x$$

$$F_y^B = F_y^B - DF_y$$

It is also possible to apply the P-Delta correction to the member stiffness matrix instead of the member end forces. If the member runs from joint A to joint B, (as shown on the preceding page) the following equations must hold.

$$\Delta Y_A + DF = \frac{12EI}{L^3} \Delta v_A + \frac{6EI}{L^2} \Delta \phi_A - \frac{12EI}{L^3} \Delta v_B + \frac{6EI}{L^2} \Delta \phi_B$$

$$\Delta Y_B - DF = \frac{12EI}{L^3} \Delta v_A - \frac{6EI}{L^2} \Delta \phi_A + \frac{12EI}{L^3} \Delta v_B - \frac{6EI}{L^2} \Delta \phi_B$$

Since

$$DF = \frac{\Delta v_B - \Delta v_A}{L} \quad P = \frac{P}{L} \Delta v_B - \frac{P}{L} \Delta v_A$$

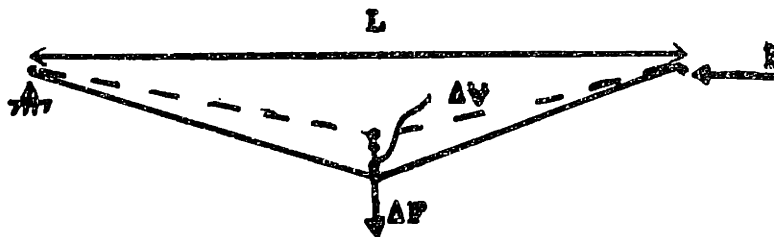
the force deformation equations can be written

$$\Delta Y_A = \left(\frac{12EI}{L^3} + \frac{P}{L} \right) \Delta v_A + \frac{6EI}{L^2} \Delta \phi_A - \left(\frac{12EI}{L^3} + \frac{P}{L} \right) \Delta v_B + \frac{6EI}{L^2} \Delta \phi_B$$

$$\Delta Y_B = - \left(\frac{12EI}{L^3} + \frac{P}{L} \right) \Delta v_A - \frac{6EI}{L^2} \Delta \phi_A + \left(\frac{12EI}{L^3} + \frac{P}{L} \right) \Delta v_B - \frac{6EI}{L^2} \Delta \phi_B$$

and the correction occurs in the stiffness matrix rather than the member forces.

Although the two methods appear identical, the stiffness matrix correction is in fact superior, because it causes a more rapid amplification as P approaches the buckling load. The reason for this can be readily seen from the example that follows, a two member, three jointed beam, with an axial load of $P = n\Delta P$, and a vertical load increment of ΔF .



Since the axial force in each member is P , the corrective force is

$$DFY = \frac{2PAV}{L/2} = \frac{4PAV}{L}$$

so

$$\Delta V = \frac{L^3}{48EI} \left(\Delta F + \frac{4PAV}{L} \right)$$

if the force correction method is used, the only value of ΔV available is that of the previous step, and thus the relationship becomes

$$\Delta V_n = \frac{L^3}{48EI} \left(\Delta F + \frac{4PAV_{n-1}}{L} \right)$$

if the stiffness matrix correction is used, it is possible to use the current value of Δv since

$$\frac{48EI}{L^3} \Delta v_n = \Delta F + \frac{4P\Delta v_n}{L}$$

so

$$\left[\frac{48EI}{L^3} - \frac{4P}{L} \right] \Delta v_n = \Delta F$$

and

$$\Delta v_n = \frac{\Delta F}{\frac{48EI}{L^3} - \frac{4P}{L}}$$

Thus the major advantage of the stiffness correction is that it doesn't lag a step behind, the way the force correction does. In practice it turns out that this difference of one step may lead to a significant discrepancy between the two methods, depending on the size of the load increment. It should be noted that in both methods the axial force in the member is the axial force obtained from the previous load increment, P_{n-1} , since the axial force for the n th increment is unknown.

One disadvantage of the stiffness correction is that the value of Δv_n can become negative. This occurs when the value of $\frac{4P}{L}$ becomes greater than $\frac{48EI}{L^3}$. Theoretically this should not occur, since buckling comes when

$$\frac{48EI}{L^3} - \frac{4P}{L} = 0$$

and hence
$$P_{cr} = \frac{12EI}{L^2}$$

In practice, however, the fact that a finite load increment is being used, causes the value of $\frac{48EI}{L^3} - \frac{4P}{L}$ to change from a very small positive number to a very small negative number, missing the zero point. Thus the stiffness correction method must be used carefully, since once a value of ΔV becomes negative, the buckling load has been exceeded, and the results are no longer valid.

2.3 The Change in Geometry

In the linear models, the change in geometry is handled by changing the joint coordinates at every increment. Thus at every step, the joint displacements are added to the old joint coordinates, and a new set of rotation matrices and lengths are computed for each member. This procedure makes no allowance for member curvature, and hence the only way to reproduce member deformation is to subdivide a member into several segments, since in all the linear models a member is assumed to be a straight line between joints. Thus the effect of the change in geometry is only considered for the structure as a whole, and no attempt is made to consider individual member geometry.

2.4 The Bending Model

Within the elastic range the bending model is completely linear and retains precisely the same stiffness matrix for

each increment. At each increment the moments at both ends of every member are checked against the plastic moment for that member. If either of the end moments is greater than the plastic moment, the member stiffness matrix is revised assuming that there is a hinge at that end of the member, and using the principle of static condensation to accomplish the modification.

The principle of static condensation states that the basic stiffness equations can be partitioned into two separate sets of equations, one associated with unknown joint loads and the other with the known joint loads. Thus the basic stiffness equation

$$\Delta F = KAU$$

becomes

$$\begin{bmatrix} \Delta F_1 \\ \Delta F_2 \end{bmatrix} = \begin{bmatrix} K_{11} & K_{12} \\ K_{21} & K_{22} \end{bmatrix} \begin{bmatrix} \Delta U_1 \\ \Delta U_2 \end{bmatrix}$$

where ΔF_1 is the column matrix of unknown joint loads, ΔF_2 is the matrix of known joint loads, ΔU_1 is the displacement of the joints whose joint loads are unknown and ΔU_2 is the displacement of the joints whose joint loads are known. By matrix multiplication, the partitioned equations can be written as follows

$$\Delta F_1 = K_{11} \Delta U_1 + K_{12} \Delta U_2$$

$$\Delta F_2 = K_{21} \Delta U_1 + K_{22} \Delta U_2$$

$$\text{If } \Delta F_2 = 0$$

$$\Delta U_2 = -K_{22}^{-1} K_{21} \Delta U_1$$

so

$$\Delta F_1 = K_{11} \Delta U_1 - K_{12} K_{22}^{-1} K_{21} \Delta U_1$$

$$\Delta F_1 = \left[K_{11} - K_{12} K_{22}^{-1} K_{21} \right] \Delta U_1$$

The matrix $\left[K_{11} - K_{12} K_{22}^{-1} K_{21} \right]$ is the statically condensed stiffness matrix and is the one used in the bending model to account for the formation of a plastic hinge. As an example, suppose the matrix is to be modified to account for a plastic hinge at the A end of the member. The original member stiffness equation would look like this.

$$\begin{bmatrix} \Delta X_A \\ \Delta V_A \\ \Delta M_B \\ \Delta X_B \\ \Delta V_B \\ \Delta M_B \end{bmatrix} = \begin{bmatrix} \frac{AE}{L} & 0 & 0 & -\frac{AE}{L} & 0 & 0 \\ 0 & \frac{12EI}{L^3} & \frac{6EI}{L^2} & 0 & -\frac{12EI}{L^3} & \frac{6EI}{L^2} \\ 0 & \frac{6EI}{L^2} & \frac{4EI}{L} & 0 & -\frac{6EI}{L^2} & \frac{2EI}{L} \\ -\frac{AE}{L} & 0 & 0 & \frac{AE}{L} & 0 & 0 \\ 0 & -\frac{12EI}{L^3} & -\frac{6EI}{L^2} & 0 & \frac{12EI}{L^3} & -\frac{6EI}{L^2} \\ 0 & \frac{6EI}{L^2} & \frac{2EI}{L} & 0 & -\frac{6EI}{L^2} & \frac{6EI}{L} \end{bmatrix} \begin{bmatrix} \Delta u_A \\ \Delta v_A \\ \Delta \phi_A \\ \Delta u_B \\ \Delta v_B \\ \Delta \phi_B \end{bmatrix}$$

The partitioned equations are shown below, note that if there is a hinge at A end, the only known joint load is ΔM_A which is zero.

$$\begin{bmatrix} \Delta X_A \\ \Delta V_A \\ \Delta X_B \\ \Delta V_B \\ \Delta M_B \\ \Delta M_A \end{bmatrix} = \begin{bmatrix} \frac{AE}{L} & 0 & -\frac{AE}{L} & 0 & 0 & 0 \\ 0 & \frac{12EI}{L^3} & 0 & -\frac{12EI}{L^3} & \frac{6EI}{L^2} & \frac{6EI}{L^2} \\ -\frac{AE}{L} & 0 & \frac{AE}{L} & 0 & 0 & 0 \\ 0 & -\frac{12EI}{L^3} & 0 & +\frac{12EI}{L^3} & -\frac{6EI}{L^2} & -\frac{6EI}{L^2} \\ 0 & \frac{6EI}{L^2} & 0 & -\frac{6EI}{L^2} & \frac{4EI}{L} & \frac{2EI}{L} \\ 0 & \frac{6EI}{L^2} & 0 & -\frac{6EI}{L^2} & \frac{2EI}{L} & \frac{4EI}{L} \end{bmatrix} \begin{bmatrix} \Delta u_A \\ \Delta v_A \\ \Delta u_B \\ \Delta v_B \\ \Delta \phi_B \\ \Delta \phi_A \end{bmatrix}$$

$$K_{12} K_{22}^{-1} K_{21} = \begin{bmatrix} 0 & 0 & 0 & 0 & 0 \\ 0 & \frac{9EI}{L^3} & 0 & -\frac{9EI}{L^3} & \frac{3EI}{L} \\ 0 & 0 & 0 & 0 & 0 \\ 0 & -\frac{9EI}{L^3} & 0 & \frac{9EI}{L^3} & -\frac{3EI}{L^2} \\ 0 & \frac{3EI}{L} & 0 & -\frac{3EI}{L^2} & \frac{EI}{L} \end{bmatrix}$$

The final modified member stiffness equation,

$P_1 = \left[K_{11} - K_{12} K_{22}^{-1} K_{21} \right] U_1$, is shown below with zeroes on the partitioned row and column.

$$\begin{bmatrix} \Delta X_A \\ \Delta V_A \\ \Delta M_A \\ \Delta X_B \\ \Delta V_B \\ \Delta M_B \end{bmatrix} = \begin{bmatrix} \frac{AE}{L} & 0 & 0 & -\frac{AE}{L} & 0 & 0 \\ 0 & \frac{3EI}{L^3} & 0 & 0 & -\frac{3EI}{L^3} & \frac{3EI}{L^2} \\ 0 & 0 & 0 & 0 & 0 & 0 \\ -\frac{AE}{L} & 0 & 0 & \frac{AE}{L} & 0 & 0 \\ 0 & -\frac{3EI}{L^3} & 0 & 0 & \frac{3EI}{L^3} & \frac{3EI}{L^2} \\ 0 & \frac{3EI}{L^2} & 0 & 0 & \frac{3EI}{L^2} & \frac{3EI}{L} \end{bmatrix} \begin{bmatrix} \Delta u_A \\ \Delta v_A \\ \Delta \phi_A \\ \Delta u_B \\ \Delta v_B \\ \Delta \phi_B \end{bmatrix}$$

The procedure for a plastic hinge at the B end is similar, except that the matrix is partitioned around ΔM_B instead of ΔM_A . If a hinge forms at both ends of a member,

the modified stiffness matrix has only axial stiffness terms as shown below.

$$K_M = \begin{bmatrix} \frac{AE}{L} & 0 & 0 & -\frac{AE}{L} & 0 & 0 \\ 0 & 0 & 0 & 0 & 0 & 0 \\ 0 & 0 & 0 & 0 & 0 & 0 \\ -\frac{AE}{L} & 0 & 0 & \frac{AE}{L} & 0 & 0 \\ 0 & 0 & 0 & 0 & 0 & 0 \\ 0 & 0 & 0 & 0 & 0 & 0 \end{bmatrix}$$

In order to prevent the zero elements in the modified member stiffness matrices from causing a singularity in the global stiffness matrix, a small correction factor is added to each non-axial term in the modified member stiffness matrix. This correction corresponds to an elasto-plastic stress strain law, where the plastic part of the curve has a finite but small stiffness. In the Bending Model this stiffness is one-thousandth of the original stiffness, which means, in effect, that the value of Young's Modulus in the plastic range is one-thousandth of the elastic value, whereas in a purely elasto-plastic system Young's Modulus would be zero in the plastic range.

2.5 The Interaction Model

The Interaction Model is basically similar to the Bending Model, but the criteria for the formation of a plastic hinge

are different. In the Interaction Model a plastic hinge is formed when

$$\frac{.847|M|}{M_p} + \frac{1|F|}{P_y} = 1.0$$

This formula corresponds to the A.I.S.C. interaction formula, where M is the moment at the end of the member, P is the axial force in the member, P_y is area of the member multiplied by the yield stress, and M_p is the plastic moment for the member.

In all other respects the Interaction Model is identical to the Bending Model. The same bilinear stress strain assumptions are used, and the stiffness matrix is modified to account for a plastic hinge in the same way.

2.6 The Latona Model

In the Latona Model the assemblage of the stiffness matrix closely parallels the procedure described at the beginning of the chapter. The principal assumption is that small changes in displacement can be linearly related to small changes in member forces. In order for this to be true, the member must be analyzed in the undeformed position, which means that individual member stability is not considered. It is this assumption that makes it possible to let $\Delta \epsilon = \Delta u'$ and $\Delta \phi' = \Delta v''$ and write the equations

$$\Delta P = a_{11}\Delta u' + a_{12}\Delta v''$$

$$\Delta M = a_{21}\Delta u' + a_{22}\Delta v''$$

which relate the incremental forces directly to the incremental displacements.

Each member is divided up into a series of cross-sections and fibers, with the stresses being monitored at every intersection of a cross-section and fiber for each member. The first step in the assemblage of the stiffness matrix is the calculation of the flexibility coefficients b_{11} , b_{12} , b_{21} , b_{22} from the fiber dimensions and stress state at each cross-section. The integration over the cross-section is accomplished by simply summing over each fiber for all the fibers in the cross-section. Once the flexibility coefficients have been computed, the member flexibility matrix, f_{11} through f_{33} , is computed by summing the appropriate flexibility term for each cross-section over all the cross-sections in the member. The member flexibility matrix, f , is then inverted, to get k , and the member stiffness matrix, K , is formed using k , T_1 and T_2 . The member stiffness matrix is then rotated into global coordinates and added to the frame stiffness matrix.

After the new joint displacements and forces have been computed by the stiffness method, the inverse of the original member stress-strain assumption,

$$\Delta u' = b_{11}\Delta P + b_{12}\Delta M$$

$$\Delta v'' = b_{21} \Delta P + b_{22} \Delta M$$

is used to calculate the incremental strains $\Delta u'$ and $\Delta v''$ at each cross-section. From these strains, the state of stress, and hence the value of ϵ , can be calculated at the intersection of each cross-section and each fiber. This now makes it possible to recalculate the stiffness coefficients b_{11} , b_{12} , b_{21} , b_{22} and the cycle begins again.

In summary, the assumption is made in the Latona Model that small changes in member forces can be linearly related to member strains, and that the geometry of the member in the deformed position is a straight line. A method of control cross-sections and fibers is used to assemble the stiffness matrix and monitor the stresses and strains. The stiffness matrix is reassembled for every load increment and the cycle is continued until all increments of load have been applied to the structure.

2.7 The Complex Model

The primary difference between the Latona Model and the Complex Model is that the geometrical assumptions made in the Latona Model are not made in the Complex Model. In the Complex Model the geometry of the structure in the deformed position is considered, and hence the rotations are not restricted to being small. Thus $\Delta \epsilon \neq \Delta u'$ and $\Delta \phi' \neq \Delta v''$, so

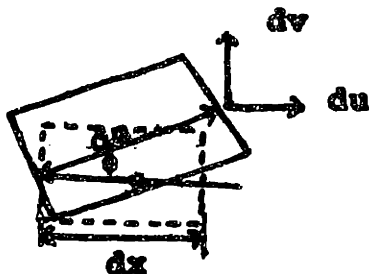
that the relationship between incremental member forces and incremental strains must be written as

$$\Delta H = b_{11} \Delta \epsilon + b_{12} \Delta \phi'$$

$$\Delta M = b_{12} \Delta \epsilon + b_{22} \Delta \phi'$$

and it becomes considerably harder to relate the incremental member forces (ΔH , ΔM) to the incremental member deformations (Δu , Δv) than it was in the other models.

The relationship between incremental deformation and incremental strain can be derived by considering the member element, originally of length dx , shown below



By geometry

$$du = ds \cos \phi - dx$$

$$dv = ds \sin \phi$$

now

$$e = \frac{ds - dx}{dx} = \frac{ds}{dx} - 1$$

so

$$ds = (1 + e) dx$$

by substitution

$$u' = \frac{du}{dx} = (1 + e) \cos \phi - 1$$

$$v' = \frac{dv}{dx} = (1 + e) \sin \phi$$

in incremental form these equations become

$$\Delta u' = \Delta \epsilon \cos \phi - (1 + \epsilon) \sin \phi \Delta \phi$$

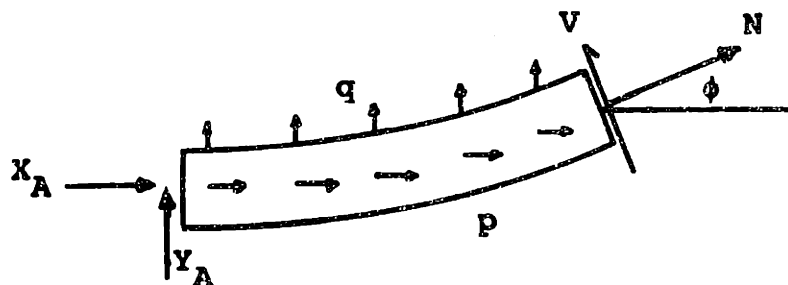
$$\Delta v' = \Delta \epsilon \sin \phi + (1 + \epsilon) \cos \phi \Delta \phi$$

integrating these equations once gives

$$\Delta u = \Delta u_A + \int_0^x \Delta \epsilon \cos \phi \, dx - \int_0^x (1 + \epsilon) \sin \phi \Delta \phi \, dx$$

$$\Delta v = \Delta v_A + \int_0^x \Delta \epsilon \sin \phi \, dx + \int_0^x (1 + \epsilon) \cos \phi \Delta \phi \, dx$$

The relationship between end forces and member forces comes from the force diagram below



Clearly by geometry

$$X_A + P = -N \cos \phi + V \sin \phi, \text{ where } P = \int_0^x p \, dx$$

$$Y_A + Q = -N \sin \phi - V \cos \phi, \text{ where } Q = \int_0^x q \, dx$$

Multiplying the top equation by $\cos \phi$, the bottom equation by $\sin \phi$ and adding gives

$$N = -(X_A + P) \cos \phi - (Y_A + Q) \sin \phi$$

Multiplying the top equation by $\sin \phi$, the bottom equation by $\cos \phi$ and adding gives

$$V = (X_A + P) \sin \phi - (Y_A + Q) \cos \phi$$

in incremental form these equations become

$$\Delta u' = \Delta \epsilon \cos \phi - (1 + \epsilon) \sin \phi \Delta \phi$$

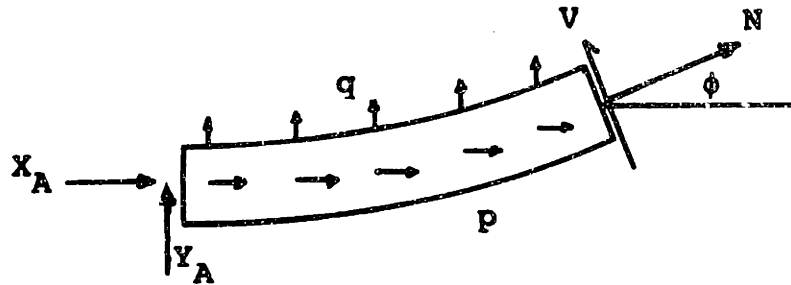
$$\Delta v' = \Delta \epsilon \sin \phi + (1 + \epsilon) \cos \phi \Delta \phi$$

integrating these equations once gives

$$\Delta u = \Delta u_A + \int_0^x \Delta \epsilon \cos \phi \, dx - \int_0^x (1 + \epsilon) \sin \phi \Delta \phi \, dx$$

$$\Delta v = \Delta v_A + \int_0^x \Delta \epsilon \sin \phi \, dx + \int_0^x (1 + \epsilon) \cos \phi \Delta \phi \, dx$$

The relationship between end forces and member forces comes from the force diagram below



Clearly by geometry

$$X_A + P = -N \cos \phi + V \sin \phi, \text{ where } P = \int_0^x p \, dx$$

$$Y_A + Q = -N \sin \phi - V \cos \phi, \text{ where } Q = \int_0^x q \, dx$$

Multiplying the top equation by $\cos \phi$, the bottom equation by $\sin \phi$ and adding gives

$$N = -(X_A + P) \cos \phi - (Y_A + Q) \sin \phi$$

Multiplying the top equation by $\sin \phi$, the bottom equation by $\cos \phi$ and adding gives

$$V = (X_A + P) \sin \phi - (Y_A + Q) \cos \phi$$

In incremental form these equations become

$$\Delta H = -(\Delta X_A + \Delta P) \cos \phi - (\Delta Y_A + \Delta Q) \sin \phi + \left[(X_A + P) \sin \phi - (Y_A + Q) \cos \phi \right] \Delta \phi$$

$$\Delta V = (\Delta X_A + \Delta P) \sin \phi - (\Delta Y_A + \Delta Q) \cos \phi + \left[(X_A + P) \cos \phi + (Y_A + Q) \sin \phi \right] \Delta \phi$$

In the first equation the term in brackets is equivalent to V and in the second equation the term in brackets is equivalent to $-H$. When this substitution is made the incremental equations become

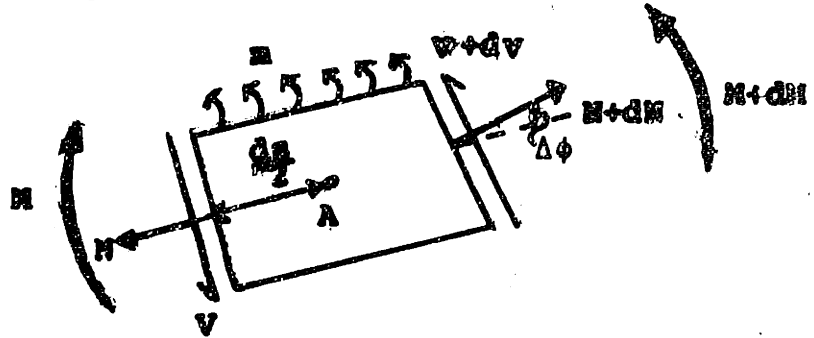
$$\Delta H = -(\Delta X_A + \Delta P) \cos \phi - (\Delta Y_A + \Delta Q) \sin \phi + V \Delta \phi$$

$$\Delta V = (\Delta X_A + \Delta P) \sin \phi - (\Delta Y_A + \Delta Q) \cos \phi - H \Delta \phi$$

with $\Delta P = \int_0^x \Delta p \, dx$, $\Delta Q = \int_0^x \Delta q \, dx$

where Δp is an incremental axial distributed load and Δq is an incremental transverse distributed load.

The incremental equation for moment equilibrium can be derived by considering the element of length ds shown below



Summing moments about A gives

$$-H + V \frac{ds}{2} + (V + dV) \frac{ds}{2} + m + H + dH = 0$$

If $\cos \Delta \phi$ is assumed to be one.

If $dv ds$ is assumed to be zero and $(1 + \epsilon) dx$ is substituted for ds the equation becomes

$$dM + V (1 + \epsilon) dx + m dx = 0$$

in incremental form this becomes

$$\Delta \left[\frac{dM}{dx} + V (1 + \epsilon) + m \right] = 0$$

or

$$\frac{d}{dx} (\Delta M) + \Delta V (1 + \epsilon) + V \Delta \epsilon + \Delta m = 0$$

substituting $\Delta V = (\Delta X_A + \Delta P) \sin \phi - (\Delta Y_A + \Delta Q) \cos \phi - N \Delta \phi$ into the equation gives

$$\frac{d}{dx} (\Delta M) = N(1+\epsilon)\Delta\phi - V\Delta\epsilon - (\Delta X_A + \Delta P)(1+\epsilon)\sin\phi + (\Delta Y_A + \Delta Q)(1+\epsilon)\cos\phi - \Delta m$$

$$\text{Since } \Delta N = b_{11}\Delta\epsilon + b_{12}\Delta\phi'$$

$$\text{and } \frac{d}{dx} (\Delta M) = \frac{d}{dx} (b_{21}\Delta\epsilon) + \frac{d}{dx} (b_{22}\Delta\phi')$$

the two equations involving ΔN are now combined to eliminate ΔN and the two equations involving $\frac{d}{dx} (\Delta M)$ are combined to eliminate $\frac{d}{dx} (\Delta M)$. This relationship, shown on the next page, involves the incremental end forces and the incremental displacements. Although it is an exceedingly complicated relationship, the manipulations that follow make it possible to express this relationship in a form very similar to the traditional stiffness solution described at the beginning of this chapter.

$$\Delta \epsilon = - \frac{b_{12}}{b_{11}} \Delta \phi' + \frac{V}{b_{11}} \Delta \phi - \frac{\Delta X_A \cos \phi}{b_{11}} - \frac{\Delta Y_A \sin \phi}{b_{11}} - \frac{\Delta P \cos \phi}{b_{11}} - \frac{\Delta Q \sin \phi}{b_{11}}$$

and by integrating $\frac{d}{dx} (b_{22} \Delta \phi')$ once and solving for $\Delta \phi'$

$$\begin{aligned} \Delta \phi' &= - \frac{\Delta M_A}{b_{22}} - \frac{b_{21}}{b_{22}} \Delta \epsilon + \frac{1}{b_{22}} \int_0^x N(1+\epsilon) \Delta \phi \, dx - \frac{1}{b_{22}} \int_0^x V \Delta \epsilon \, dx \\ &\quad - \frac{\Delta X_A}{b_{22}} \int_0^x (1+\epsilon) \sin \phi \, dx + \frac{\Delta Y_A}{b_{22}} \int_0^x (1+\epsilon) \cos \phi \, dx \\ &\quad - \frac{1}{b_{22}} \int_0^x \left[\Delta P(1+\epsilon) \sin \phi - \Delta Q(1+\epsilon) \cos \phi + \Delta m \right] dx \end{aligned}$$

Defining

$$F1 = - \frac{b_{12}}{b_{11}} \Delta \phi' + \frac{V}{b_{11}} \Delta \phi$$

$$F2 = - \frac{\Delta P \cos \phi}{b_{11}} - \frac{\Delta Q \sin \phi}{b_{11}}$$

$$F3 = - \frac{b_{21}}{b_{22}} \Delta \epsilon + \frac{1}{b_{22}} \int_0^x \left[N(1+\epsilon) \Delta \phi - V \Delta \epsilon \right] dx$$

$$F4 = - \frac{1}{b_{22}} \int_0^x \left[\Delta P(1+\epsilon) \sin \phi - \Delta Q(1+\epsilon) \cos \phi + \Delta m \right] dx$$

the incremental equations become

$$\Delta \epsilon = - \frac{\Delta X_A \cos \phi}{B_{11}} - \frac{\Delta Y_A \sin \phi}{B_{11}} + F1 + F2$$

$$\Delta \phi' = \frac{-\Delta X_A}{B_{22}} \int_0^x (1+\epsilon) \sin \phi \, dx + \frac{\Delta Y_A}{B_{22}} \int_0^x (1+\epsilon) \cos \phi \, dx - \frac{\Delta M_A}{B_{22}} + F3 + F4$$

$$\Delta \phi = \Delta \phi_A - \Delta X_A \int_0^x \frac{dx}{B_{22}} \int_0^x (1+\epsilon) \sin \phi \, dx + \Delta Y_A \int_0^x \frac{dx}{B_{22}} \int_0^x (1+\epsilon) \cos \phi \, dx$$

$$- \Delta M_A \int_0^x \frac{dx}{B_{22}} + \int_0^x F3 \, dx + \int_0^x F4 \, dx$$

$$\Delta u = \Delta u_A + \int_0^x \cos \phi \Delta \epsilon \, dx - \int_0^x (1+\epsilon) \sin \phi \Delta \phi \, dx$$

$$\Delta v = \Delta v_A + \int_0^x \sin \phi \Delta \epsilon \, dx + \int_0^x (1+\epsilon) \cos \phi \Delta \phi \, dx$$

In this form the expressions for $\Delta \epsilon$, $\Delta \phi'$ and $\Delta \phi$ depend upon each other, since $\Delta \epsilon$ is a function of $F1$, which is in turn a function of $\Delta \phi'$ and $\Delta \phi$, and both $\Delta \phi'$ and $\Delta \phi$ are functions of $F3$, which is in turn a function of $\Delta \epsilon$. In order to solve these relationships, it is necessary to use an incremental formulation where a new set of incremental strains is assumed, and then checked for accuracy. In the

incremental formulation the constants F1 and F3 become

$$F1_n = \frac{-b_{12}}{b_{11}} \Delta \phi'_n + \frac{V}{b_{11}} \Delta \phi_n$$

$$F3_n = \frac{-b_{21}}{b_{22}} \Delta \epsilon_n + \frac{1}{b_{22}} \int_0^x \left[N(1+\epsilon) \Delta \phi_n - V \Delta \epsilon_n \right] dx$$

and the incremental strains become

$$\Delta \epsilon_{n+1} = - \frac{\Delta X_A \cos \phi}{b_{11}} - \frac{\Delta Y_A \sin \phi}{b_{11}} + F1_n + F2$$

$$\Delta \phi'_{n+1} = \frac{-\Delta X_A}{b_{22}} \int_0^x (1+\epsilon) \sin \phi dx + \frac{\Delta Y_A}{b_{22}} \int_0^x (1+\epsilon) \cos \phi dx - \frac{\Delta M_A}{b_{22}} + F3_n + F4$$

$$\Delta \phi_{n+1} = \Delta \phi_A - \Delta X_A \int_0^x \frac{dx}{b_{22}} \int_0^x (1+\epsilon) \sin \phi dx + \Delta Y_A \int_0^x \frac{dx}{b_{22}} \int_0^x (1+\epsilon) \cos \phi dx$$

$$- \Delta M_A \int_0^x \frac{dx}{b_{22}} + \int_0^x F3_n dx + \int_0^x F4 dx$$

$$\Delta u_{n+1} = \Delta u_A + \int_0^x \cos \phi \Delta \epsilon_{n+1} dx - \int_0^x (1+\epsilon) \sin \phi \Delta \phi_n dx$$

$$\Delta v_{n+1} = \Delta v_A + \int_0^x \sin \phi \Delta \epsilon_n dx + \int_0^x (1+\epsilon) \cos \phi \Delta \phi_{n+1} dx$$

By integrating over the length of the member in the expression for $\Delta \phi_{n+1}$, Δu_{n+1} and Δv_{n+1} , equations for $\Delta \phi_B$, Δu_B and Δv_B

can be found, and it becomes possible to relate the incremental member displacements to the incremental member loads as follows.

$$\begin{aligned} \Delta\phi_B - \Delta\phi_A &= -\Delta X_A \int_0^L \frac{dx}{b_{22}} \int_0^x (1+\epsilon) \sin \phi \, dx + \Delta Y_A \int_0^L \frac{dx}{b_{22}} \int_0^x (1+\epsilon) \cos \phi \, dx \\ &\quad - \Delta M_A \int_0^L \frac{dx}{b_{22}} + \int_0^L F3_n \, dx + \int_0^L F4 \, dx \\ \Delta u_B - \Delta u_A &= -\Delta X_A \int_0^L \frac{\cos^2 \phi}{b_{11}} \, dx - \Delta Y_A \int_0^L \frac{\sin \phi \cos \phi}{b_{11}} \, dx + \int_0^L F1_n \cos \phi \, dx \\ &\quad - \int_0^L (1+\epsilon) \sin \phi \Delta\phi_n \, dx + \int_0^L F2 \cos \phi \, dx \\ \Delta v_B - \Delta v_A &= \Delta\phi_A \int_0^L (1+\epsilon) \cos \phi \, dx - \Delta X_A \int_0^L (1+\epsilon) \cos \phi \, dx \int_0^x \frac{dx}{b_{22}} \int_0^x (1+\epsilon) \sin \phi \, dx \\ &\quad + \Delta Y_A \int_0^L (1+\epsilon) \cos \phi \, dx \int_0^x \frac{dx}{b_{22}} \int_0^x (1+\epsilon) \cos \phi \, dx - \Delta M_A \int_0^L (1+\epsilon) \cos \phi \, dx \int_0^x \frac{dx}{b_{22}} \\ &\quad + \int_0^L \sin \phi \Delta\epsilon_n \, dx + \int_0^L (1+\epsilon) \cos \phi \, dx \int_0^x F3_n \, dx + \int_0^L (1+\epsilon) \cos \phi \, dx \int_0^x F4 \, dx \end{aligned}$$

If

$$HO(x) = \int_0^x \frac{dx}{b_{22}}$$

$$H1(x) = \int_0^x \frac{dx}{b_{22}} \int_0^x (1+\epsilon) \sin \phi \, dx$$

$$H2(x) = \int_0^x \frac{dx}{b_{22}} \int_0^x (1+\epsilon) \cos \phi \, dx$$

and

$$f_{11} = \int_0^L \frac{\cos^2 \phi}{b_{11}} \, dx$$

$$f_{12} = \int_0^L \frac{\sin \phi \cos \phi}{b_{11}} \, dx$$

$$f_{21} = \int_0^L (1+\epsilon) H1(x) \cos \phi \, dx$$

$$f_{22} = \int_0^L -(1+\epsilon) H2(x) \cos \phi \, dx$$

$$f_{23} = \int_0^L (1+\epsilon) H0(x) \cos \phi \, dx$$

$$f_{31} = H1(L)$$

$$f_{32} = -H2(L)$$

$$f_{33} = HO(L)$$

$$T'_{A_1} = \int_0^L F1_n \cos \phi \, dx - \int_0^L (1+\epsilon) \sin \phi \, \Delta \phi_n \, dx$$

$$T'_{A_2} = \int_0^L \sin \phi \, \Delta \epsilon_n + \int_0^L (1+\epsilon) \cos \phi \, dx \int_0^L F3_n \, dx$$

$$T'_{A_3} = \int_0^L F3_n \, dx$$

$$T_{A_1} = \int_0^L F2 \cos \phi \, dx$$

$$T_{A_2} = \int_0^L (1+\epsilon) \cos \phi \, dx \int_0^x F4 \, dx$$

$$T_{A_3} = \int_0^L F4 \, dx$$

$$T_{I_{23}} = \int_0^L (1+\epsilon) \cos \phi \, dx$$

the incremental force displacement equations become

$$\Delta u_B - \Delta u_A = -f_{11} \Delta X_A - f_{12} \Delta Y_A + O \Delta M_A + T'_{A_1} + T_{A_1}$$

$$\Delta v_B - \Delta v_A - T'_{I_{23}} \phi_A = -f_{21} \Delta X_A - f_{22} \Delta Y_A - f_{23} \Delta M_A + T'_{A_2} + T_{A_2}$$

$$\Delta \phi_B - \Delta \phi_A = -f_{31} \Delta X_A - f_{32} \Delta Y_A - f_{33} \Delta M_A + T'_{A_3} + T_{A_3}$$

In matrix form this becomes

$$\Delta u_B - T_1 \Delta u_A = -f \Delta P_A + T'_A + T_A$$

where

$$T_1 = \begin{bmatrix} 1 & 0 & 0 \\ 0 & 1 & \int_0^L (1+\epsilon) \cos \phi dx \\ 0 & 0 & 1 \end{bmatrix}$$

multiplying both sides of the equation by $K = f^{-1}$ gives

$$K \Delta u_B - K T_1 \Delta u_A = -\Delta P_A + K T'_A + K T_A$$

so

$$\Delta P_A = K T_1 \Delta u_A - K \Delta u_B + K T'_A + K T_A$$

now

$$\Delta X_B = -\Delta X_A - \Delta P$$

$$\Delta Y_B = -\Delta Y_A - \Delta Q$$

$$\Delta M_B = -\Delta X_A \int_0^L (1+\epsilon) \sin \phi dx + \Delta Y_A \int_0^L (1+\epsilon) \cos \phi dx - \Delta M_A -$$

$$\int_0^L \left[(1+\epsilon) (\Delta P \sin \phi - \Delta Q \cos \phi) + \Delta M \right] dx + \int_0^L \left[N(1+\epsilon) \Delta \phi - V \Delta \epsilon \right] dx$$

so if

$$T_2 = \begin{bmatrix} -1 & 0 & 0 \\ 0 & -1 & 0 \\ -\int_0^L (1+\epsilon) \sin \phi dx & \int_0^L (1+\epsilon) \cos \phi dx & -1 \end{bmatrix}$$

then $\Delta P_B = T_2 \Delta P_A + T_B$

If the effect of the distributed loads and moments is contained in the matrix T_B then the following matrix equation holds

$$\Delta P_B = T_2 \Delta P_A = T_2 K T_1 \Delta u_A - T_2 K \Delta u_B + T_2 K T'_A + T_2 K T_A + T_B$$

This now gives a relationship between applied forces and displacements at either end. The required matrices and a brief summary of the solution procedure appear on the following pages.

$$f = \begin{bmatrix} \int_0^L \frac{\cos^2 \phi}{b_{11}} dx & \int_0^L \frac{\sin \phi \cos \phi}{b_{11}} dx & 0 \\ \int_0^L (1+\epsilon) H_1(x) \cos \phi dx & \int_0^L -(1+\epsilon) H_2(x) \cos \phi dx & \int_0^L (1+\epsilon) H_0(x) \cos \phi dx \\ H_1(L) & -H_2(L) & H_0(L) \end{bmatrix}$$

$$T_1 = \begin{bmatrix} 1 & 0 & 0 \\ 0 & 1 & \int_0^L (1+\epsilon) \cos \phi dx \\ 0 & 0 & 1 \end{bmatrix}$$

$$T_1^* = \begin{bmatrix} -1 & 0 & 0 \\ 0 & -1 & 0 \\ 0 & 0 & -1 \end{bmatrix}$$

$$T_A = \left[\begin{array}{l} \int_0^L F1_n \cos \phi \, dx - \int_0^L (1+\epsilon) \sin \phi \, \Delta \phi_n \, dx \\ \int_0^L \sin \phi \, \Delta \epsilon_n \, dx + \int_0^L (1+\epsilon) \cos \phi \, dx \int_0^L F3_n \, dx \\ \int_0^L F3_n \, dx \end{array} \right]$$

$$T_A = \left[\begin{array}{l} \int_0^L F2 \cos \phi \, dx \\ \int_0^L (1+\epsilon) \cos \phi \, dx \int_0^x F4 \, dx \\ \int_0^L F4 \, dx \end{array} \right]$$

$$T_2 = \left[\begin{array}{ccc} -1 & 0 & 0 \\ 0 & -1 & 0 \\ -\int_0^L (1+\epsilon) \sin \phi \, dx & \int_0^L (1+\epsilon) \cos \phi \, dx & -1 \end{array} \right]$$

$$T_B = \begin{bmatrix} -\Delta P(L) \\ -\Delta Q(L) \\ \int_0^L [(1+\epsilon)(\Delta P \sin \phi - \Delta Q \cos \phi) + \Delta m] dx + \\ \int_0^L [N(1+\epsilon)\Delta \phi_n - z\epsilon_n] dx \end{bmatrix}$$

and the matrix equations become

$$\Delta P_A = K_{AA} \Delta U_A + K_{AB} \Delta U_B + FEP_A$$

$$\Delta P_B = K_{BA} \Delta U_A + K_{BB} \Delta U_B + FEP_B$$

where

$$f^{-1} = K$$

$$K_{AA} = KT_1$$

$$K_{AB} = KT_1' = -K$$

$$K_{BA} = T_2 KT_1$$

$$K_{BB} = T_2 K$$

$$FEP_A = KT_A + KT_A'$$

$$FEP_B = T_2 FEP_A + T_B$$

With these matrices the solution becomes quite similar to a traditional stiffness method solution. At any give increment of load ϕ' , ϕ , ϵ , N , and V are known. This makes it

possible to form the flexibility coefficients b_{11} , b_{12} , b_{21} , and b_{22} by integrating over the member, and also the member stiffness matrices K_{AA} , K_{AB} , K_{BA} , and K_{BB} . The vectors T_A and T_B can be formed and the global stiffness matrix assembled. Since the fixed end forces depend on T_A' which in turn depends on Δc , $\Delta \phi$ and $\Delta \phi'$, an iterative solution is required. The iteration starts by assuming a new Δc , $\Delta \phi$ and $\Delta \phi'$ for each member. This makes it possible to compute T_A' , FEF_A and FEF_B and solve the equation $EAU^* = AP - AQ$ where AQ is the vector of fixed end forces and AP the vector of applied loads. From AU^* it is possible to compute approximate member end forces and get a new estimate of Δc , $\Delta \phi$ and $\Delta \phi'$. This process continues until two solutions are within an acceptable tolerance, at which point the new value of ϕ' , ϕ , c , M and V are computed and the whole process is repeated again.

The Complex Model is the only model that includes member stability. Because the numerical solution is based on an incremental approach, the only simplifying assumption made about deformation is that $\Delta \phi$ is small enough to take it as a differential, and therefore $\sin \Delta \phi = \Delta \phi$ and $\cos \Delta \phi = 1$. This is a safe assumption as long as the loading increments are reasonably small, and since the accuracy of any tangent formulation depends on the size of the loading increments anyway, this assumption seems entirely justified. In all other respects, the Complex Model is theoretically

exact, within the limits of any incremental approach, and can be confidently used as a yardstick against which other models can be compared.

3.0 MEMBER STUDY - ELASTIC

In this chapter, the behavior of the Complex Model is discussed, and the relative importance of the two elastic non-linear effects, the P-Delta effect, and the effect of change in geometry, is examined. Although the Complex Model is the only model capable of representing member deformations, and hence member instability, the simple expedient of subdividing a member into a number of smaller members makes it possible to reproduce member buckling with the other models as well. Because of this, it is possible to use the other models to check the Complex Model, provided that enough submembers are used in the simpler models. In addition, the relative importance of the various non-linear effects can be evaluated, since each effect can be included separately in the simple models.

3.1 Behavior of the Complex Model

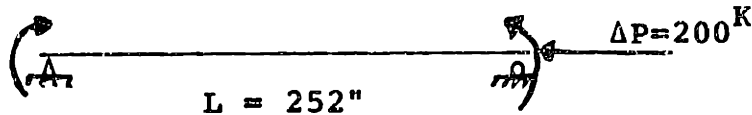
Three basic types of loading were examined; an axially loaded member with small end moments (single curvature), an axially loaded member with a concentrated vertical load in the center, and an axially loaded member with a prescribed vertical displacement applied at the center. Only in the second case were boundary conditions other than hinged ends considered. In all cases, the member was a W14 x 142, modeled with six fibers and twenty-six sections. A previous

thesis done by Raymond W. Latona has shown that this number of fibers and cross sections will give results that are accurate to within 2½% in both the elastic and inelastic range.

The results of the first type of loading, equal end moments and an axial load, are shown in Figure 3-1, the load increments and support conditions are shown below.

$$\Delta M = 10 \text{ in}\cdot\text{K}$$

$$\Delta M = 10 \text{ in}\cdot\text{K}$$



The Euler buckling load for this member (P_E) is 7786 kips, and this value is quite close to that given by Figure 3-1. Figure 3-2 shows the same case, but with the load increments ΔP and ΔM halved. The smaller increments cause the predicted buckling load to be lower by about 400 kips, which is precisely what would be expected from a tangent formulation, since any error will give a load above the true solution.

The results of the second type of loading are shown in Figures 3-3 through 3-6. Figures 3-3 and 3-4 represent the results obtained from the case shown below, with the member length equal to 252 inches in 3-3, and 504 inches in 3-4.

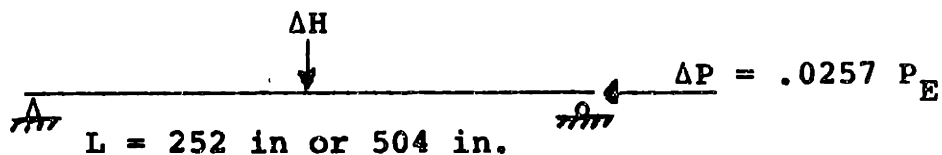


Figure 3-1. Graph of v vs P

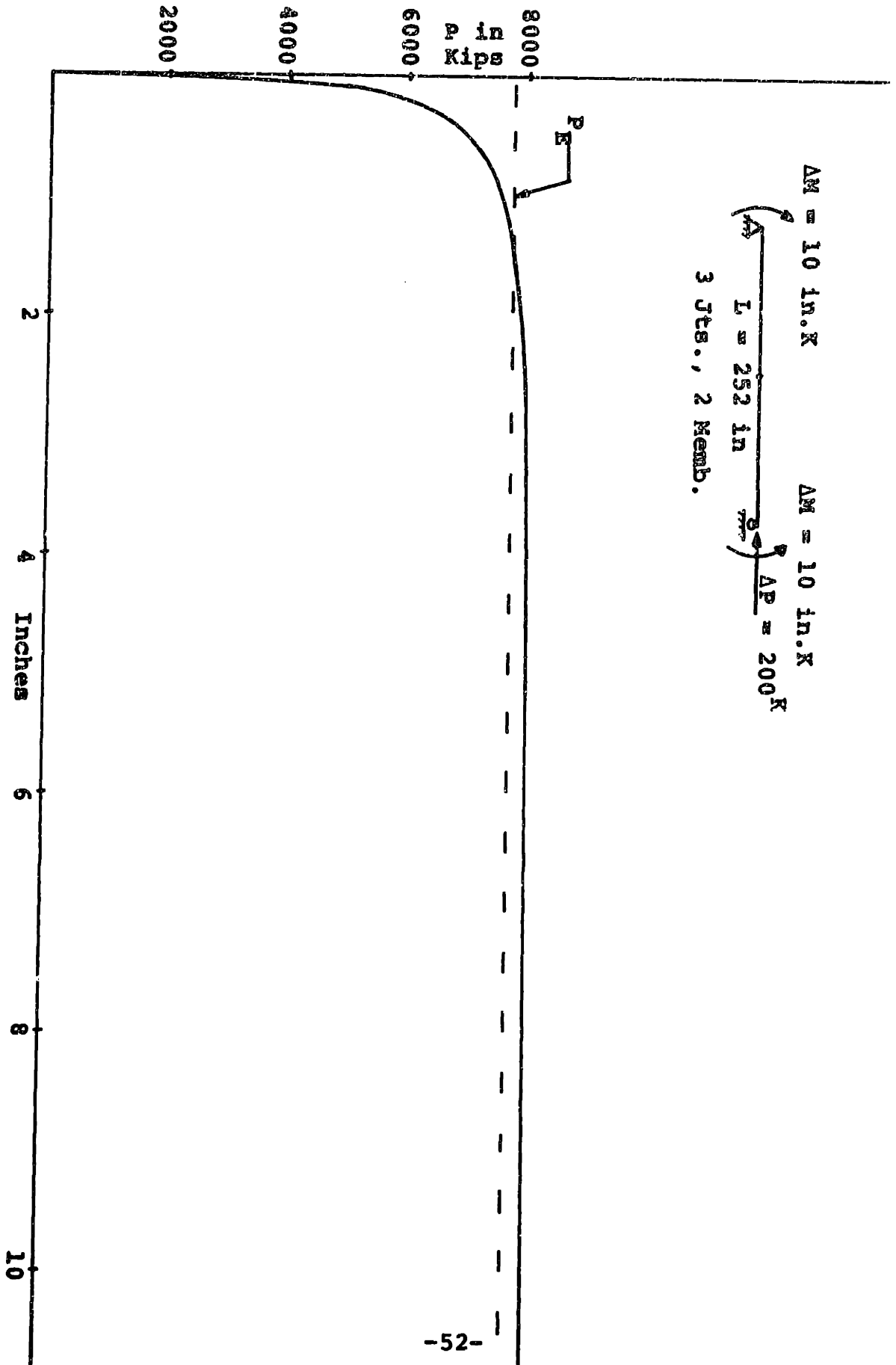


Figure 3-2. Graph of P vs V

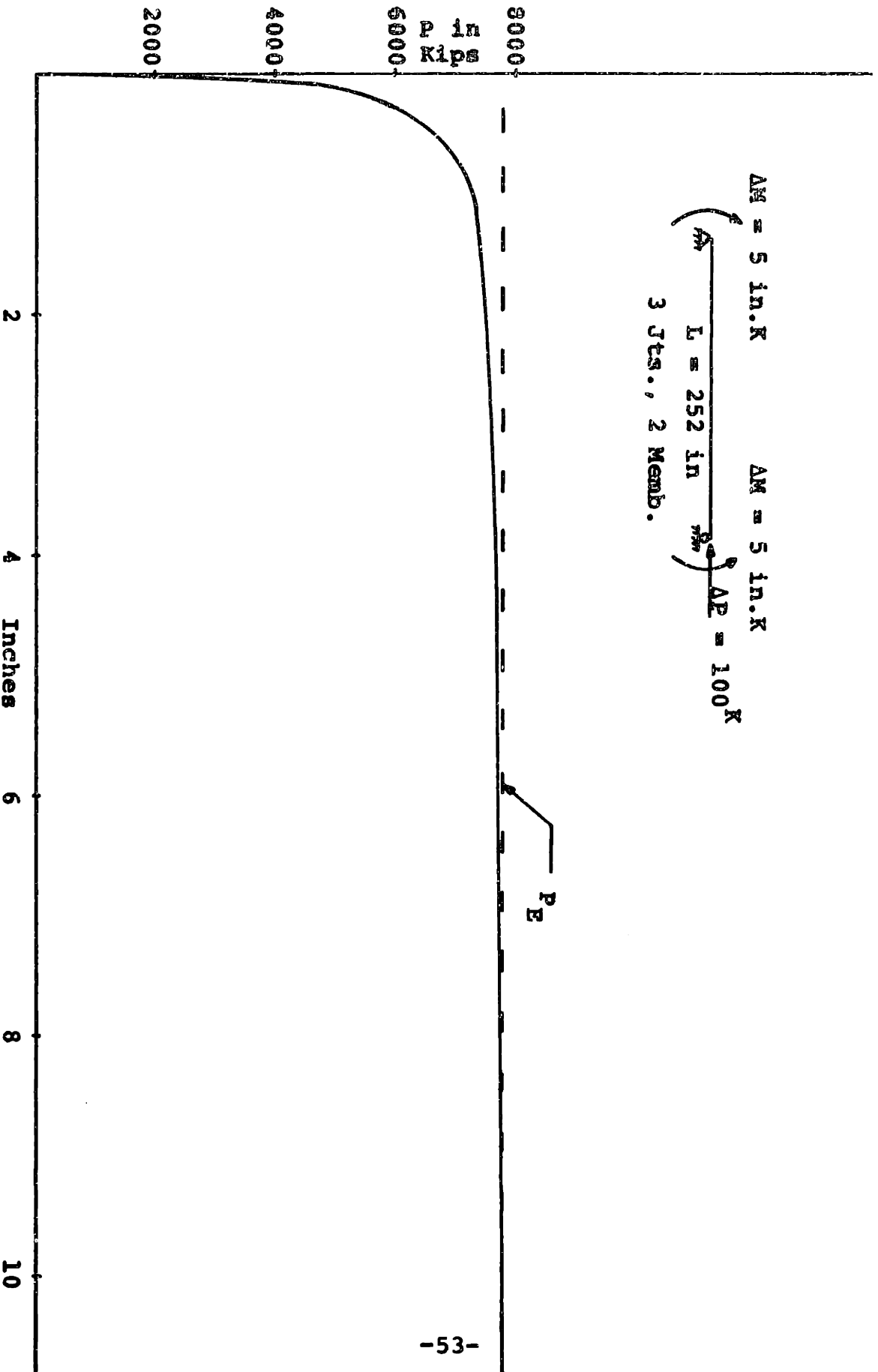


Figure 3-3. Graph of v vs P

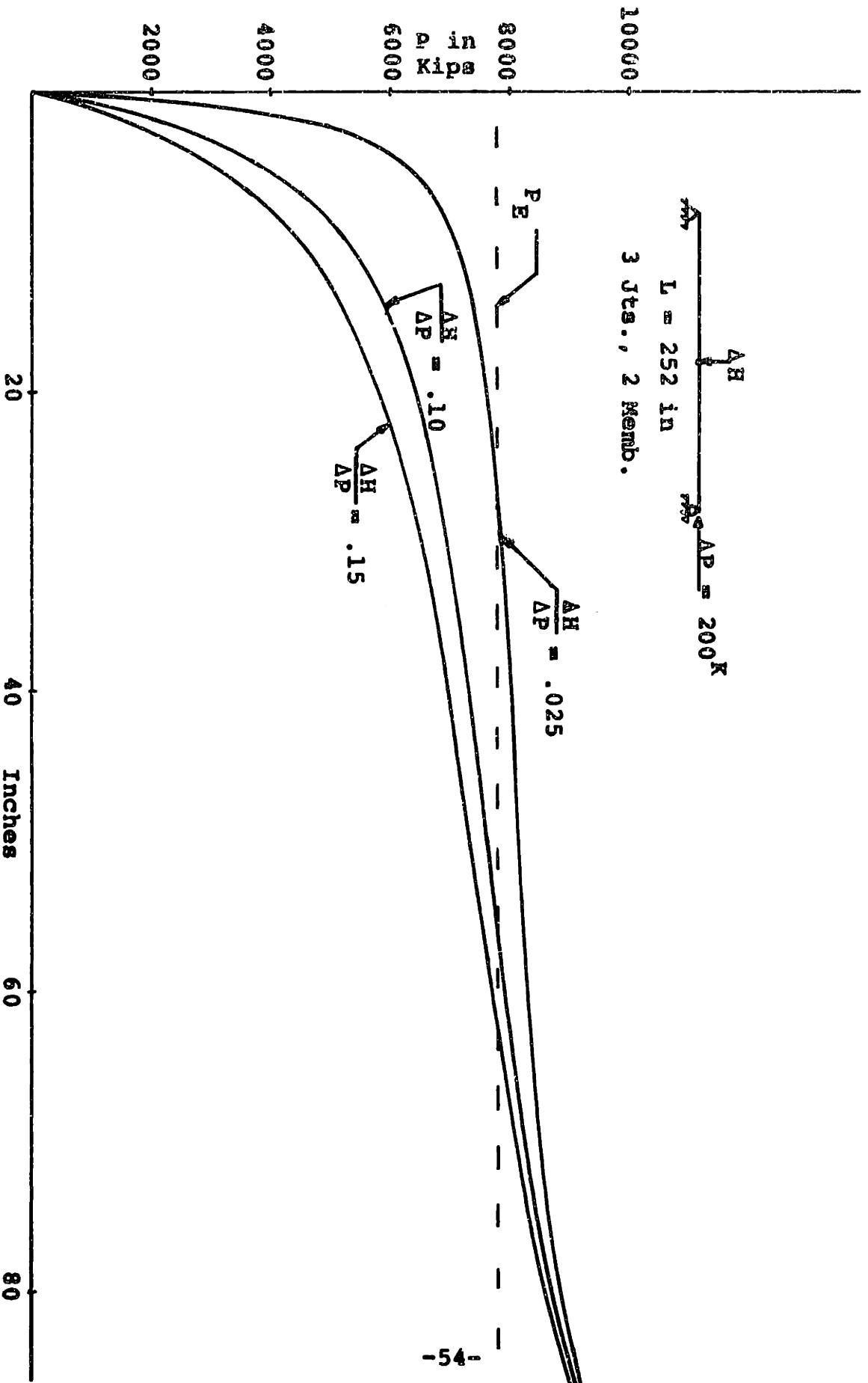
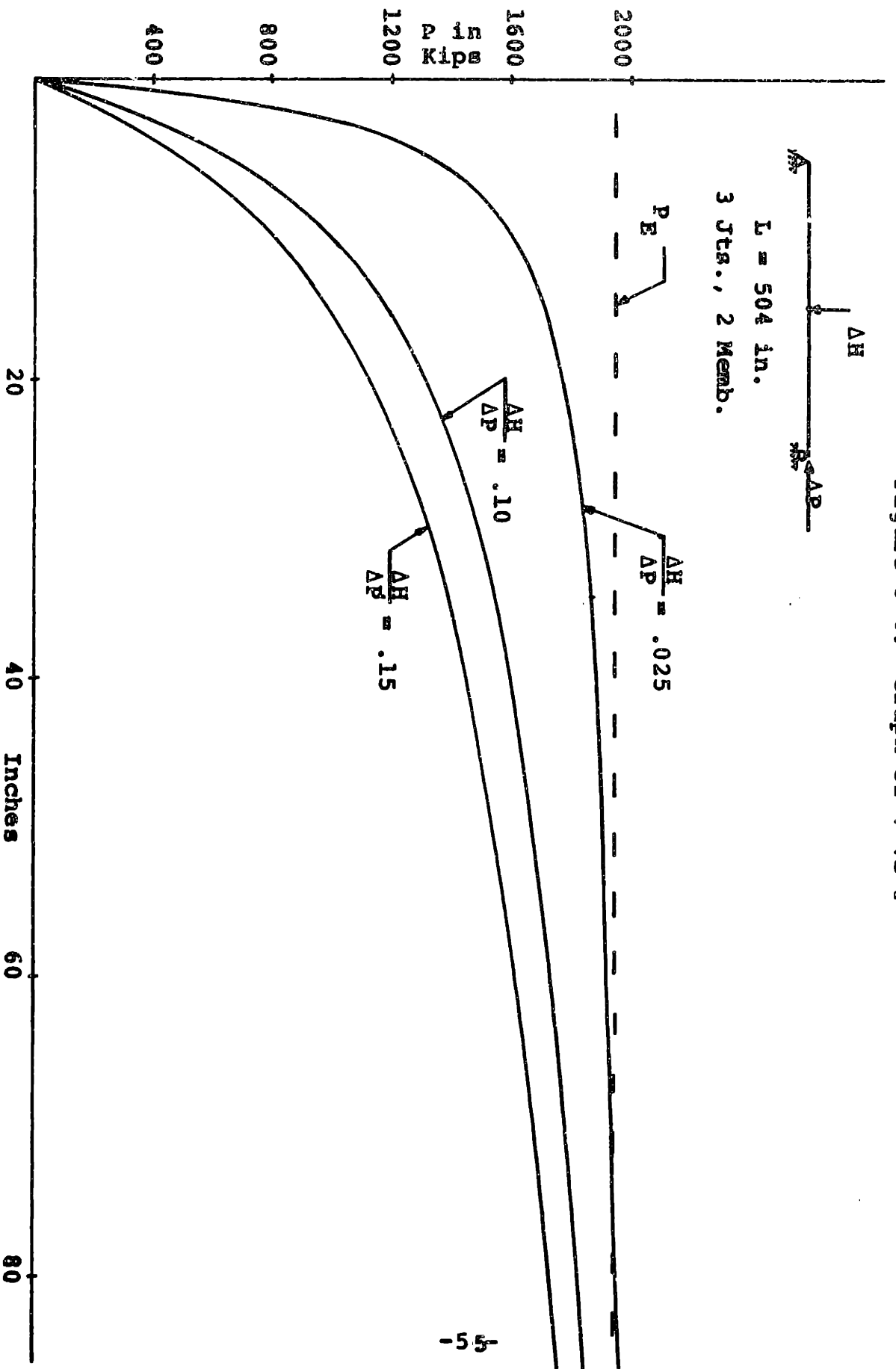


Figure 3-4. Graph of v vs P



In both cases, the critical buckling load predicted by the model, approaches the Euler buckling load as ΔH approaches zero. Since both the axial load and the horizontal load increase at each increment, even a small value of ΔH amounts to an appreciable load after thirty or forty increments, and hence may well have a sizeable effect on member stability. A precise definition of the buckling load is very difficult for this type of loading. There is no clear point of instability, instead, there is an area where the stiffness of the member is clearly decreasing, an area where it remains constant (but very small), and finally an area of increasing stiffness, although by this time the deflection has become so great that the structure is more of an arch than a beam. This is only a theoretical difficulty, however, since this member, if made of conventional steel, would already have failed inelastically.

Thus the most important parameter for this type of loading is not a precise definition of the buckling load, but rather a precise definition of the amount of deflection amplification to be expected as P approaches P_E . If the amplification factor A is defined as the ratio of the actual beam deflection, to the beam deflection that would occur if only the horizontal load were present, then the amplification factor for various ratios of P/P_E can be computed from Figures 3-3 through 3-6.

In the case of a hinged member, the theoretical midspan deflection (assuming small deformations) for a member with an axial load P and a horizontal load H is shown below.

$$v_T = \frac{HL}{4P} \left(\frac{\sin \frac{KL}{2}}{\frac{KL}{2} \cos \frac{KL}{2}} - 1 \right) , K = \sqrt{\frac{P}{EI}}$$

Since the deflection at midspan due to the horizontal load acting alone would be

$$v_H = \frac{HL^3}{48EI}$$

the amplification factor can be written as follows

$$A = \frac{v_T}{v_H} = \frac{12}{K^2 L^2} \left(\frac{\sin \frac{KL}{2}}{\frac{KL}{2} \cos \frac{KL}{2}} - 1 \right) , K = \sqrt{\frac{P}{EI}}$$

In Tables 3-1 and 3-2 the values of A obtained from Figures 3-3 and 3-4 are compared with the value of A given by the formula above. In all cases the increment of axial load, ΔP , is 2.57% of the Euler buckling load.

Table 3-1

Effect of Varying ΔH on A for Beam of Figure 3-3

P/P_E	$\Delta H/\Delta P$			Theory
	.025	.10	.15	
.5	1.92	1.92	1.92	1.98
.75	3.53	3.46	3.45	3.95
.9	7.56	6.65	5.89	9.85

Table 3-2

Effect of Varying ΔH on A for Beam of Figure 3-4

P/P_E	$\Delta H/\Delta P$			Theory
	.025	.10	.15	
.5	1.92	1.92	1.92	1.98
.75	3.71	3.55	3.45	3.95
.9	7.90	6.86	6.00	9.85

It should be noted that the theoretical predictions in ~~these tables~~ are based on the traditional linearized theory, which becomes inaccurate when the deformations cease to be small. Since the linear theory cannot predict the increase in stiffness due to the arch effect, the results given in Tables 3-1 and 3-2 appear reasonable. The agreement with the linearized theory is quite good at $P = .5 P_E$, but becomes poorer as P approaches P_E . Some of this discrepancy is undoubtedly caused by the inherent errors in any tangent solution, and some by the linear assumptions in the theory. Since the size of the solution error is directly dependent on the size of ΔP , the relationship between A and ΔP is shown in Table 3-3 for different ratios of $\Delta P/P_E$. In Table 3-3 below, the value of $\Delta H/\Delta P$ is .10, and the length of the beam is 254 inches.

Table 3-3

Effect of Varying ΔP on A for Beam of Figure 3-3

P/P_E	$\Delta P/P_E$			Linear Extrapolation		Theory
	.0257	.0128	.0064	Columns 1&2	Columns 2&3	
.5	1.92	1.96	1.98	2.01	2.00	1.98
.75	3.46	3.62	3.69	3.78	3.76	3.96
.9	6.65	7.03	7.21	7.41	7.39	9.90

Table 3-3 clearly shows that A increases as the size of ΔP decreases, and that the relationship between ΔA and ΔP is essentially linear. At $P = .5 P_E$, the linear extrapolation agrees quite closely with the linearized theory, but at higher loads there continues to be a significant discrepancy. This discrepancy is probably due to error in the theory, since the displacements at these loads are no longer small enough to justify the linear assumptions made in deriving the theoretical amplification factor. Thus the predictions of the Complex Model appear quite good. In areas where the linearized theory is valid, the Complex Model agrees very closely, in areas where the theory is less valid, the predictions of the Complex Model differ in a way that appears reasonable.

When the ends of the member are fixed rather than pinned, the theoretical amplification factor (again assuming small deformations) becomes

$$A = \frac{96}{K^3 L^3} \left[\frac{2(1 - \cos \frac{KL}{2}) - \frac{KL}{2} \sin \frac{KL}{2}}{\sin \frac{KL}{2}} \right] K = \sqrt{\frac{P}{EI}}$$

In Tables 3-4 and 3-5, the values of A obtained from Figures 3-5 and 3-6 are compared with this theoretical value for $\Delta P = .0257 P_E$, and varying ratios of $\frac{\Delta P}{\Delta H}$.

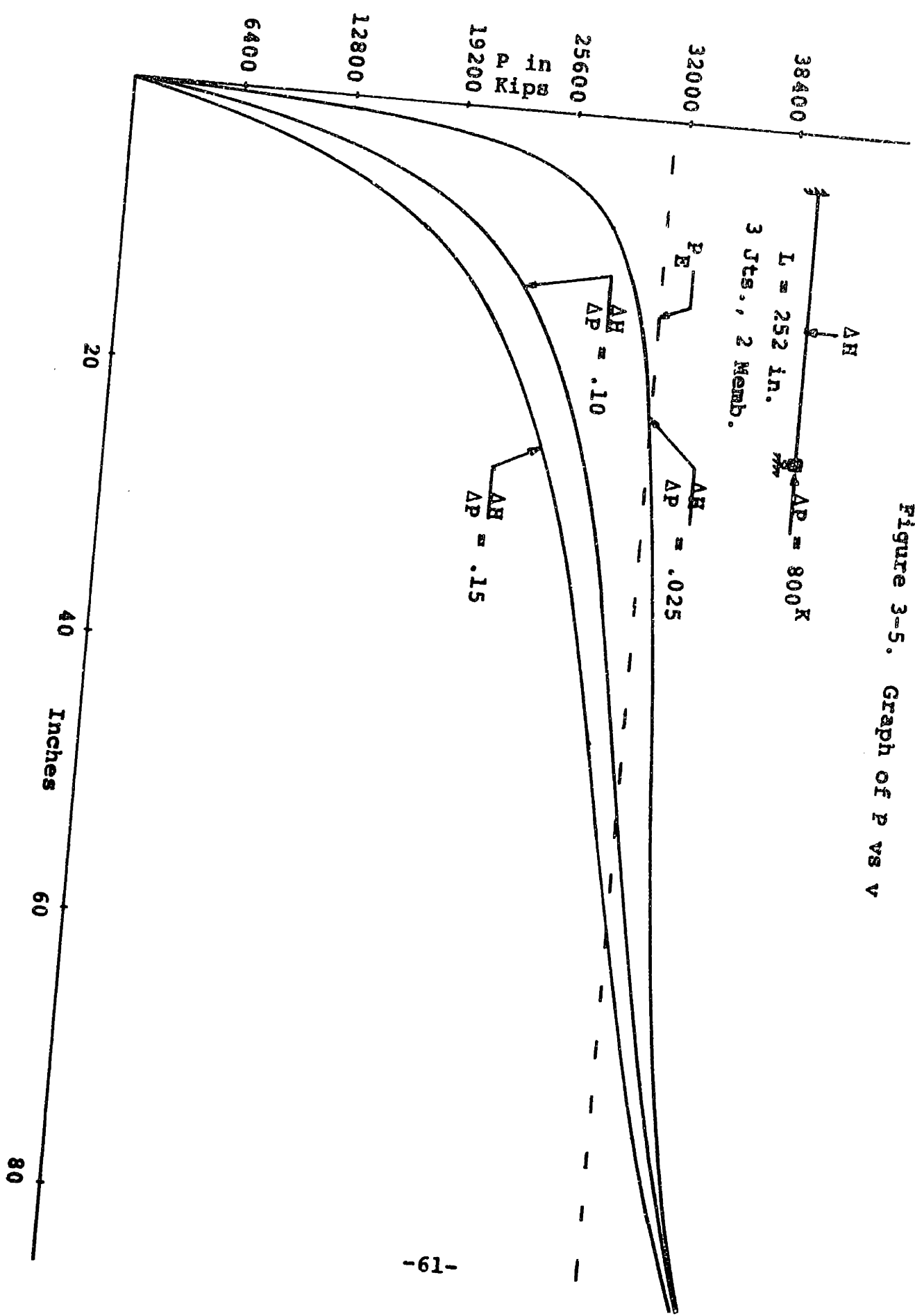


Figure 3-5. Graph of P vs V

Figure 3-6. Graph of P vs v

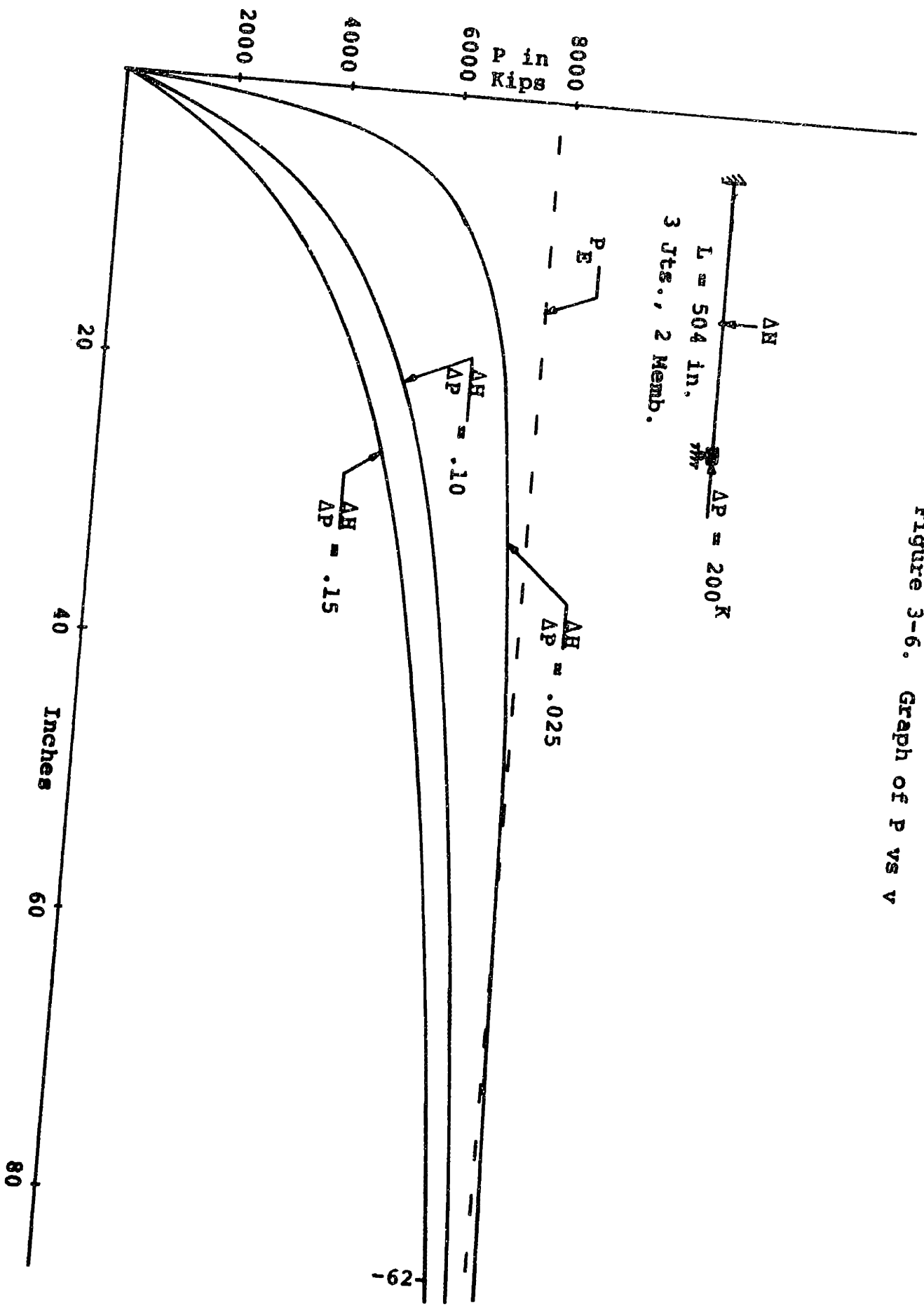


Table 3-4

Effect of Varying ΔH on A for Beam of Figure 3-5

P/P_E	$\Delta H/\Delta P$			Theory
	.025	.10	.15	
.5	1.90	1.93	1.92	1.98
.75	3.51	3.30	3.23	3.95
.90	6.55	5.89	5.44	9.84

Table 3-5

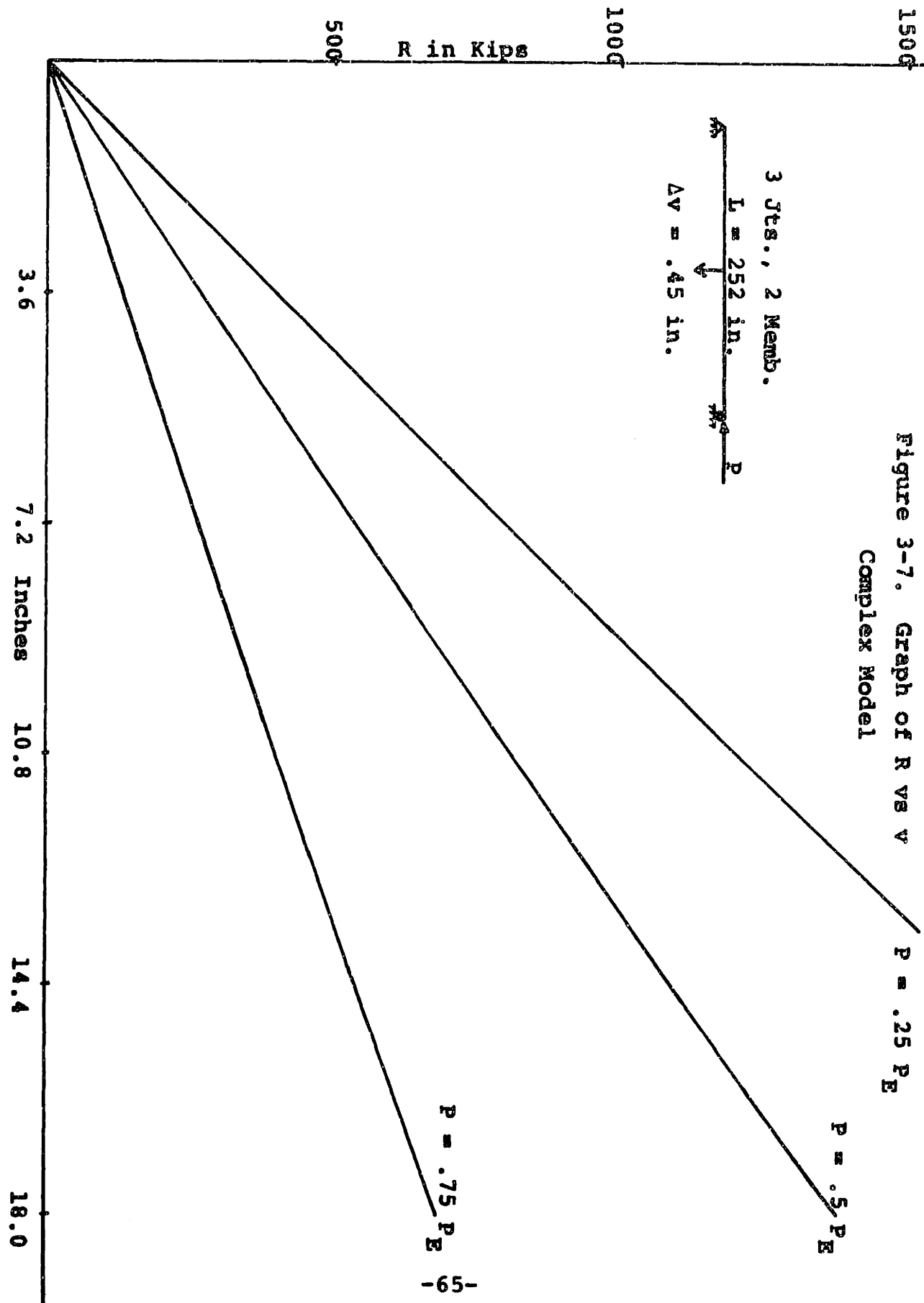
Effect of Varying ΔH on A for Beam of Figure 3-6

P/P_E	$\Delta H/\Delta P$			Theory
	.025	.10	.15	
.5	1.92	1.93	1.91	1.98
.75	3.56	3.50	3.40	3.95
.90	7.25	6.43	5.78	9.84

These tables show that the amplifications predicted by the model for the fixed ended case are very similar to those predicted for the pin ended case. Once again the agreement with the linear theory is good in the area where that theory is valid, and where the model differs from the theory, the variation seems reasonable.

Because the results of Tables 3-4 and 3-5 are so similar to those of Tables 3-1 and 3-2, it seems reasonable to assume that the error study done in Table 3-3 would apply equally well here. It should be noted, that in all cases the stiffening caused by the arch effect will increase as ΔH increases. Thus the value of A should decrease as the ratio of $\Delta H/\Delta P$ increases. This reduction cannot be predicted by the theory, since the linear assumptions used cause A to be independent of H. The results from the tables do show this reduction, however, and show that it becomes significant after P exceeds $.5 P_E$.

In the third type of loading, an axial load with a prescribed vertical displacement, the vertical displacement was applied to a member with a constant axial load, and also to a member with an increasing axial load. Figure 3-7 shows the case where the axial load was held constant and a prescribed displacement was applied at the center. The graph clearly shows that the axial load has a softening effect on the beam, and that this effect is increased as the magnitude of the axial load increases. This effect is not



quite linear, and a slight stiffening of the beam occurs. This is caused by the fact that the perturbing forces caused by the P-Delta effect are not quite linearly related to the displacement, and hence do not quite cancel out the increase in reaction which is, of course, linearly related to the displacement.

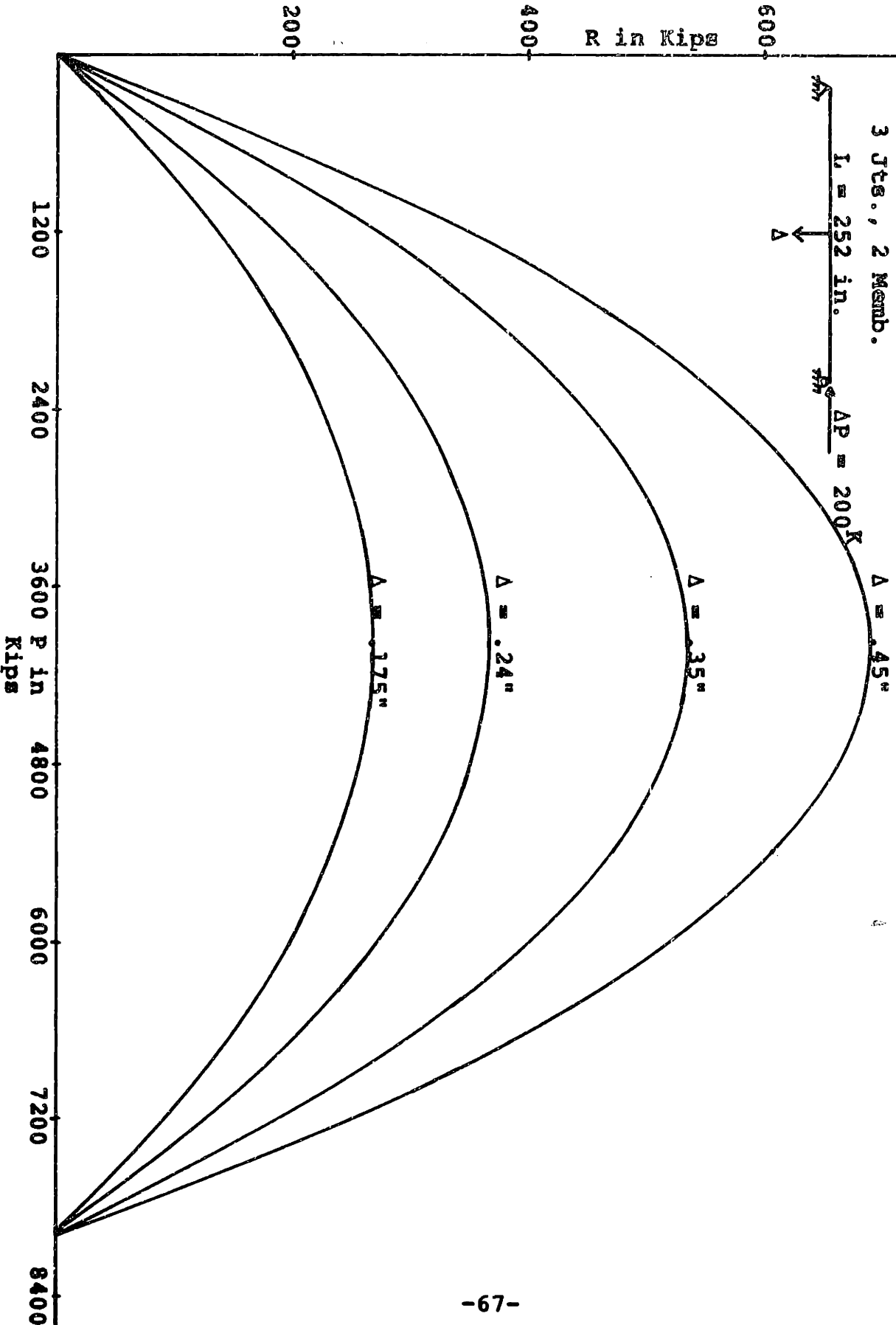
In the second case, both axial load and displacement were varied, giving the results shown in Figure 3-8 where the axial load is graphed against the vertical reaction. It is interesting to note that buckling occurs when R becomes equal to zero, and that the maximum value of R is a function of the prescribed displacement. Thus, in this situation, a decreasing value of R is not an indication of buckling until the value of R becomes negative.

In summary, three different cases have been examined, and in each of them the results obtained from the Complex Model agree with those predicted by theory. In the areas where the theory doesn't apply, or gives an upper bound, the model results appear reasonable, and differ from the theory in a predictable way. The use of a tangent type solution does cause an error, which can only be reduced by a smaller increment of load.

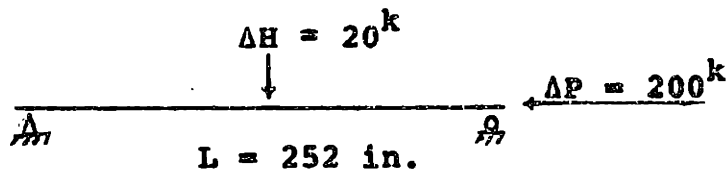
3.2 The Elastic Non-Linear Effects

Although member buckling is not considered in the linear models, buckling of the structure as a whole is accounted for by the P-Delta effect and the change in geometry. In this

Figure 3-8. Graph of R vs P
Complex Model

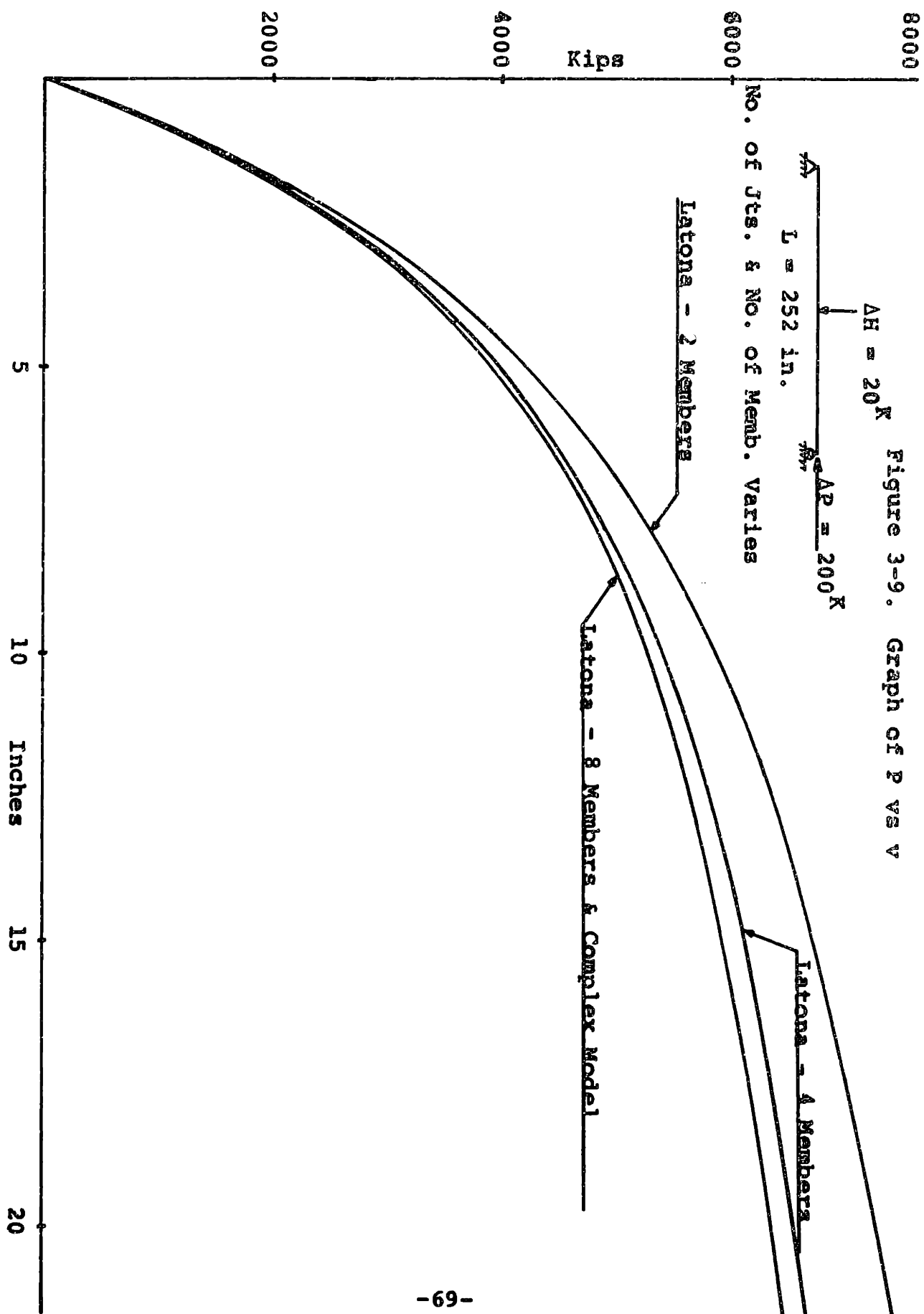


section, the structure shown below will be modeled using two, four and eight members, and the results will be compared to those obtained by the Complex Model.



Since both the Interaction Model and the Latona Model give identical results in the elastic case, only the Latona Model will be specifically discussed, although all results and conclusions are equally applicable to the Interaction Model.

Figure 3-8 compares the results from the Latona Model with those from the Complex Model. When eight members are used in the Latona Model, the results are practically identical with those given by the Complex Model. When fewer members are used, the agreement is not as good, although even the model with two members is within 15% of the Complex Model. Since it is possible to reproduce the results of the Complex Model with an eight member Latona Model, the two non-linear effects can be isolated, and compared with the correct solution. Figure 3-9 shows the behavior of the Latona Model with only the P-Delta effect, and the Latona Model with both the P-Delta effect and the change in geometry. The graph clearly shows that the results obtained from the Latona Model, when the P-Delta effect is the only non-linear



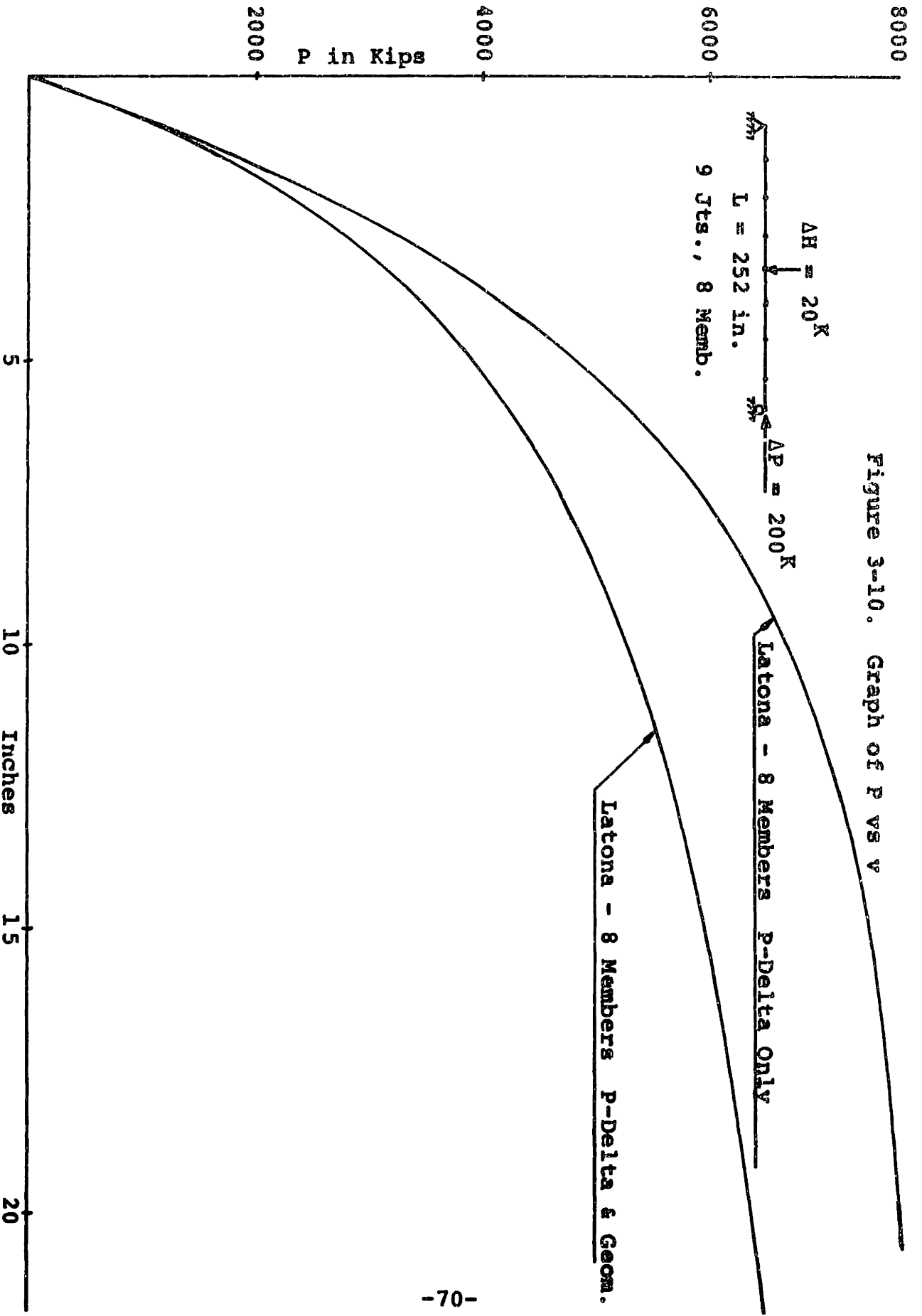


Figure 3-10. Graph of P vs V

effect considered, are considerably different from those obtained when both the P-Delta effect and the change in geometry are included. This shows that the effect of change in geometry is as important as the P-Delta effect, and that both must be included in a modified linear model, if non-linear behavior is to be accurately represented.

3.3 Summary

The behavior of the Complex Model in the elastic range has been examined, and the results given by the model conform to established theory. The major source of error in the model has been shown to be the size of the incremental load, a reduction in increment size, giving a reduction in the magnitude of the error. By subdividing the basic member into a series of submembers, it has been possible to use the two modified linear models, the Latona Model and the Interaction Model, to model buckling as well. It has been shown that a member divided into eight submembers, and analyzed by a modified linear model, will give the same results as the Complex Model, provided that both the P-Delta effect and the effect of change in geometry are included. In such an analysis it is essential that both non-linear effects be considered, since neither effect alone gives sufficiently accurate results. It should be noted that the effect of member curvature is not reproduced in the modified linear models, and hence there is no stiffening of the structure at

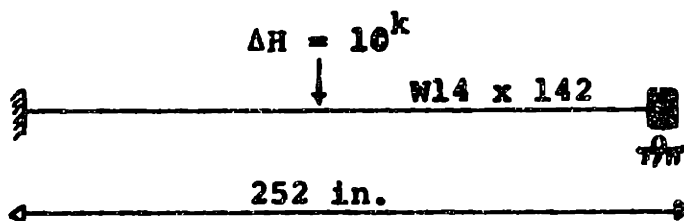
large deformations. Since this effect is rarely significant when inelastic behavior is considered, the lack of it does not seriously curtail the use of the modified linear models on realistic structures.

4.0 MEMBER STUDY - INELASTIC

In this chapter, the third non-linear effect, a change in the modulus of elasticity due to yielding, is included. Five different examples are examined, and the behavior of the various models in each example is discussed. In the first two examples no axial load is applied, member deformations are quite small, and hence the effect of yielding becomes the only important non-linear effect. In the last three examples an axial load is applied and the relative importance of all three non-linear effects is considered. In all cases the material is assumed to be A36 steel, and the section is a W14 x 142.

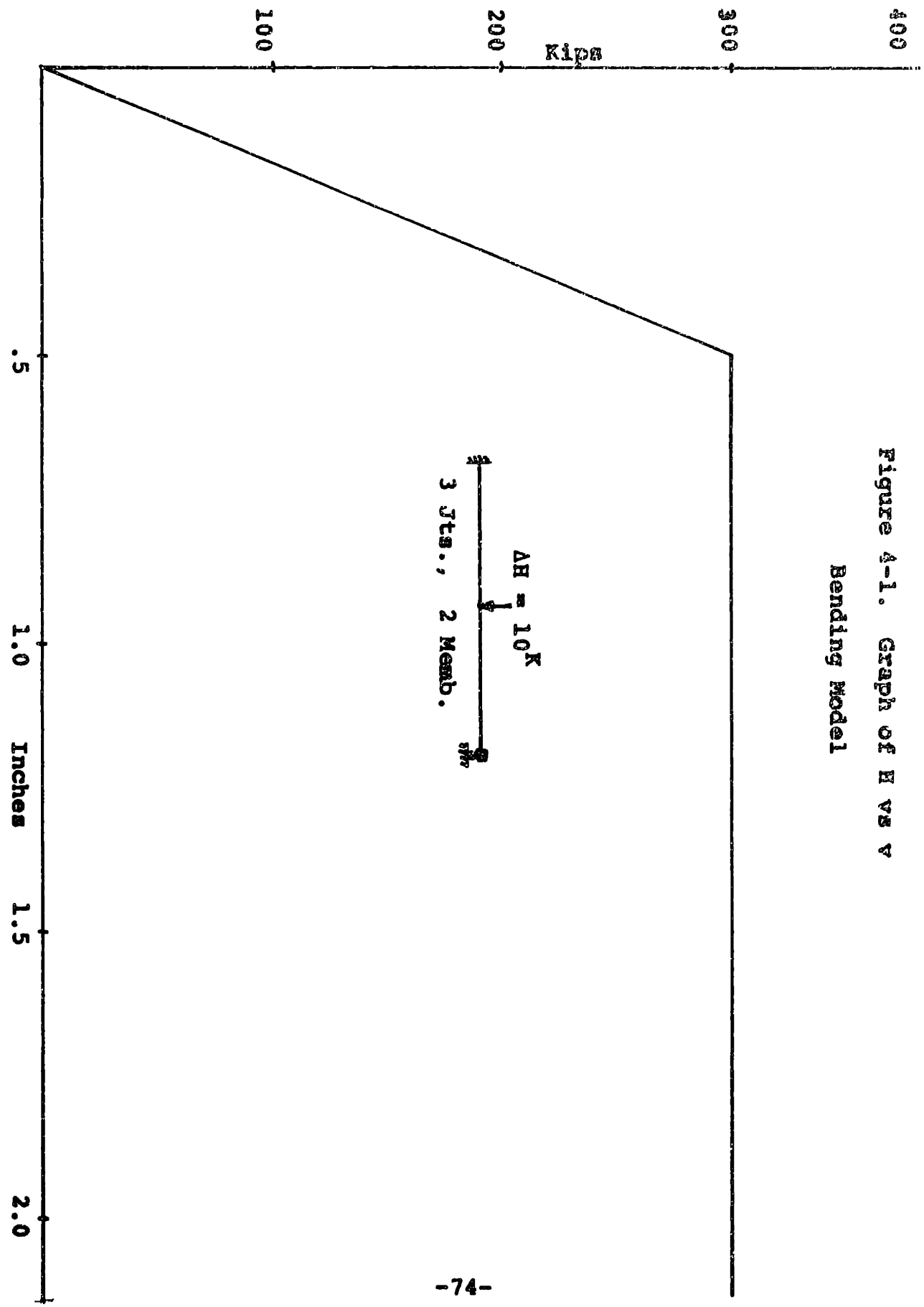
4.1 Inelastic Behavior - Without Axial Load

The first example considered is shown below, a fixed ended beam with a concentrated load at midspan.



Since the moment at both ends and the center is $\frac{HL}{8}$, the beam should fail when the beam moment equals the plastic moment for the beam. In this case, the plastic moment is 9180 in.k so the beam should fail when H reaches 291^k . Figures 4-1 through 4-4 show the predictions of the four models for this example.

Figure 4-1. Graph of H vs V
 Bending Model



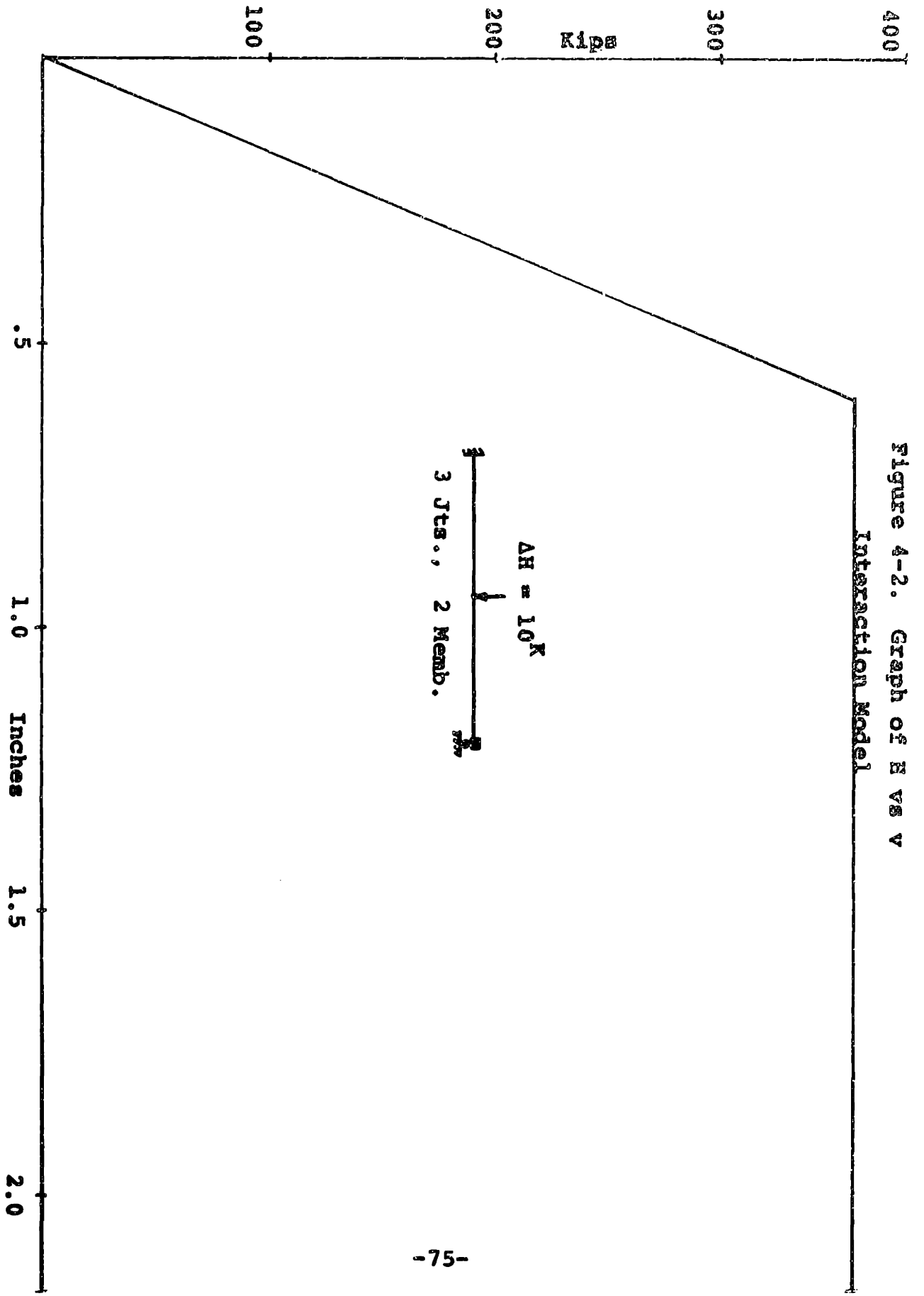
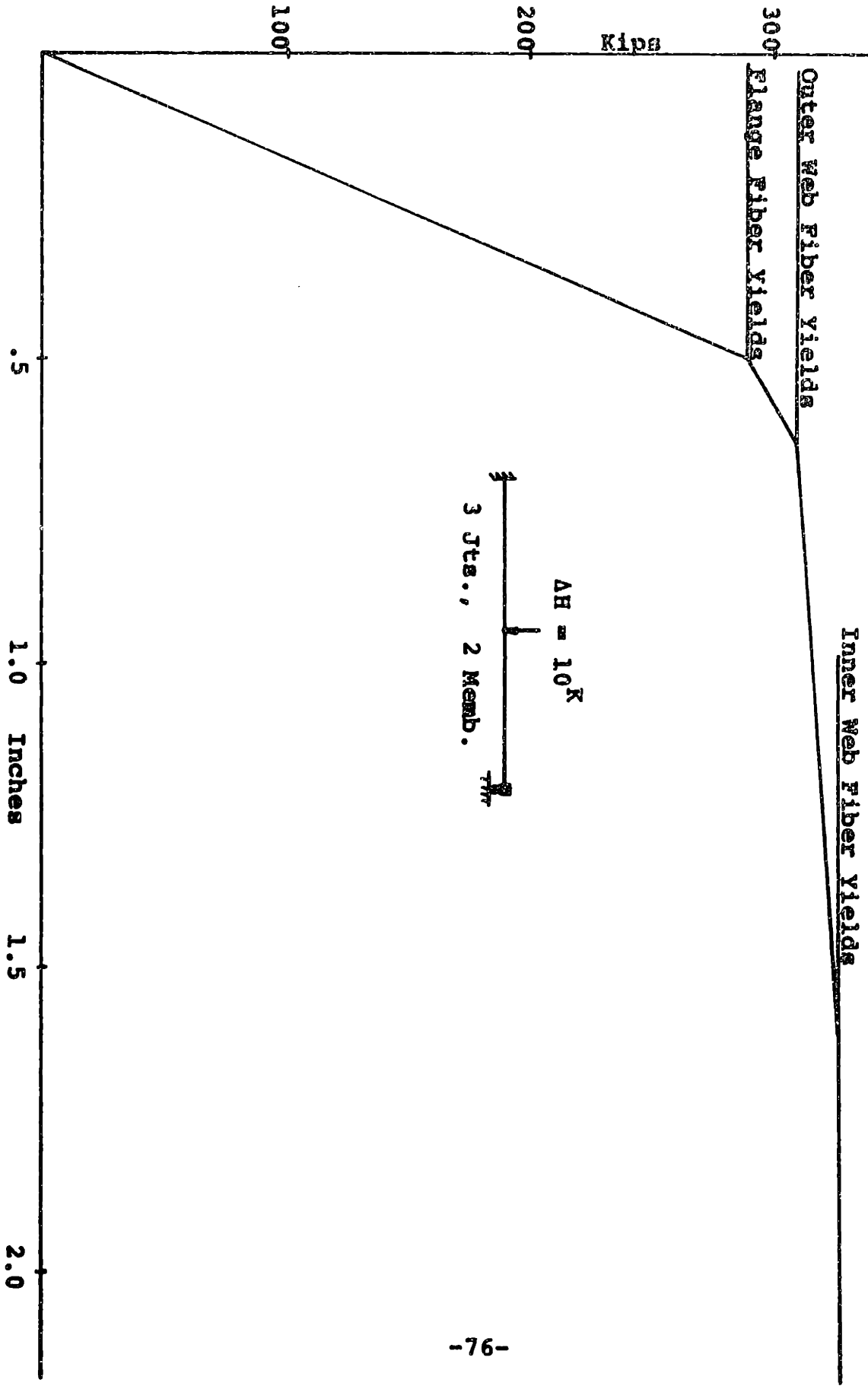


Figure 4-2. Graph of E vs V Interaction Model

Figure 4-3. Graph of H vs V
 Latona Model



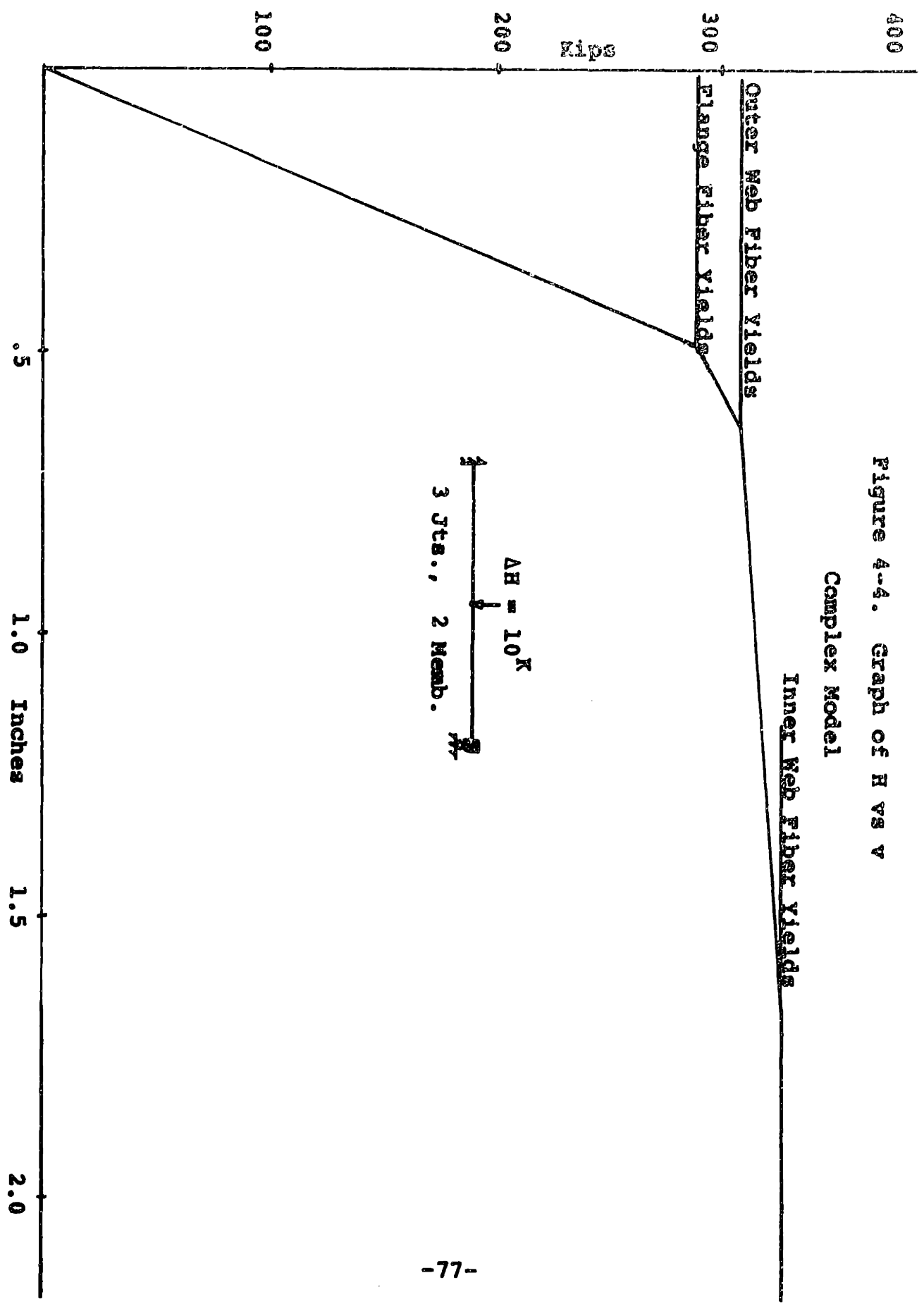
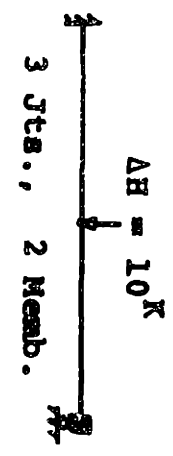


Figure 4-4. Graph of H vs v
Complex Model

Outer Web Fiber Yields

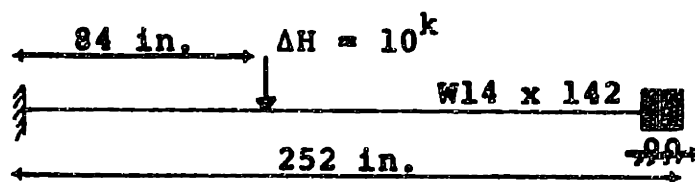
Flange Fiber Yields



The Bending Model and the Interaction Model fail abruptly since they develop hinges as soon as the inelastic criteria are met. The Bending Model gives a very good prediction of the limiting load, but the Interaction Model is high, since it meets the criteria of $.847 M/M_p = 1$. Because of this, the failure load predicted by the Interaction Model should be 1.18 times as large as that predicted by the Bending Model, and this is precisely what it is. Clearly a smaller load increment would lead to a better prediction for both models, but the error in the Bending Model is only about 3% and this certainly seems tolerable.

The Latona Model and the Complex Model both use the same fiber and section technique to check for yielding, and thus should give results that are in close agreement. This is in fact the case, but their behavior is significantly different from that of the Bending Model. The formation of the failure mechanism is markedly more gradual, and comes in two parts. The first part is the formation of a hinge, which starts when the flange fibers yield, in this case when $H = 290^k$, and ends when all the fibers at one section have yielded, in this case when $H = 330^k$. Since the three hinges required to cause failure all form at the same time in this example, a failure mechanism exists when $H = 330^k$. Unlike the Bending and Interaction Models, each hinge takes several increments to form, and there are several changes in stiffness before failure, each one corresponding to the yielding of two symmetrical fibers. It is

important to note that the spreading of yielding can only be counted on when a failure mechanism is being developed. It is perfectly possible for yielding to start and then stop, if there are alternative load paths within the structure. This phenomenon of spreading of yielding causes significant differences between the predictions of the Bending and Interaction Models, and the Latona and Complex Models, especially when the failure mechanism forms progressively rather than suddenly. In the second example, shown below, a loading pattern that causes a progressive failure mechanism is examined.



In theory, the three plastic hinges will form progressively from left to right across the member. The first one should form at the left end at a load of 246^k , the second one should form at the point of load application at a load of 316^k and the third one should form at the right end at a load of 328^k . At this point, a mechanism is formed and the structure fails. This theory assumes that a plastic hinge forms as soon as the moment in the member reaches the plastic moment, and that at that point the yielded section has no further stiffness. This is a common assumption in plastic design, but it clearly fails to account for any spreading of yielding. The theory outlined above is precisely the theory used in the Bending Model, except that the Bending

Model is not truly elasto-plastic, and consequently it should also predict this type of behavior. Figure 4-5 shows that this is in fact the case, the small residual stiffness after yielding, and the size of the load increment, cause the failure load to be 340^k instead of 330^k , but the behavior conforms very closely with the plastic theory and the formation of the three hinges is very clear. The Interaction Model, shown in Figure 4-6, behaves in a similar fashion, but because of the moment multiplier of .847 used in the AISC interaction formula, the hinges form at higher loads.

The behavior of the Complex and Latona Models is quite different, however. As can be seen from Figures 4-7 and 4-8, the first hinge forms at 255 kips, about where plastic theory indicates it should, the second hinge starts forming at 330^k , and after that the behavior becomes more complicated. The explanation for this can be found in the phenomenon of spreading of yielding. Instead of a hinge forming at once, it forms progressively, the outer fibers yielding first and then the inner fibers, until the entire section is plastic. Because of this, the second hinge forms in two separate steps, with the outer fibers yielding first and then the middle fibers yielding. In Figure 4-9, the load increment has been reduced to 2.5 kips, and the precise spreading of yielding is shown in Figure 4-10. With this smaller load increment, it becomes clear that the hinges all form progressively, and that the contribution of the inner web fiber is relatively

400

300

200

100

Kips

Figure 4-5. Graph of H vs V

Bending Model

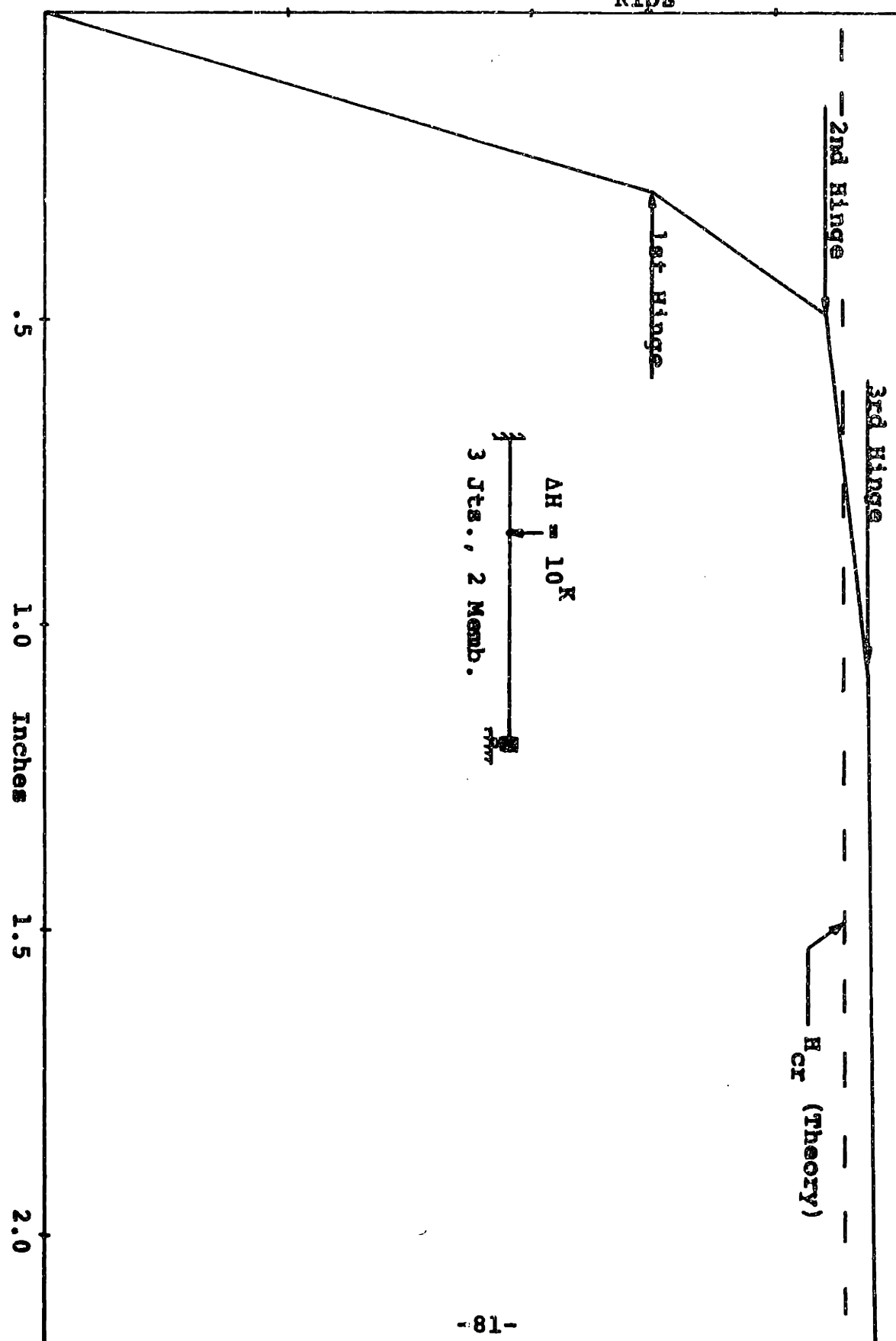
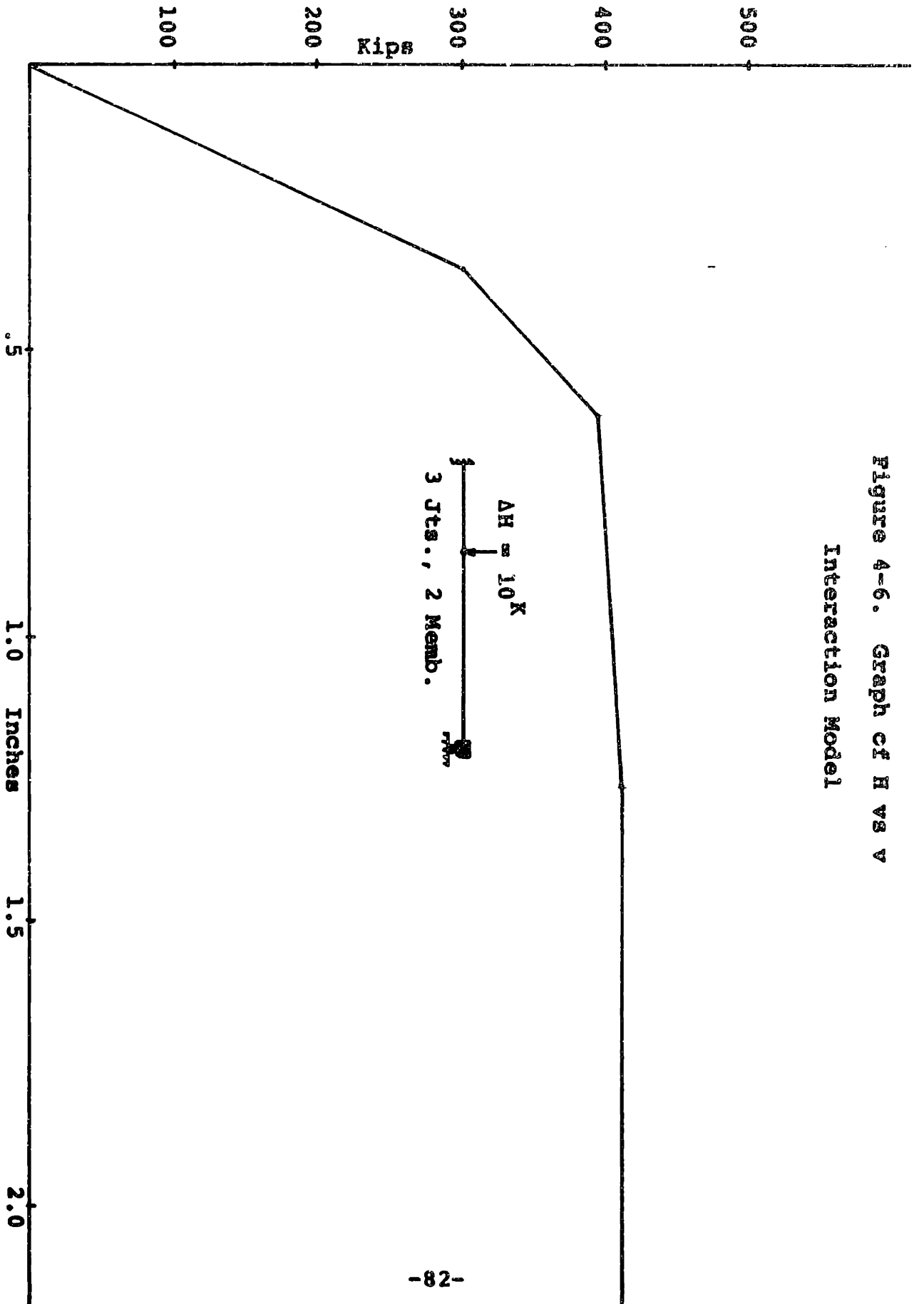


Figure 4-6. Graph of H vs V
Interaction Model



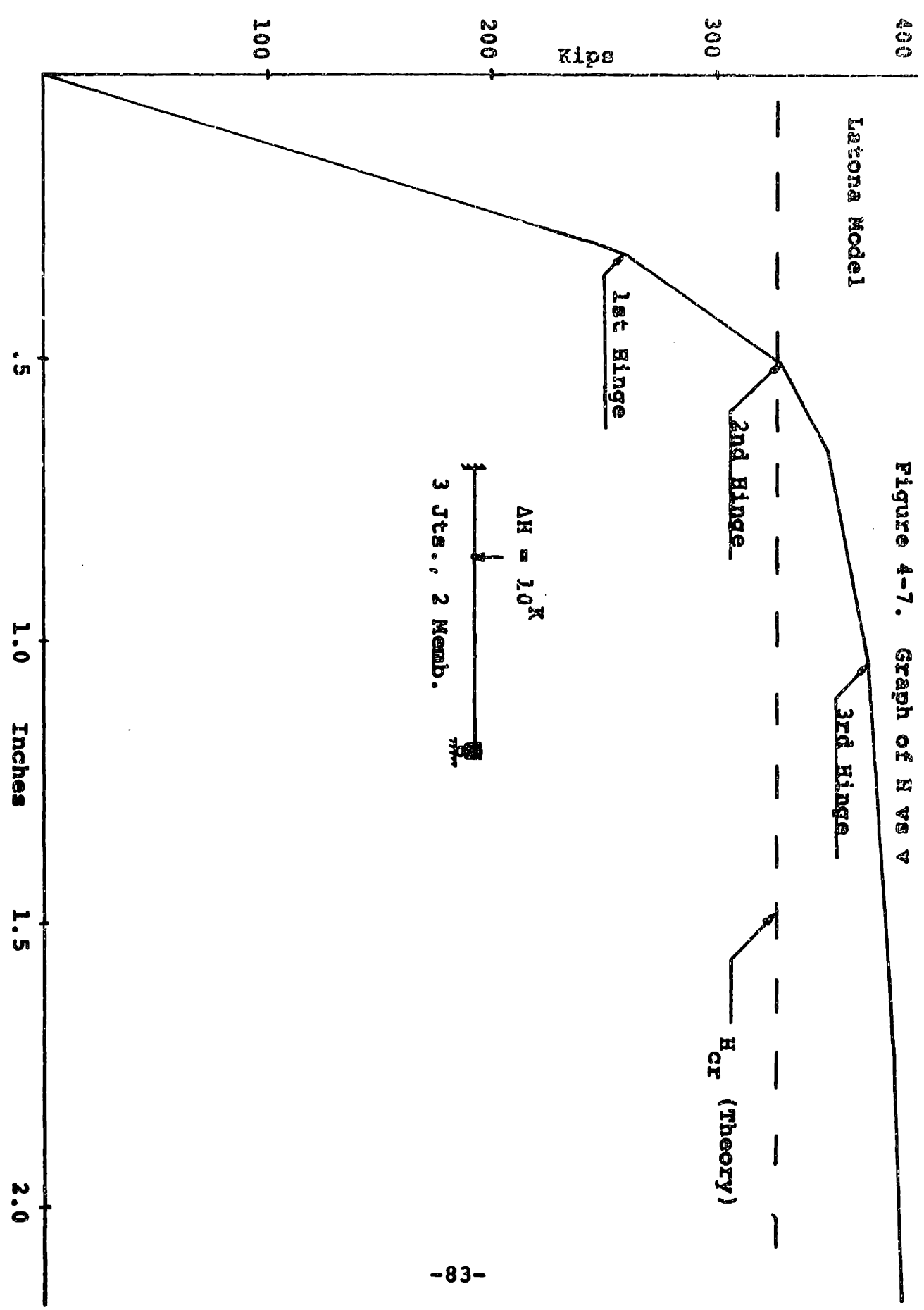


Figure 4-7. Graph of H vs V

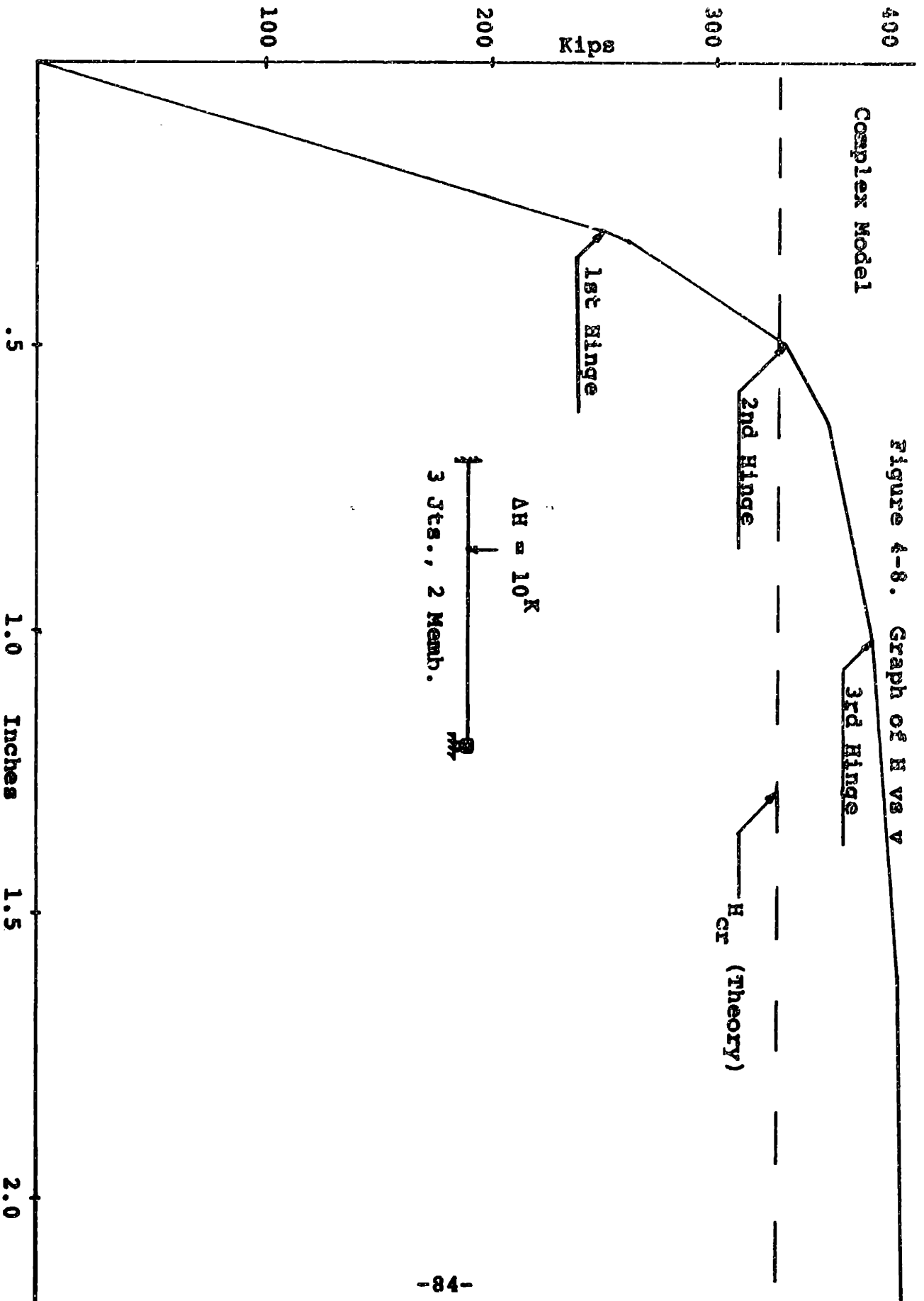


Figure 4-9. Graph of H vs V
Complex Model

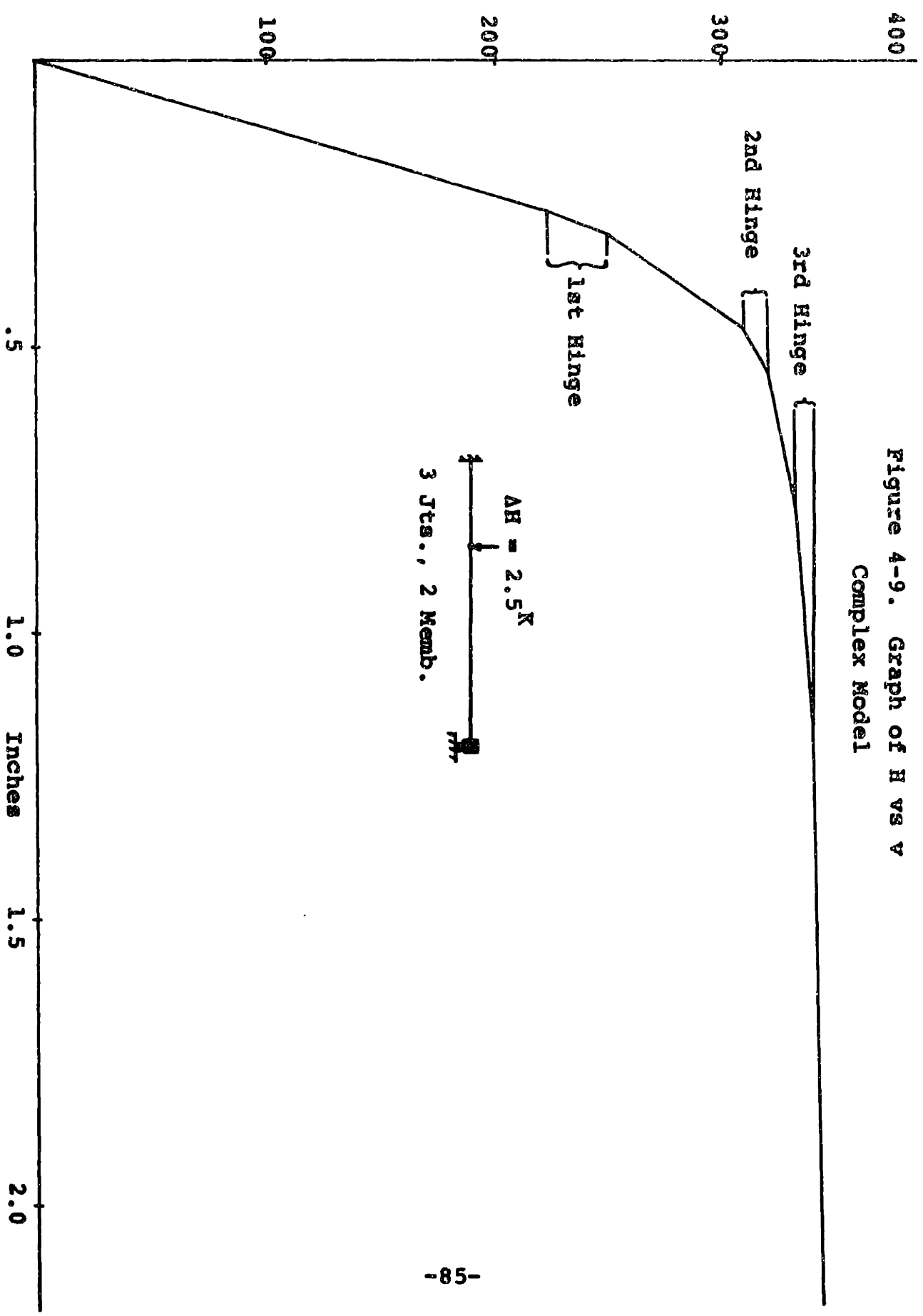
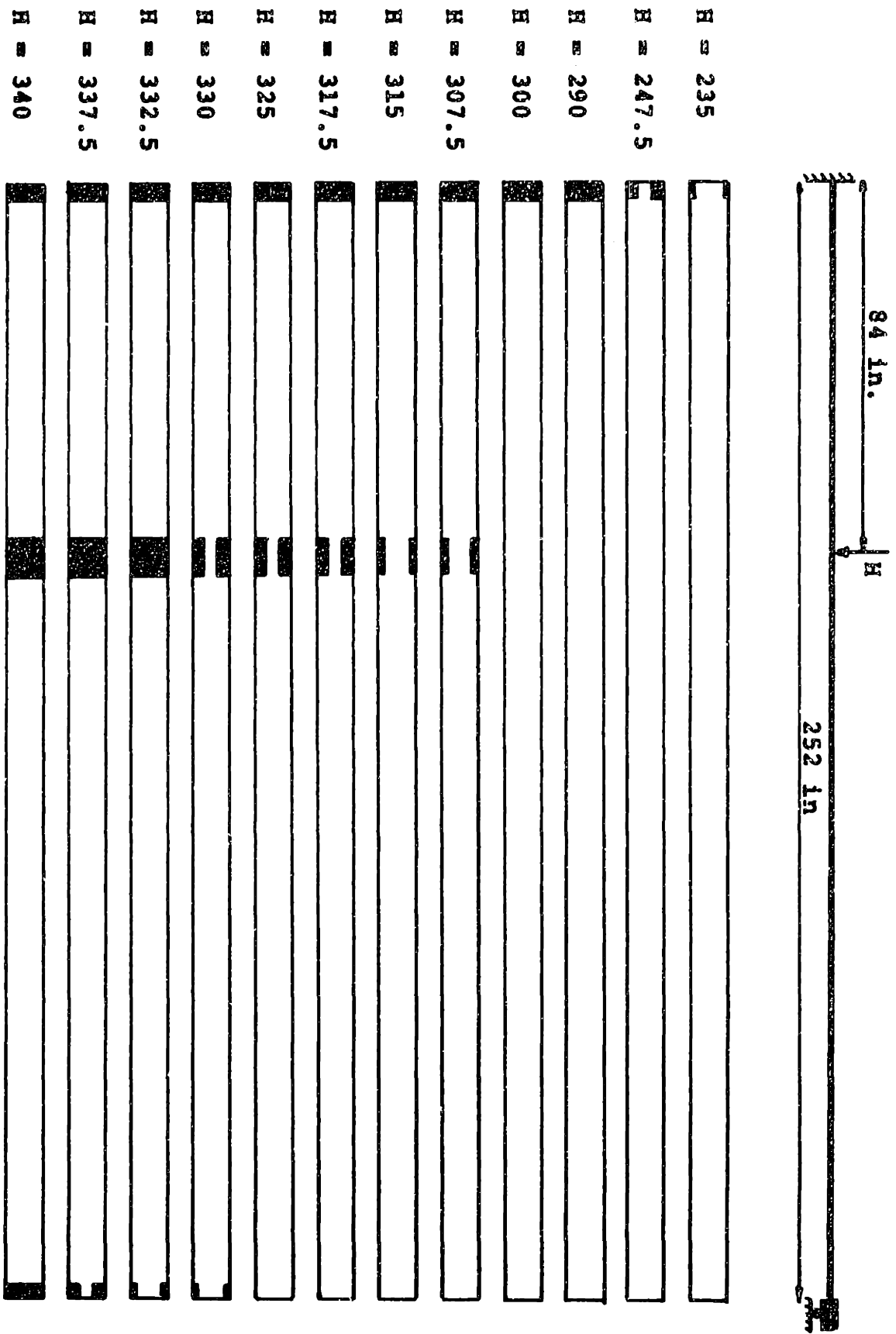


Figure 4-10. Spreading of Yielding for Beam of Figure 4-9



small. A comparison of Figures 4-9 and 4-10 shows that once the outer two fibers have yielded, the member behaves as if the entire section were plastic. Thus the formation of a hinge appears as two changes in stiffness, the first change occurring when the flange fibers yield, and the second change occurring when the outer web fibers yield. If the structure that remains, after the formation of a hinge, is sufficiently stiff, this double change of stiffness may not be very obvious. In Figure 4-9, the change in stiffness as the first hinge starts to form is much smaller than the change in stiffness as the second hinge starts, because the remaining structure is much stiffer in the case of the first hinge.

Since the size of the load increment influences the way the stresses change, it is clear that the spreading of yielding will be less accurately represented when a larger load increment is used. This is why the transition phase for the first hinge is much less clear in Figures 4-7 and 4-8. The change in stresses is so large, that both the flange fiber and the outer web fiber fail at the same increment, whereas this does not occur when the load increment is smaller. The table on the next page shows how the loads at which each hinge starts to form vary as the load increment is decreased; the failure load is defined as the load at which all sections have become plastic.

Table 4-1

**Relationship Between Load Increment and Hinge Formation
in Complex Model**

Size of Load Increment	H at Start of 1st Hinge	H at Start of 2nd Hinge	H at Start of 3rd Hinge	H at Failure
10.0	240.0	320.0	360.0	370.0
5.0	235.0	310.0	340.0	350.0
2.5	235.0	307.5	330.0	340.0
Extrapolated	230.0	300.0	320	330

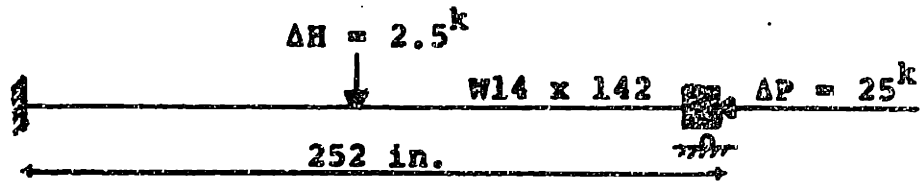
It is interesting that the reduction in H for a reduction in increment size is linear for the third hinge and the failure load, but not for the first two hinges. This is probably due to the fact that yielding is essentially complete at this point, and hence the precise order in which the fibers yielded ceases to be important. The table clearly shows that a reduction in increment size causes a reduction in failure load, although the phenomenon of spreading of yielding is important for all increment sizes.

Thus the major inelastic difference between the Bending and Interaction Models, and the Latona and Complex Models is in the way the formation of a plastic hinge is handled. In a case where one hinge will cause failure, or several hinges form at the same time causing failure, this difference is relatively unimportant. Even in a case where several plastic

hinges must form progressively in order to form a mechanism, this difference is small, and only causes small discrepancies between the predictions of the models. In all cases, the size of the load increment is important, and a reduction in load increment may greatly reduce the predicted failure load of the member, especially in the Latona and Complex Models.

4.2 Inelastic Behavior - With Axial Load

The addition of axial load greatly complicates the problem of inelastic behavior. For any significant axial load, the Bending Model becomes totally inadequate, since it makes no provision for the added stress due to the axial load. Because of this, the Bending Model will not be discussed in this section. The other three models should give reasonable results for this type of loading situation, although the two modified non-linear models will be limited by the fact that only two segments are used in the member. The first two examples used in this section illustrate opposite extremes. The first is a relatively stiff beam column where the P-Delta effect and the effect of change in geometry are relatively unimportant; the second is a very slender column where these two effects are quite important. The loading conditions for the first example are shown on the next page and the results for each model are shown in Figures 4-11 through 4-13; in the Latona and Complex Models the spreading of yielding is also shown (Figures 4-12 and 4-13).



Since the three plastic hinges necessary to form a mechanism all form simultaneously, the Interaction Model remains elastic until the criteria for yielding are met, and then fails at an axial load of 1050 kips. In the Latona and Complex Models, the failure is more gradual due to the phenomenon of spreading of yielding. Figures 4-12 and 4-13 show that the results given by the two models are practically identical for this example. The Complex Model gives a slightly higher failure load than the Latona Model, and there are slight differences in the yielding patterns, but for practical purposes, the models give the same results. In this example, the P-Delta effect and the effect of change in geometry are far less important than the effect of yielding, and don't significantly affect the behavior of the member. As a result, the inability of the Latona Model to represent these effects as accurately as the Complex Model is not important. The yielding mechanism is very important, however, as the presence of an axial load causes yielding to spread from section to section as well as from fiber to fiber. This spreading of yielding greatly decreases the stiffness of the member and causes the deflection to increase very rapidly once yielding starts.

Figure 4-11: Graph of P vs v
Interaction Model

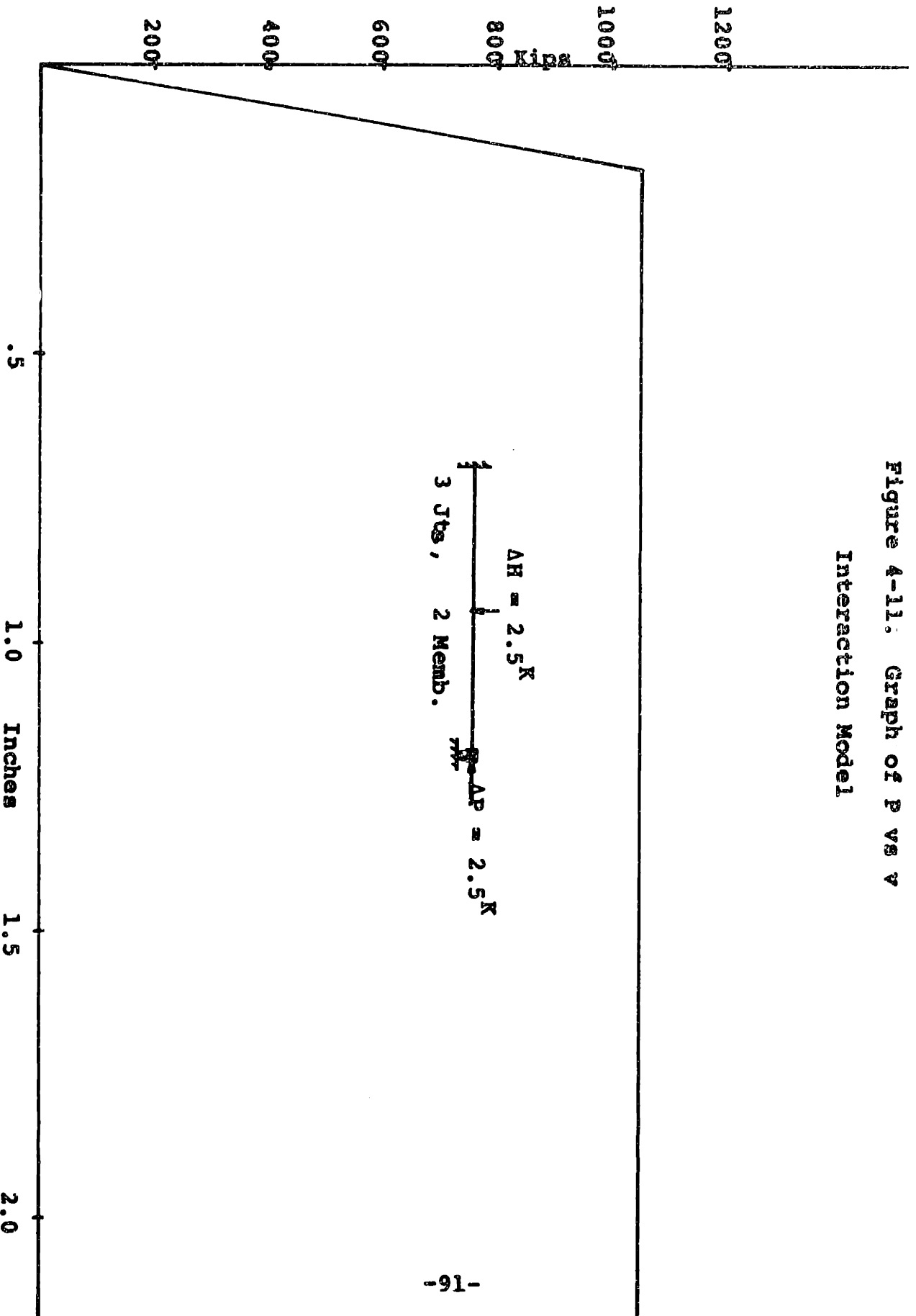
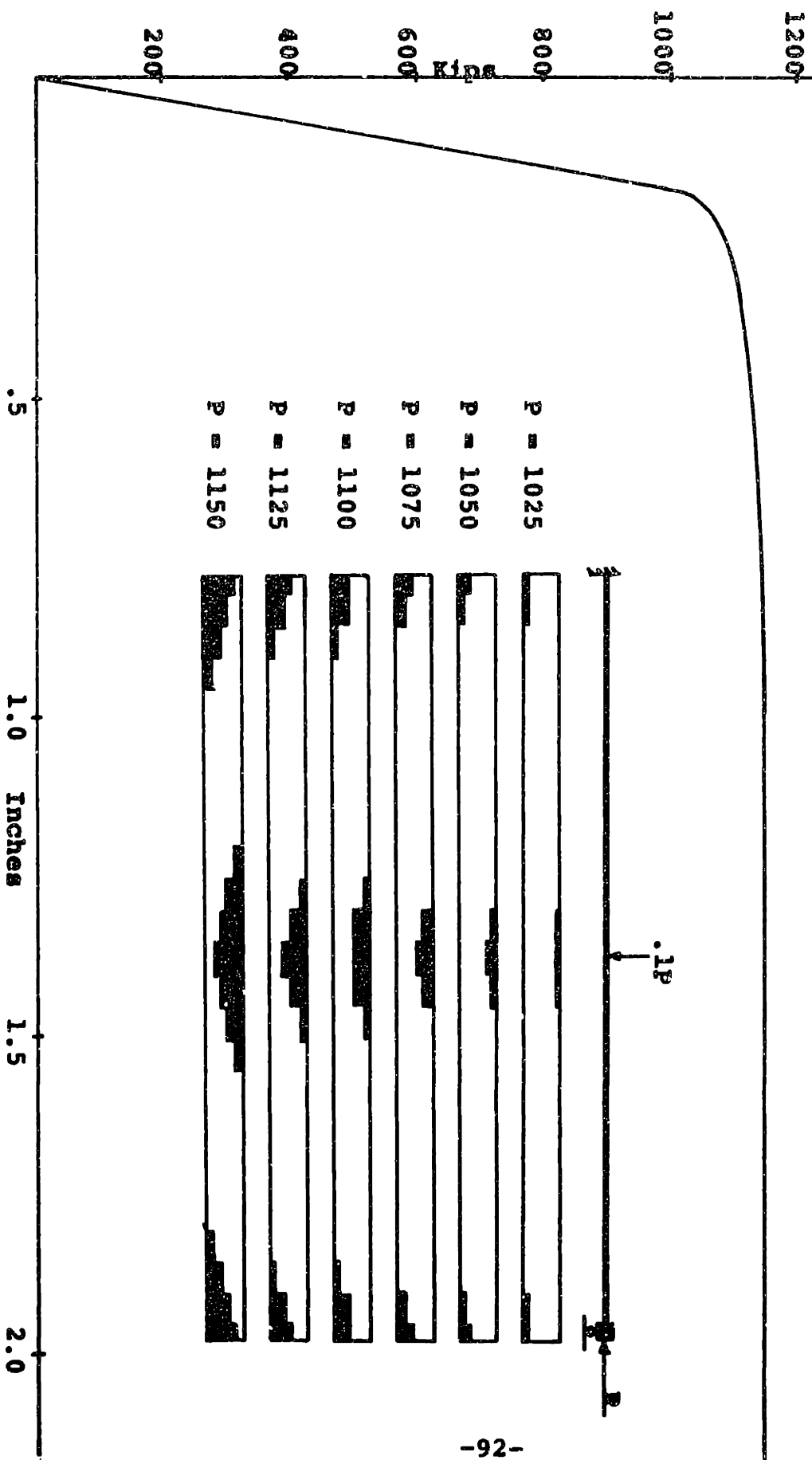
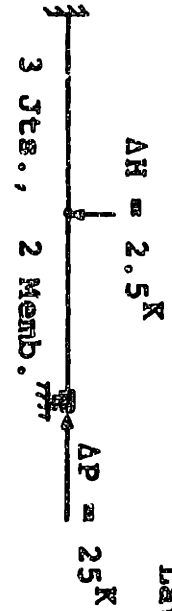
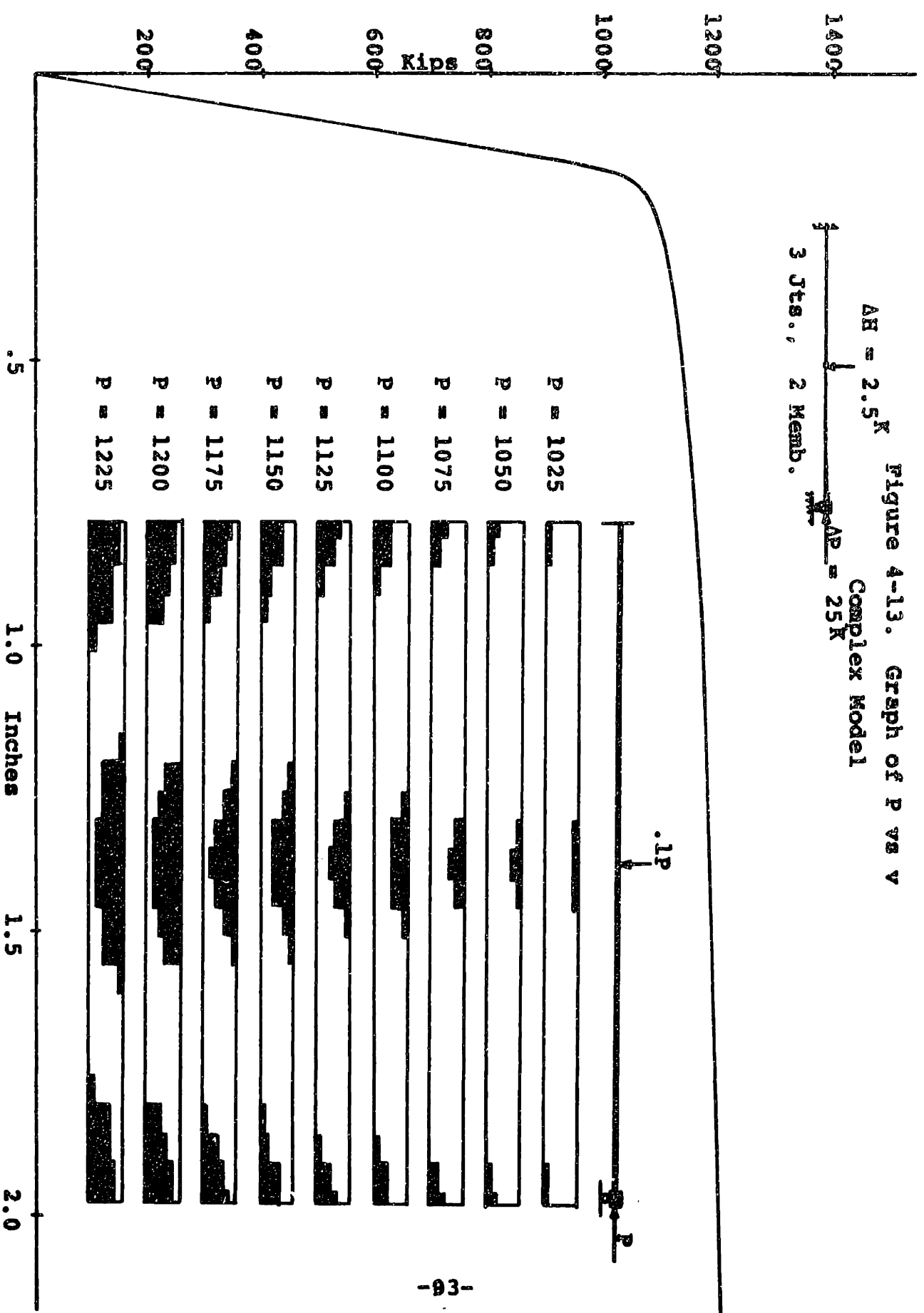


Figure A-12. Graph of P vs v

Latona Model

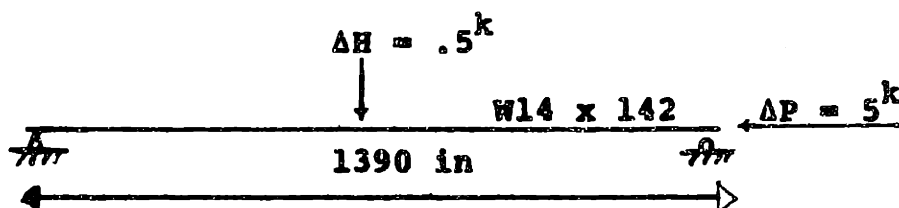


$\Delta H = 2.5K$ Figure 4-13. Graph of P vs v
 Complex Model
 3 Jts., 2 Memb. $\Delta P = 25K$



Thus the presence of an axial load makes the failure mechanism considerably more complicated, since yielding is not confined to a small area, but may well spread throughout the member. This type of behavior cannot be accounted for in the Interaction Model, but can be represented by the Latona Model and the Complex Model, and both models give essentially similar results for this case.

In the second beam column example, all the non-linear effects become important, since the member is extremely slender, and is pin ended as well. The loading conditions for this case are shown below, and the results for the three models are shown in Figures 4-14 through 4-16.



Once again the Interaction Model predicts an abrupt failure, since one mechanism is sufficient to cause collapse. The other two models predict a more gradual failure, but this time their predictions vary slightly. Unlike the first example, the Interaction Model gives a higher failure load than the Latona and Complex Models, and the Complex Model is somewhat softer than the modified linear models. Because the beam column is subdivided into only two members, the modified linear models cannot reproduce the P-Delta effect and the change in geometry as accurately as the Complex Model. By the

Figure 4-14. Graph of P vs V
Interaction Model

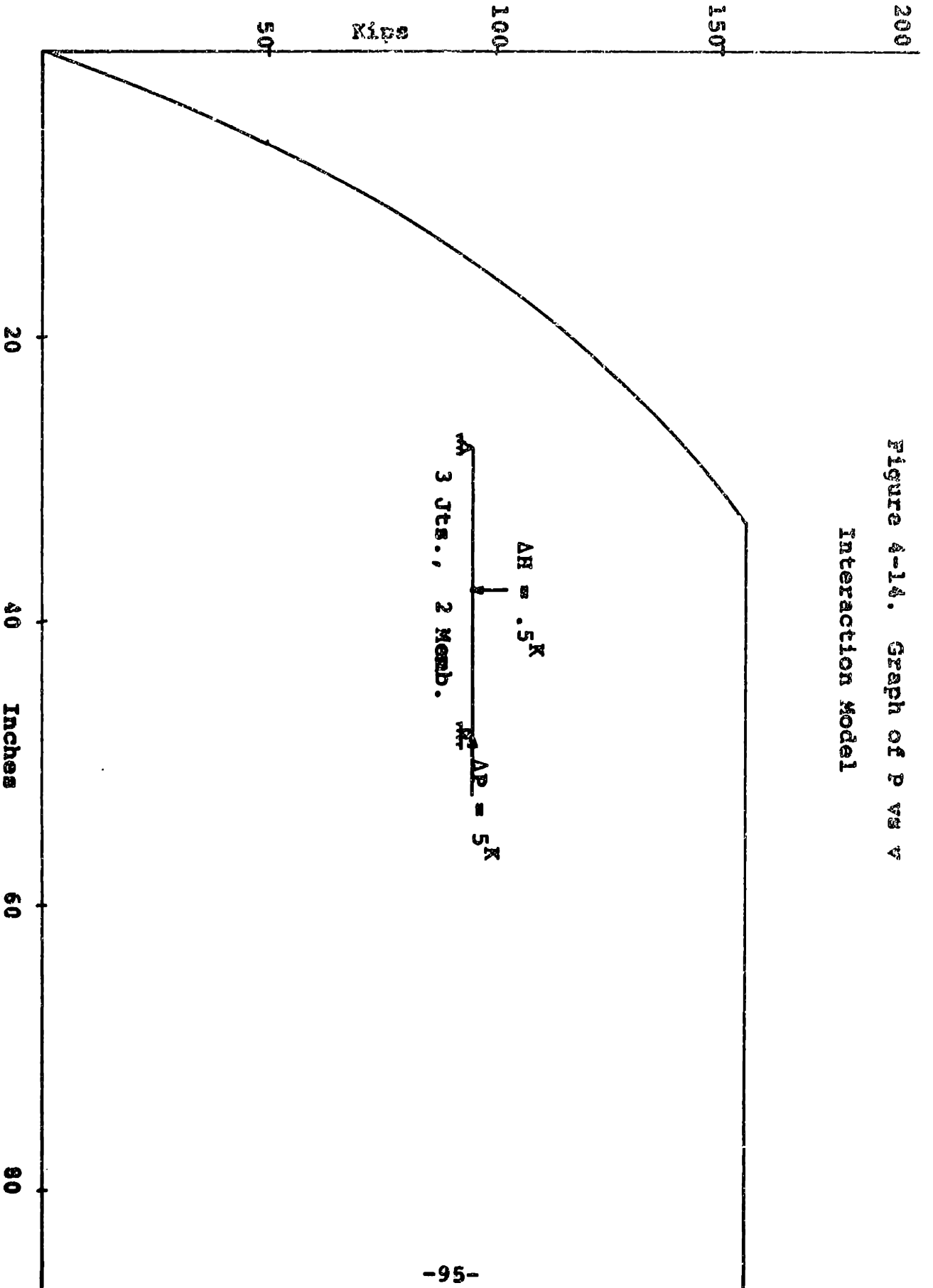
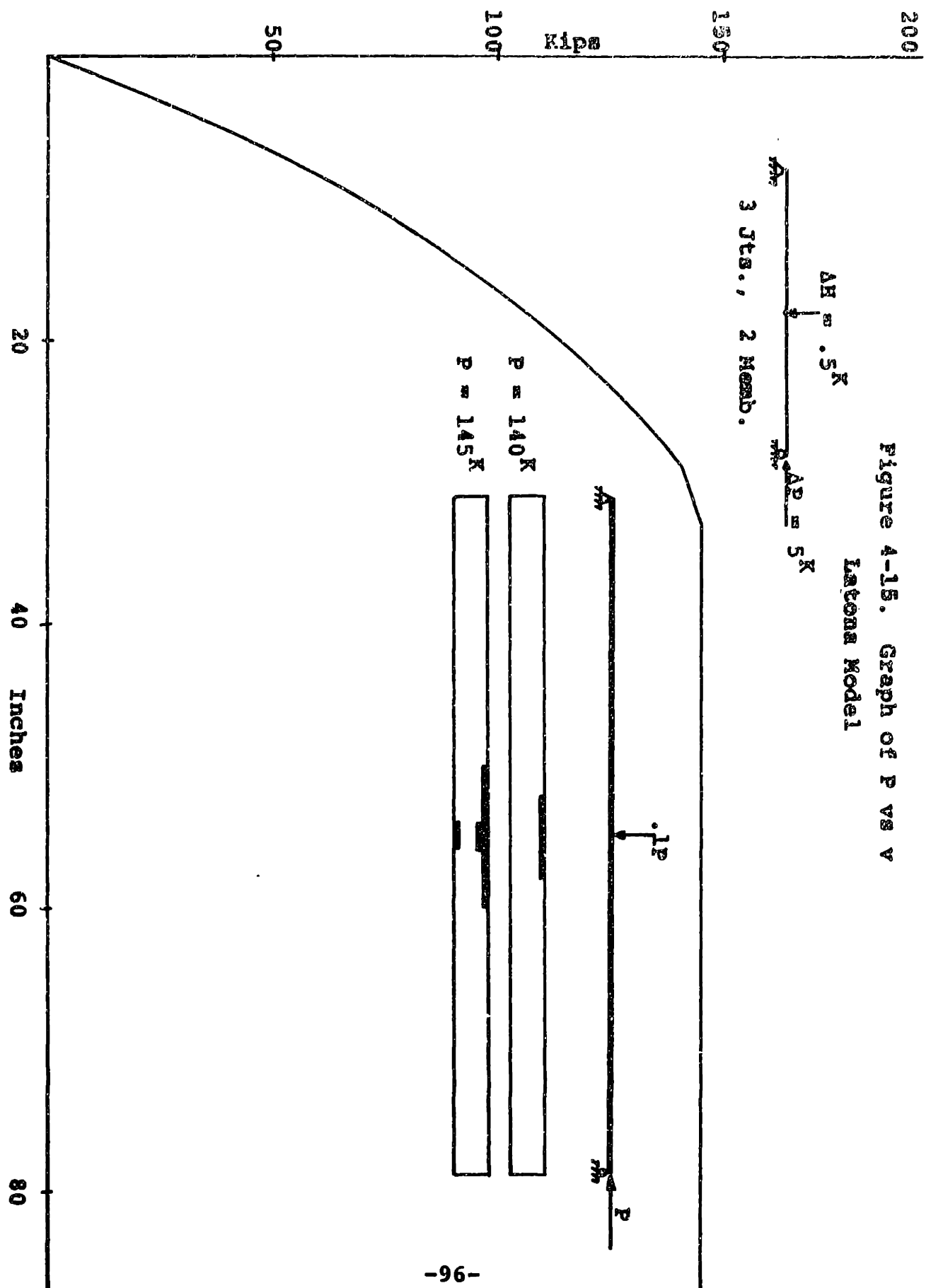
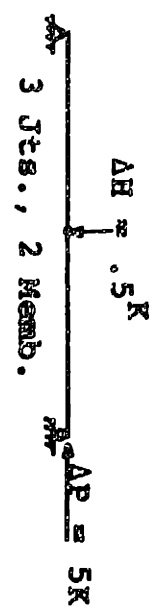


Figure 4-15. Graph of P vs V
Latona Model



200

Figure 4-16. Graph of P vs V
Complex Model



150

Kips

100

50

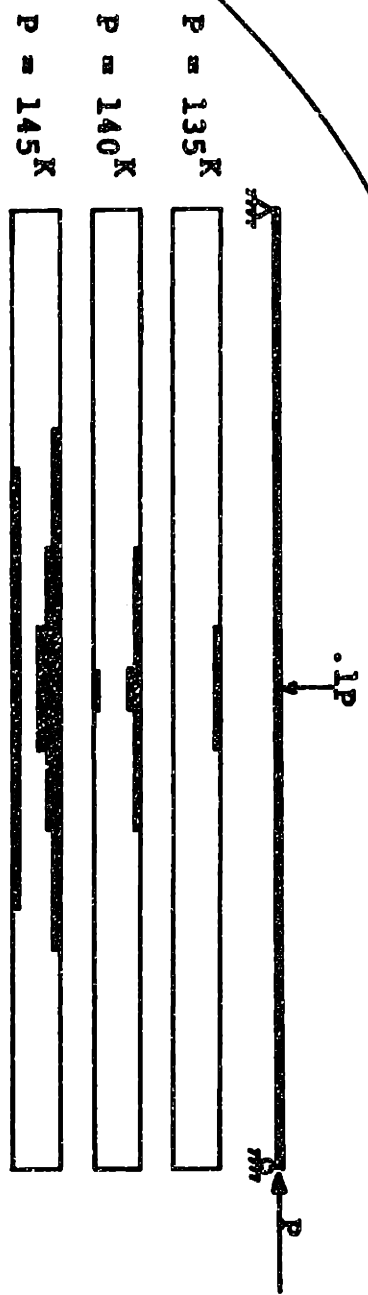
20

40

Inches

60

80



time yielding occurs in this example, the amplification factor is greater than two and the error caused by using a modified linear model with only two segments becomes significant. The differences in the spreading of yielding between the Complex Model and the Latona Model reflect this error. In the Complex Model, yielding starts one load increment earlier than in the Latona Model and spreads slightly more rapidly from section to section. This means that the beam column in the Latona Model is stiffer, just before failure, than its counterpart in the Complex Model, a result that might be important if it were part of a structure rather than just an individual member. It is interesting to note that this variation in stiffness does not significantly affect the failure load, and that both models predict failure at a load of 145 kips, 10 kips below the failure load predicted by the Interaction Model.

In the third example, a prescribed displacement is applied to a column with a constant axial load. Two conditions are examined, one where the strain hardening of the member is .1%, and one where the strain hardening is 3%. For the purposes of this thesis, % strain hardening will be defined as the ratio of the tangent stiffness after yielding to the tangent stiffness before yielding. The loading conditions for these cases are shown on the next page, and the results are shown in Figures 4-17 through 4-22 for each of the three models.

150

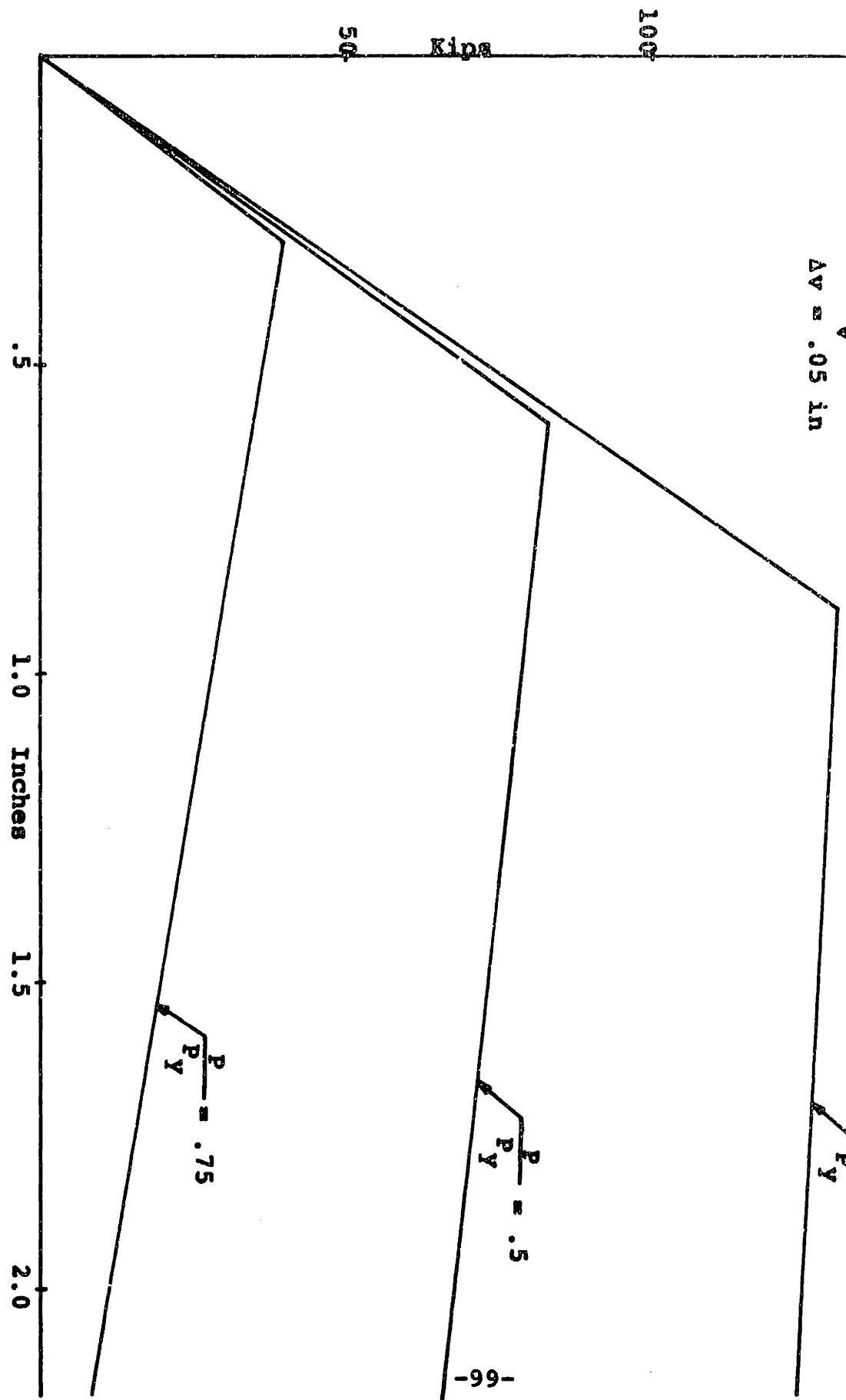
3 Jts., 2 Memb.

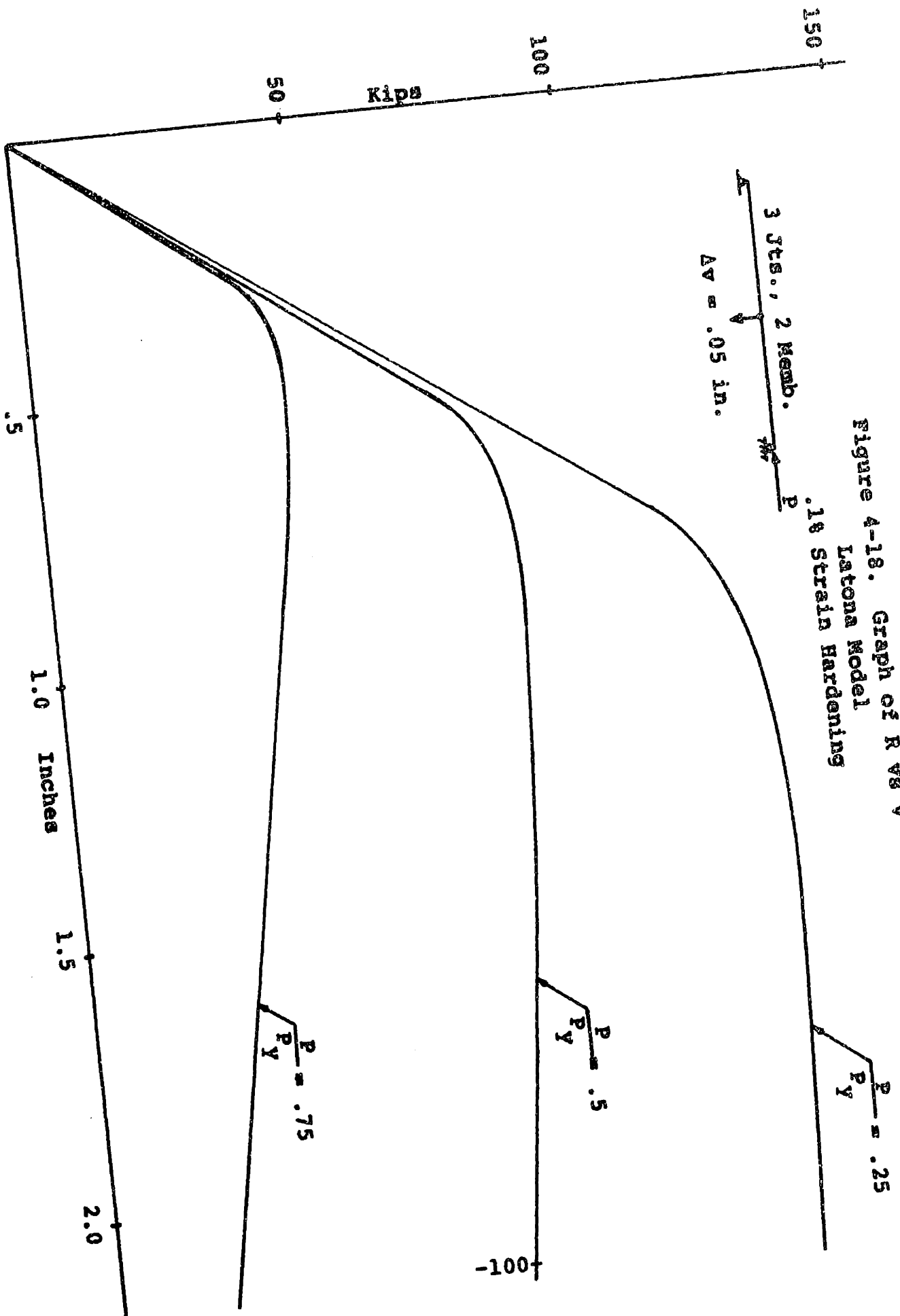
$\Delta v = .05$ in

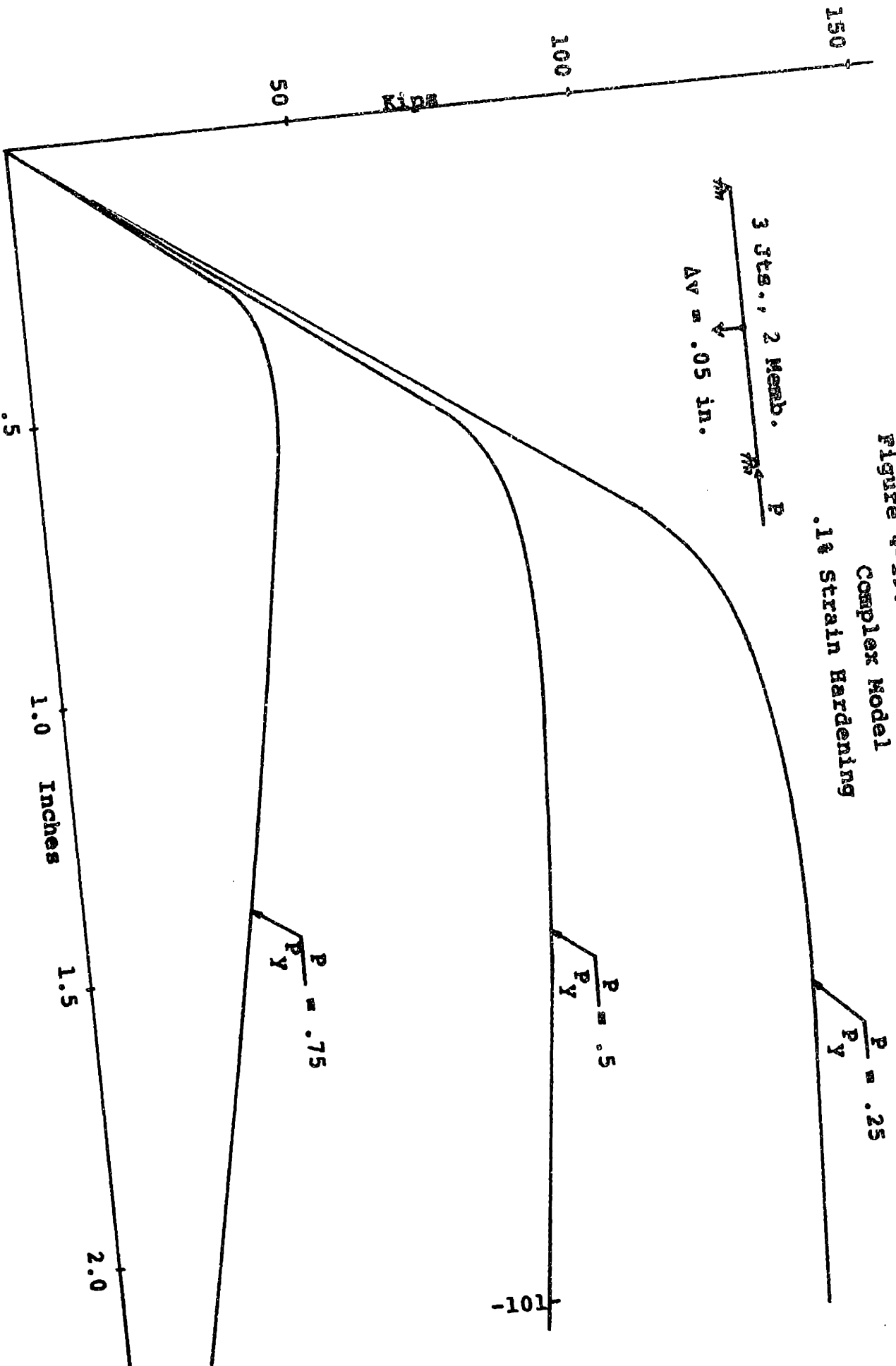


Figure 4-17. Graph of R vs v

Interaction Model
.14 Strain Hardening







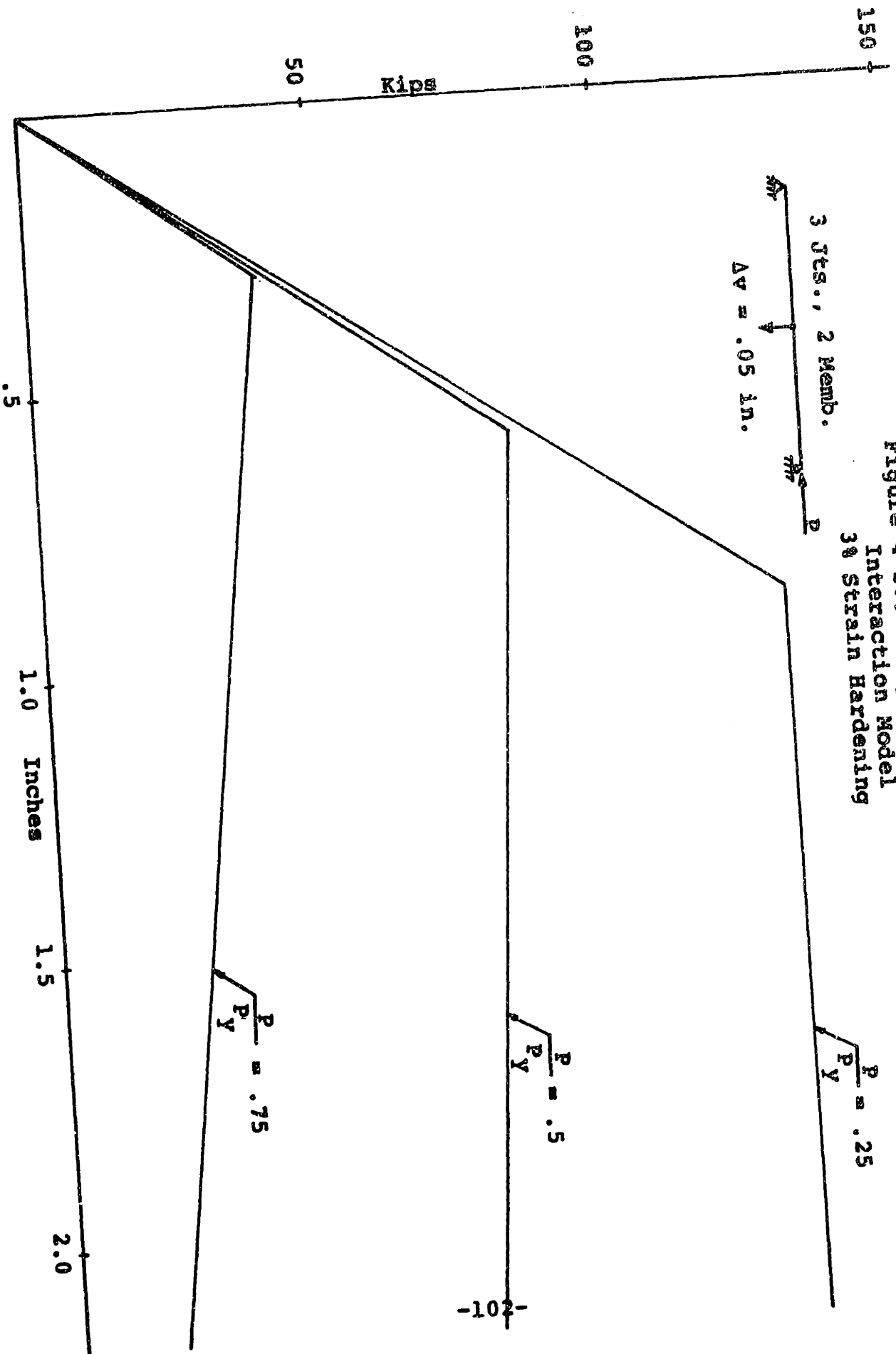
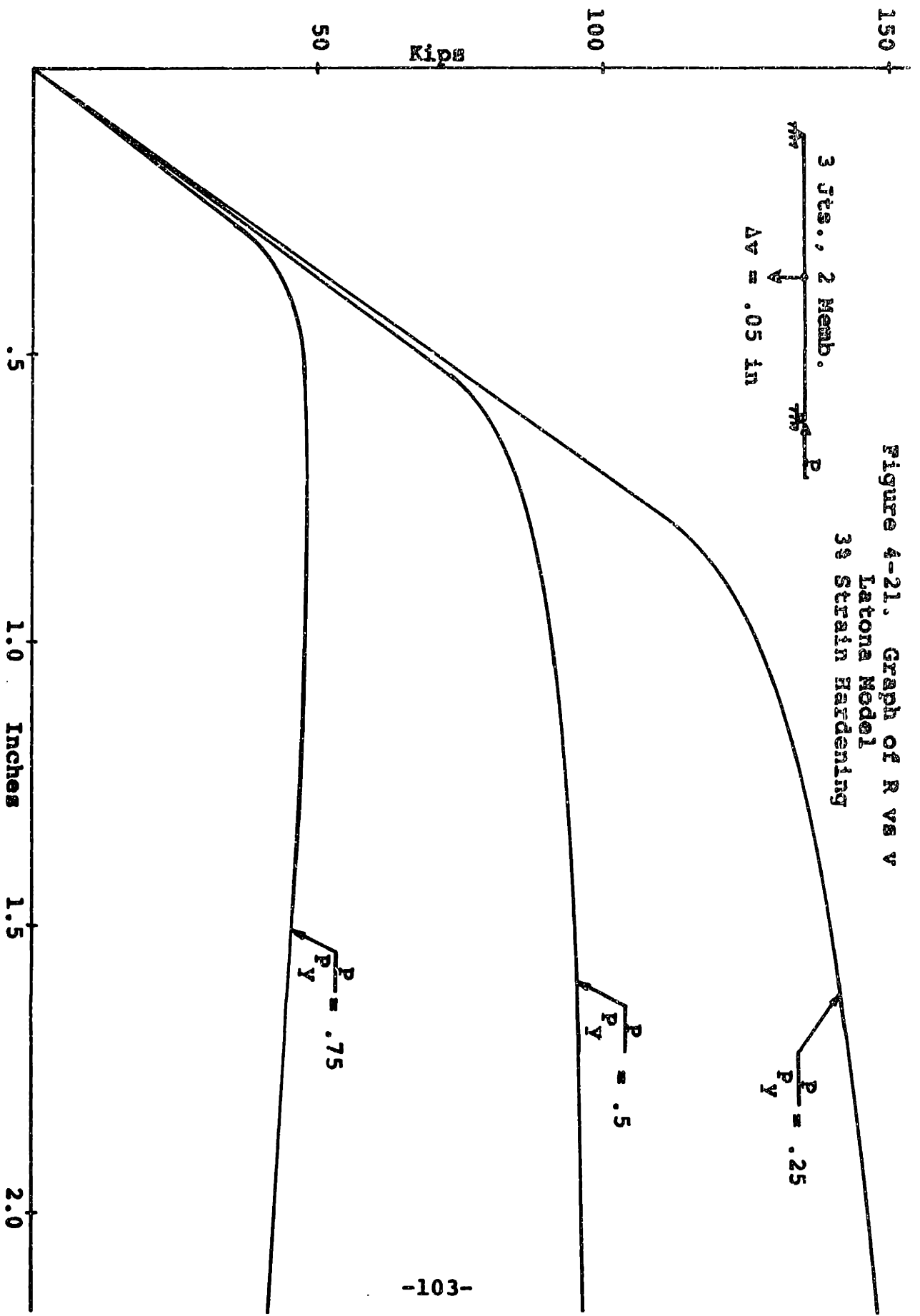


Figure 4-20. Graph of R vs V
 Interaction Model
 38 Strain Hardening



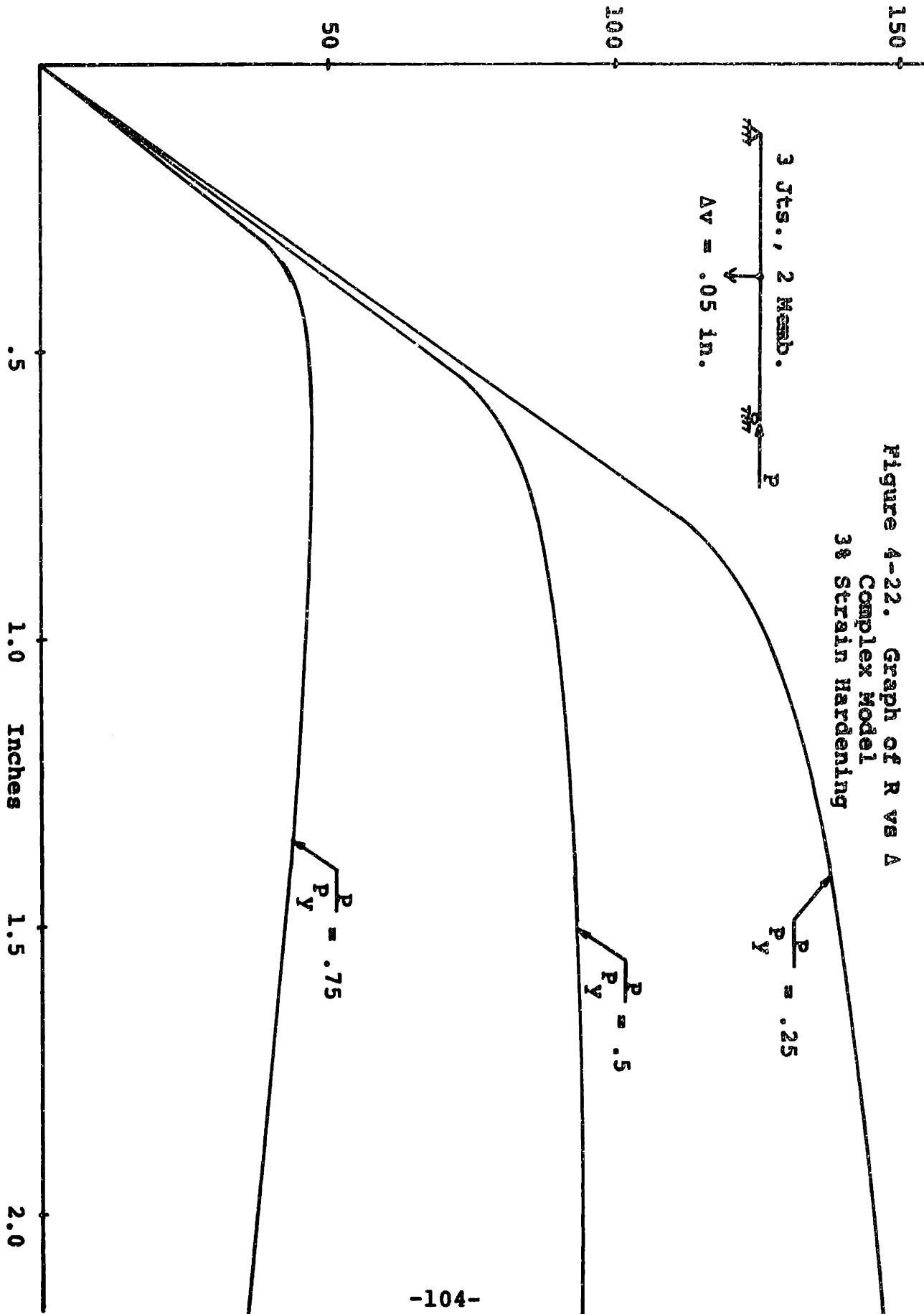
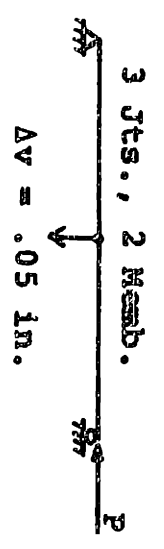
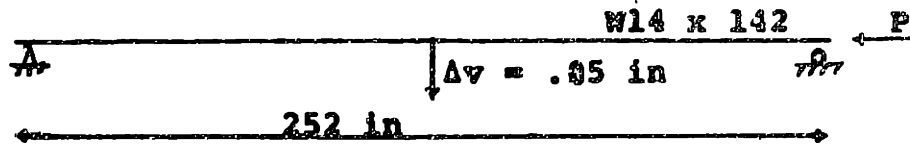
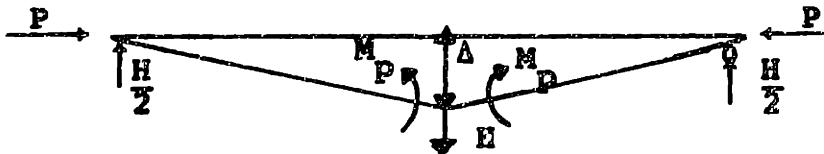


Figure 4-22. Graph of R vs Δ
 Complex Model
 3 ϕ Strain Hardening





The graphs clearly show that the slope of the curve after failure is a function of both the strain hardening and the axial load. The nature of this relationship can be better understood by examining the diagram below.



In order to satisfy equilibrium the following relationship must hold.

$$P\Delta + \frac{HL}{4} = M_P$$

This means that the relationship between H and Δ can be expressed as

$$H = \frac{4M_P}{L} - \frac{4P\Delta}{L} + \alpha \frac{48EI\Delta}{L^3}$$

where α is the percent strain hardening. Differentiating H with respect to Δ gives

$$\frac{dH}{d\Delta} = \frac{4}{L} \left(\frac{12EI\alpha}{L^2} - P \right)$$

and it can be seen that the slope after failure is a function

of both P and α . This approximation agrees very closely with the results given by the Interaction Model, while the Latona and Complex Models predict higher slopes and non-linear behavior after yielding, especially in the case of 3% strain hardening. Since the complicated models are much more sensitive to the size of the displacement increment than the Interaction Model, some of this discrepancy may be due to the size of the load increment, but in all models, the slope after yielding is clearly a function of both the axial load and the percent strain hardening.

4.3 Summary

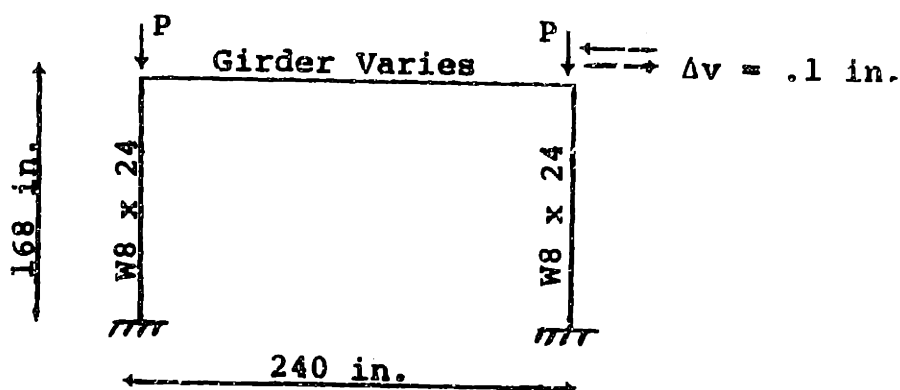
Thus the ability of each of the models to accurately represent the behavior of a member is dependent on the increment size and the type of loading for that particular member. When an axial load is present, yielding spreads along the member as well as through it, and the concept of a plastic hinge forming at a set location may not be valid. Of the three non-linear effects, the spreading of yielding is the most important, and in most practical cases, a modified linear model with two segments can represent the other effects sufficiently accurately. The other two effects can be important, however, and in the case of slender members or materials with a higher yield point, may well become significant.

5.0 FRAME STUDY - INELASTIC

In this chapter several single bay single story frames are examined in an attempt to investigate the importance of such parameters as axial load, ratio of beam plastic moment to column plastic moment, ratio of girder stiffness to column stiffness, and the percent of strain hardening. In all cases, an axial load is first applied to the frame which is then cycled through a series of displacement reversals by prescribing displacements. In the simple models, the values of the plastic moment are suitably modified, the column moment being reduced to account for the axial load in the Bending Model, and the girder moment being reduced to account for the multiplier of .847 in the Interaction Model. The chapter is divided into two basic sections. The first is a parametric study involving three different types of frames and two different ratios of column axial load to column yield load. The frames consist of a frame where the girder is stiffer and stronger than the column, a frame where the girder is weaker and more flexible than the column, and a frame where the girder is stiffer, but weaker, than the column. In the second section, the effects of load increment and percent strain hardening are examined for the single bay single story frame in Latona's thesis, since this frame exhibited significant differences between the complicated and simple models in that thesis.

5.1 Parametric Study

The frames used in the parametric study have the members and dimensions shown below. In all cases, the columns are W8 x 24, and the girders are varied to make the stiffness and strength ratios work out. The percent strain hardening is always .1%, and the loading is a prescribed displacement increment of .1 inches as shown below.



The results for the first case, where the girder is stronger and stiffer than the column, are shown in Figures 5-1 through 5-8. Figures 5-1 through 5-4 show the results for the four models when the ratio of axial load to yield load $\left(\frac{P}{P_Y}\right)$ is .2, Figures 5-5 through 5-8 show the results when $\frac{P}{P_Y}$ is .4. As was shown in Chapter 4, the slope of the R-Δ curve after a mechanism has developed, is dependent on both P and the strain hardening percentage α. In the case of a single story single bay frame this relationship is

$$\frac{dH}{d\Delta} = \frac{2}{h} \left(\left[\frac{12EI}{h^2} \frac{(1+6\gamma)}{(4+6\gamma)} \right] \alpha - P \right), \quad \gamma = \frac{I_g h}{I_c L}$$

Since α is .001, the slope after a mechanism has formed should

Figure 5-1. Graph of R vs Δ

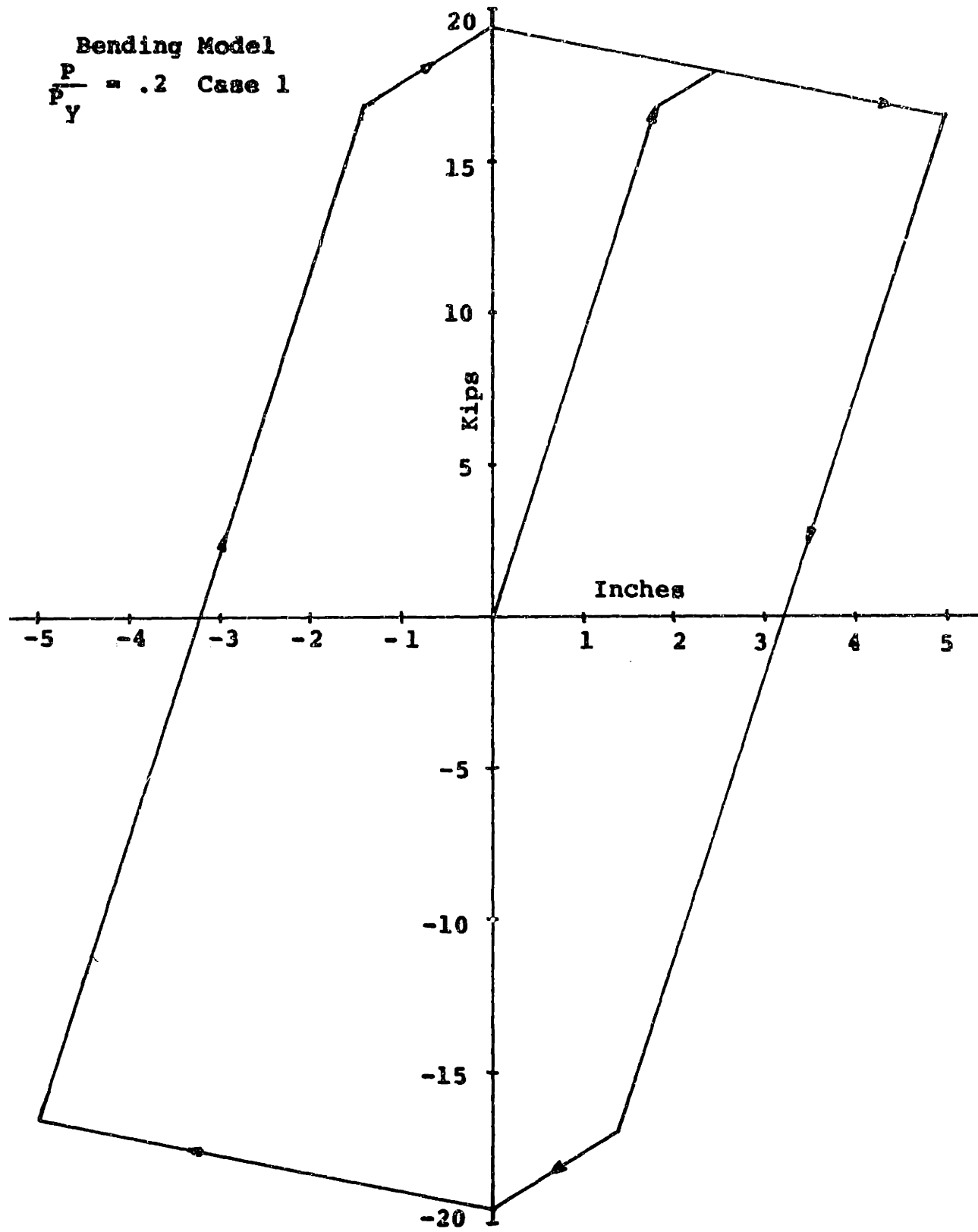


Figure 5-2. Graph of R vs Δ

Interaction Model

$$\frac{P}{P_y} = .2 \text{ Case 1}$$

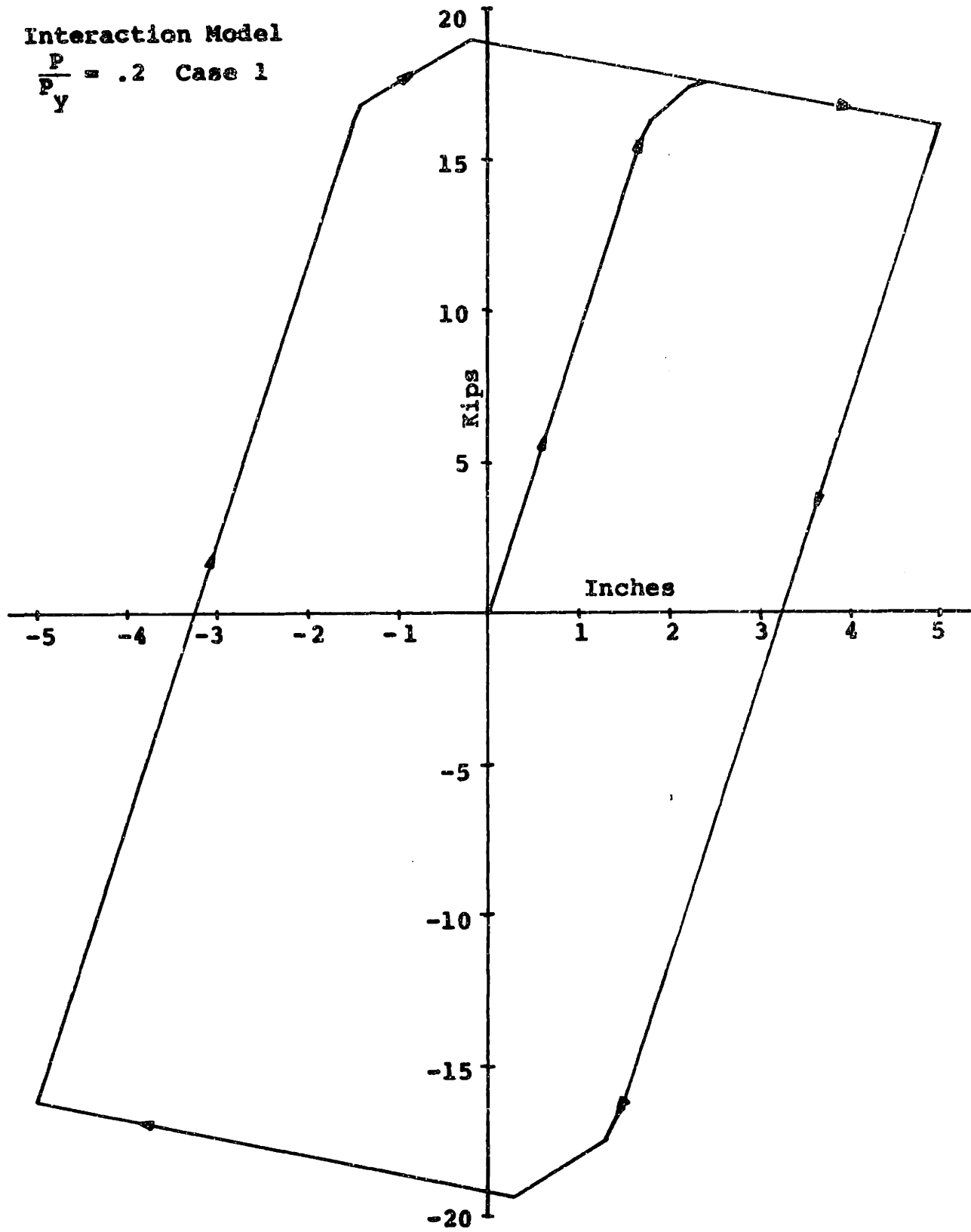


Figure 5-3. Graph of R vs A

Latona Model
 $\frac{P}{Y} = .2$ Case 1

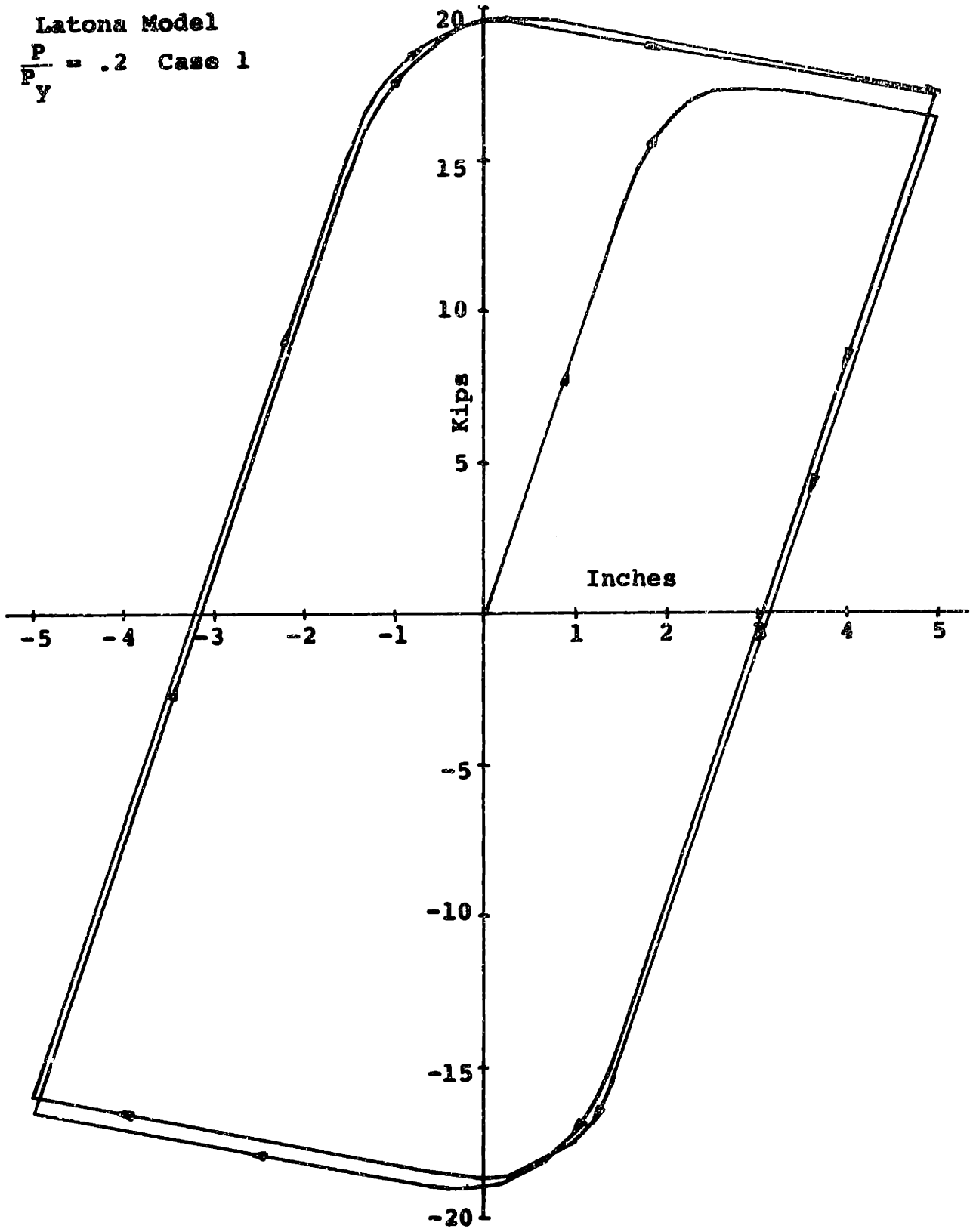


Figure 5-4. Graph of R vs Δ

Complex Model
 $\frac{P}{y} = .2$ Case 1

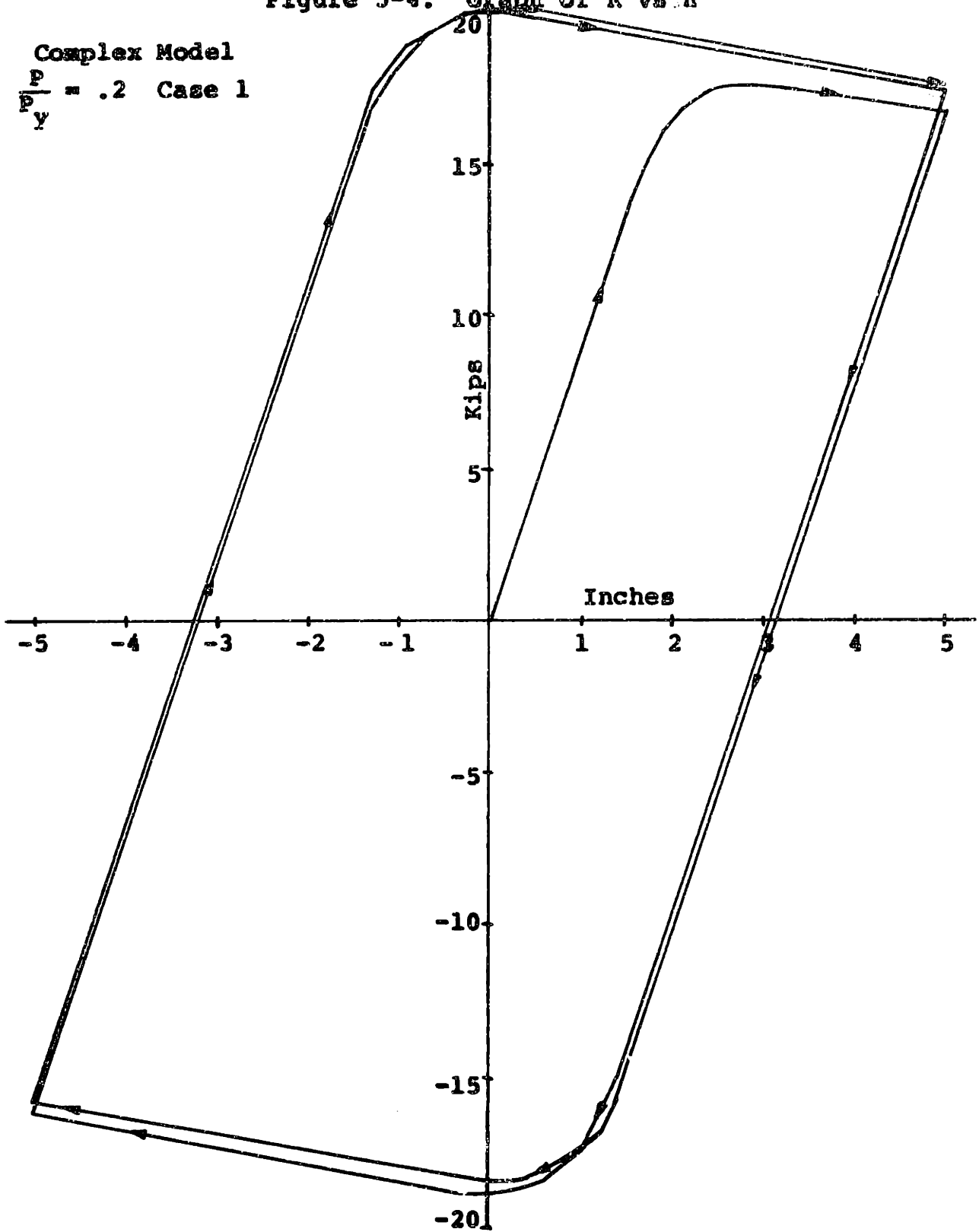


Figure 5-5. Graph of R vs Δ

Bending Mode.
 $\frac{P}{P_y} = .4$ Case 1

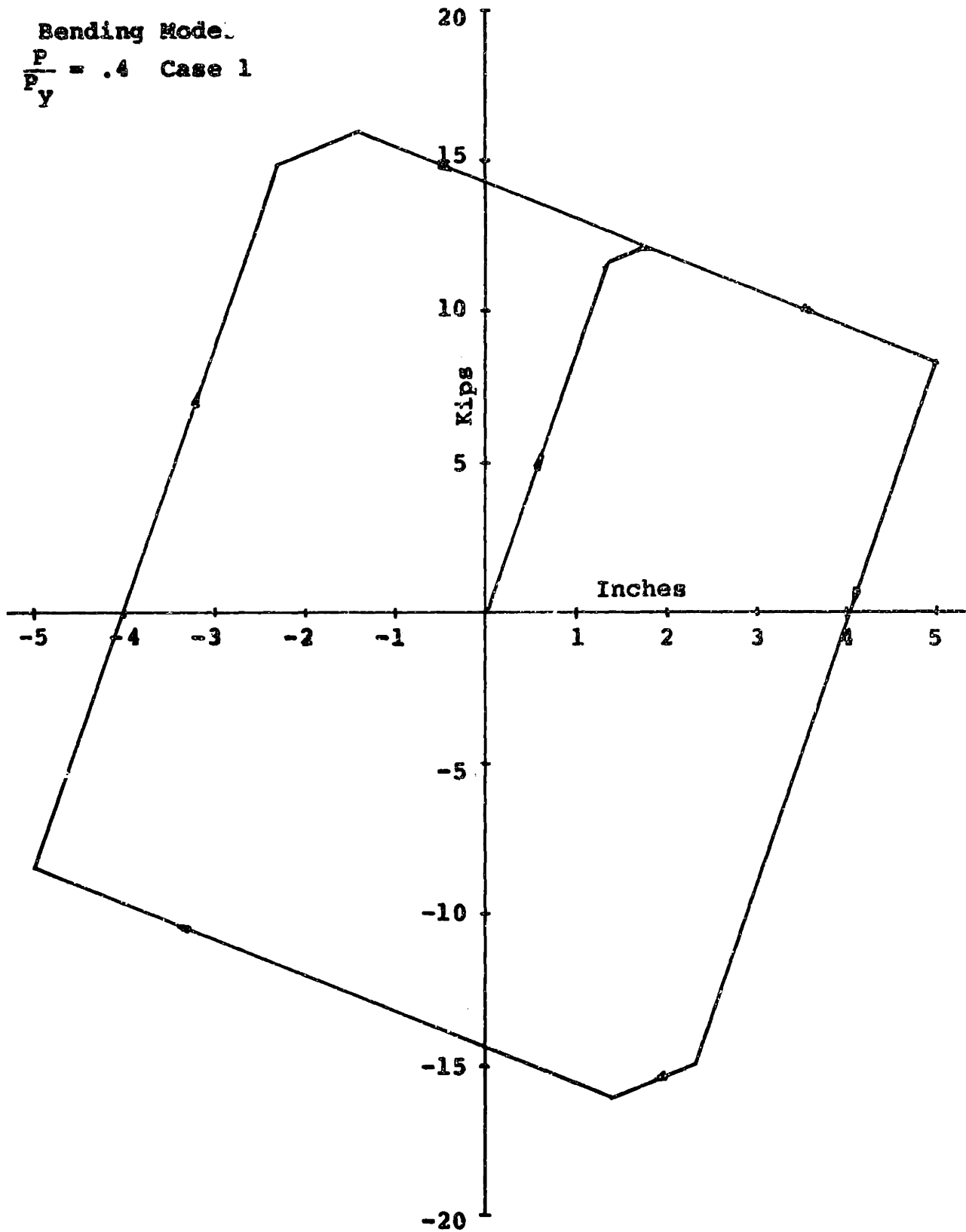


Figure 5-6. Graph of R vs Δ

Interaction Model

$$\frac{P}{P_y} = .4 \quad \text{Case 1}$$

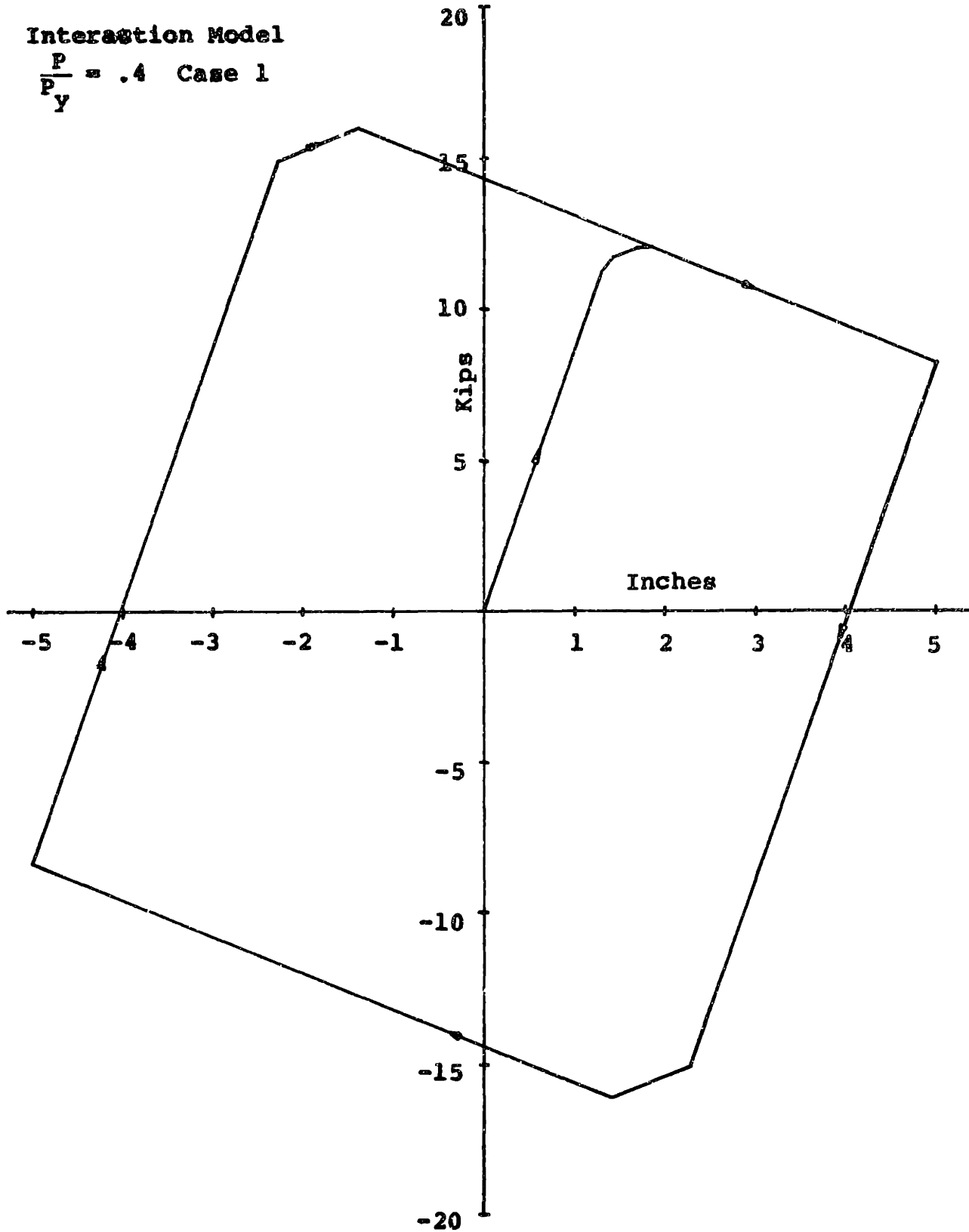


Figure 5-7. Graph of H vs Δ

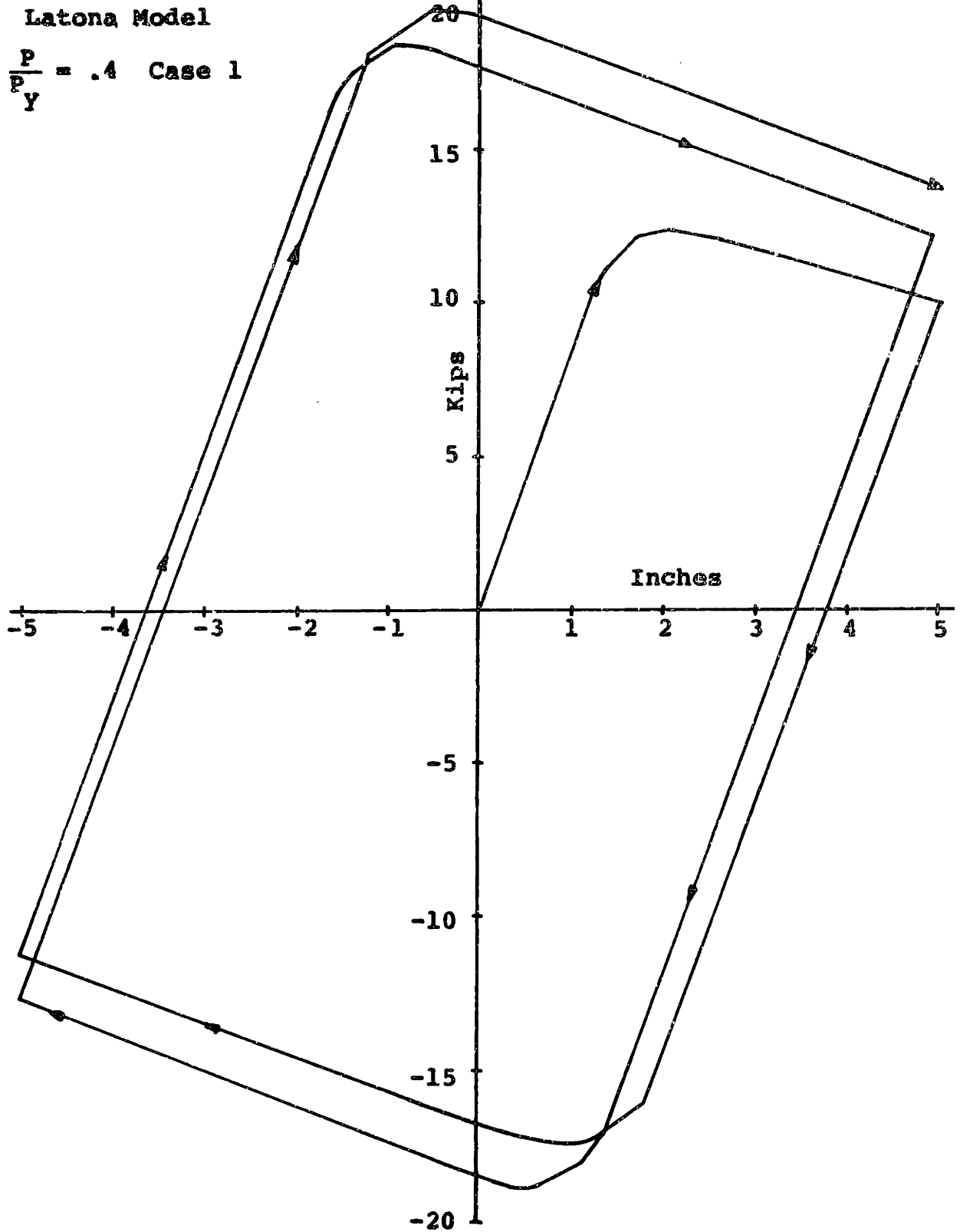
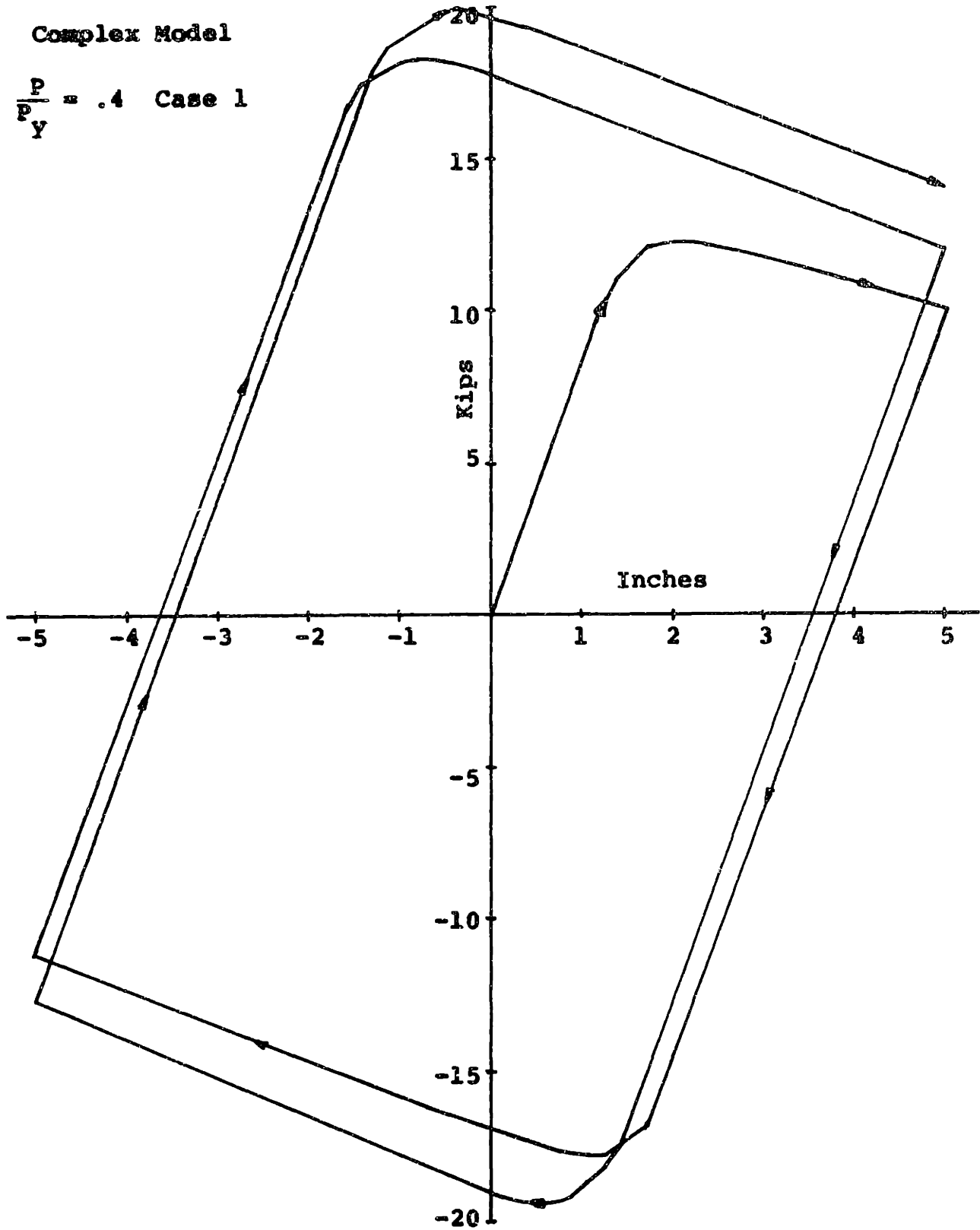


Figure 5-8. Graph of H vs Δ

Complex Model

$\frac{P}{P_Y} = .4$ Case 1



be quite close to $-\frac{2P}{h}$ in the simple models, and this is in fact the case.

When the axial load is relatively small, there is very little difference between the four models. The two simple models are definitely trilinear, while the Latona and Complex Models give a more gradual failure, and a slightly higher failure load. The Bending Model fails at a slightly higher load than the Interaction Model, since the Bending Model does not account for the increased axial force due to frame sideways, but in general, all four models give quite similar results.

This is not the case when $\frac{P}{P_y}$ is .4, however. The larger axial load causes a significant change in the behavior of the Latona and Complex Models. The behavior of the simple models remains quite similar, with the exception of the downward slope of the R-Δ curve, which is now twice as large since the axial load has doubled. The force displacement curve is a stable loop, however, which is no longer true for the Latona and Complex Models. Instead, these models show an increase in force at each cycle so that each loop becomes narrower and higher, although in all other respects, the models behave as expected, and give quite similar results. Thus this unsteady behavior is the only major difference between the complicated and simple models for this case, and it is this behavior that is further explored in the second section of this chapter.

The results for the second type of frame, where the girder is weaker and more flexible than the column, are shown in Figures 5-9 through 5-16 with Figures 5-9 through 5-12 being the results for $\frac{P}{P_Y} = .2$ and Figures 5-13 through 5-16 being the results for $\frac{P}{P_Y} = .4$. The results for this frame are very similar to those for the first frame, with no major difference between the four models for a small axial load, and a significant difference between the complicated and simple models for a large axial load. Once again the Complex and Latona Models show an increase in resisting force at each cycle, so that the force deformation loop becomes progressively higher and narrower, while the Bending and Interaction Models do not show this behavior, and the force deformation loop for these models remains stable for both values of axial load. In all the models, the slope of the R-Δ curve after the formation of a mechanism is dependent on the magnitude of the axial load, and agrees well with the value of $-\frac{2P}{h}$, mentioned earlier in this chapter.

In both of the frames examined so far, plastic hinges will develop first at the base of a column. Thus both cases involve initial column yielding at the bottom of the frame, regardless of where the second set of hinges occurs at the top. In the third frame, this situation is avoided by greatly increasing the column yield strength in the frame of case 1. This means that the girder is stiffer than the column but

Figure 5-9. Graph of R vs Δ

Bending Model
 $\frac{P}{P_Y} = .2$ Case 2

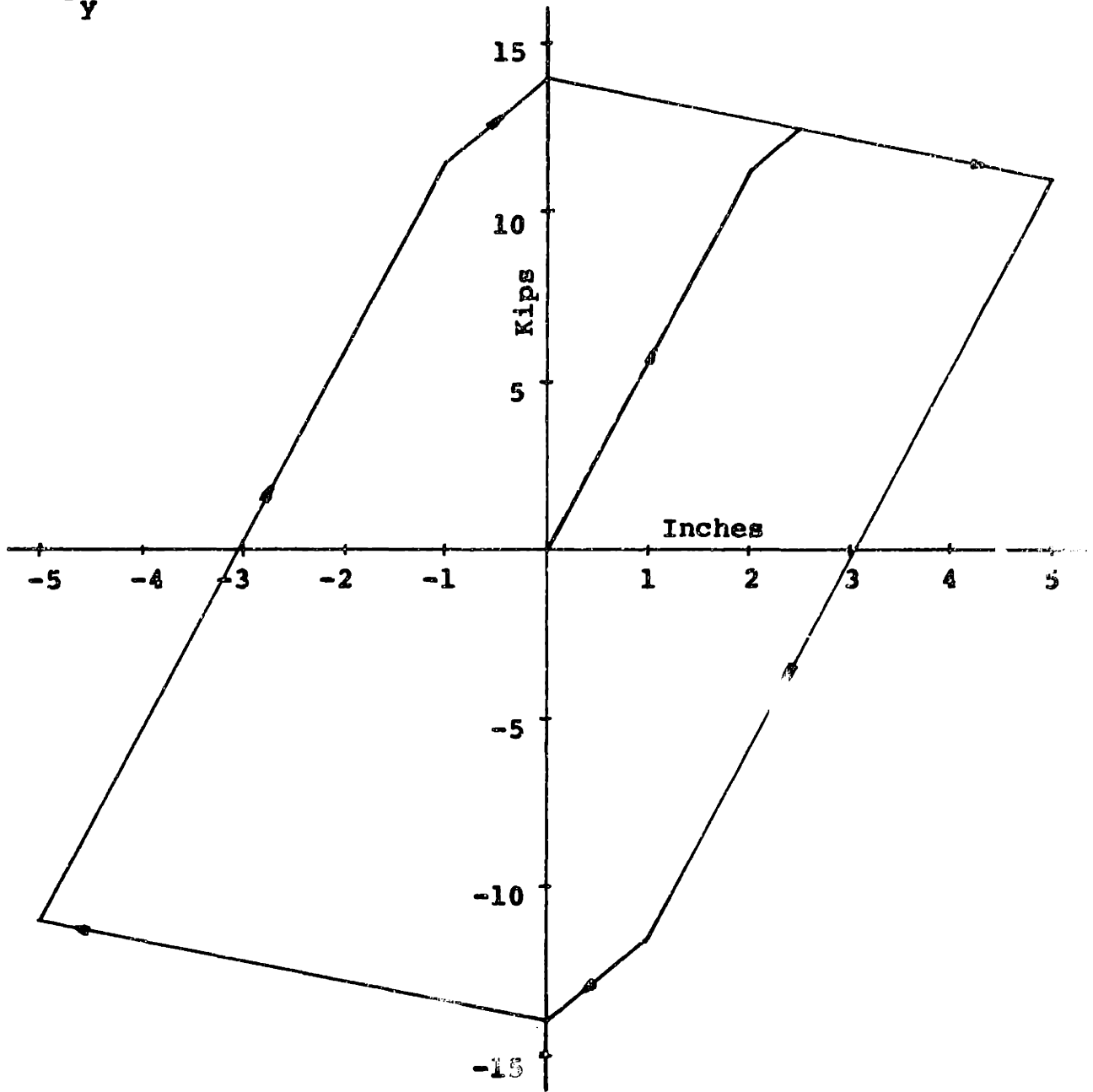


Figure 5-10. Graph of R vs A

Interaction Model

$$\frac{P}{P_y} = .2 \text{ Case 2}$$

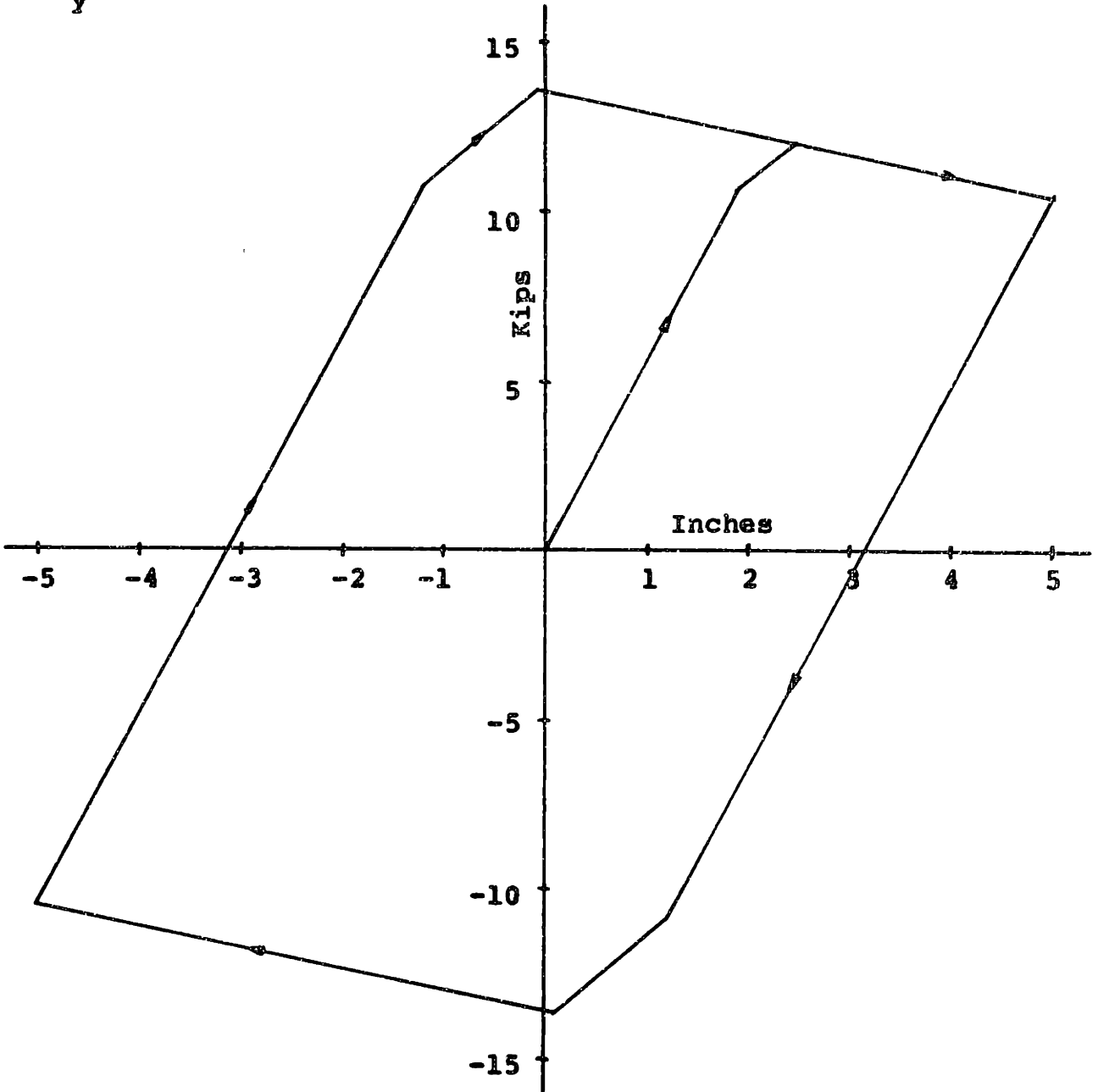


Figure 5-11. Graph of R vs Δ

Latona Model

$$\frac{P}{P_Y} = .2 \text{ Case 2}$$

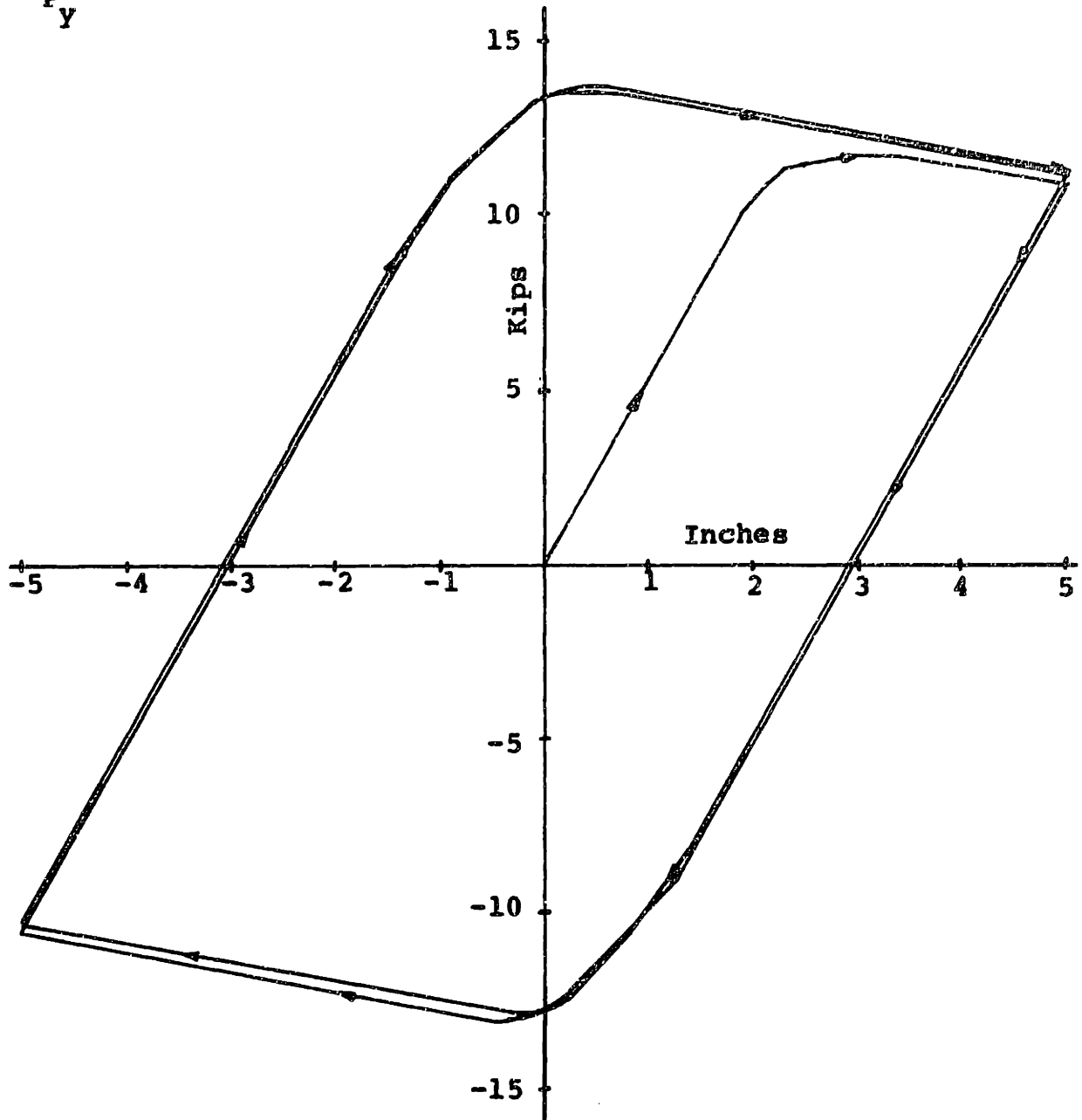


Figure 5-12. Graph of R vs Δ

Complex Model

$\frac{P}{P_y} = .2$ Case 2

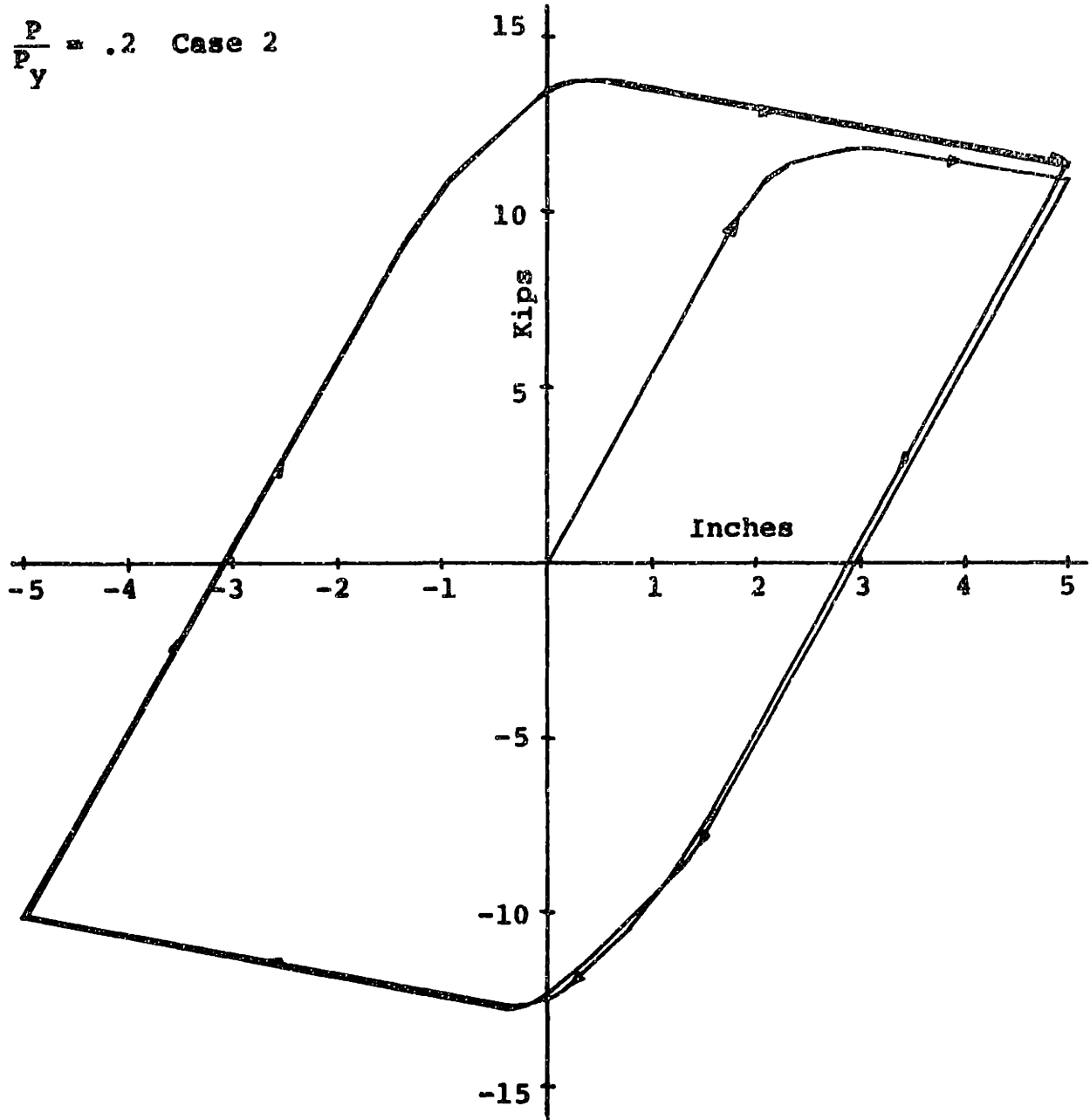


Figure 5-13. Graph of R vs Δ

Bending Model

$$\frac{P}{P_Y} = .4 \quad \text{Case 2}$$

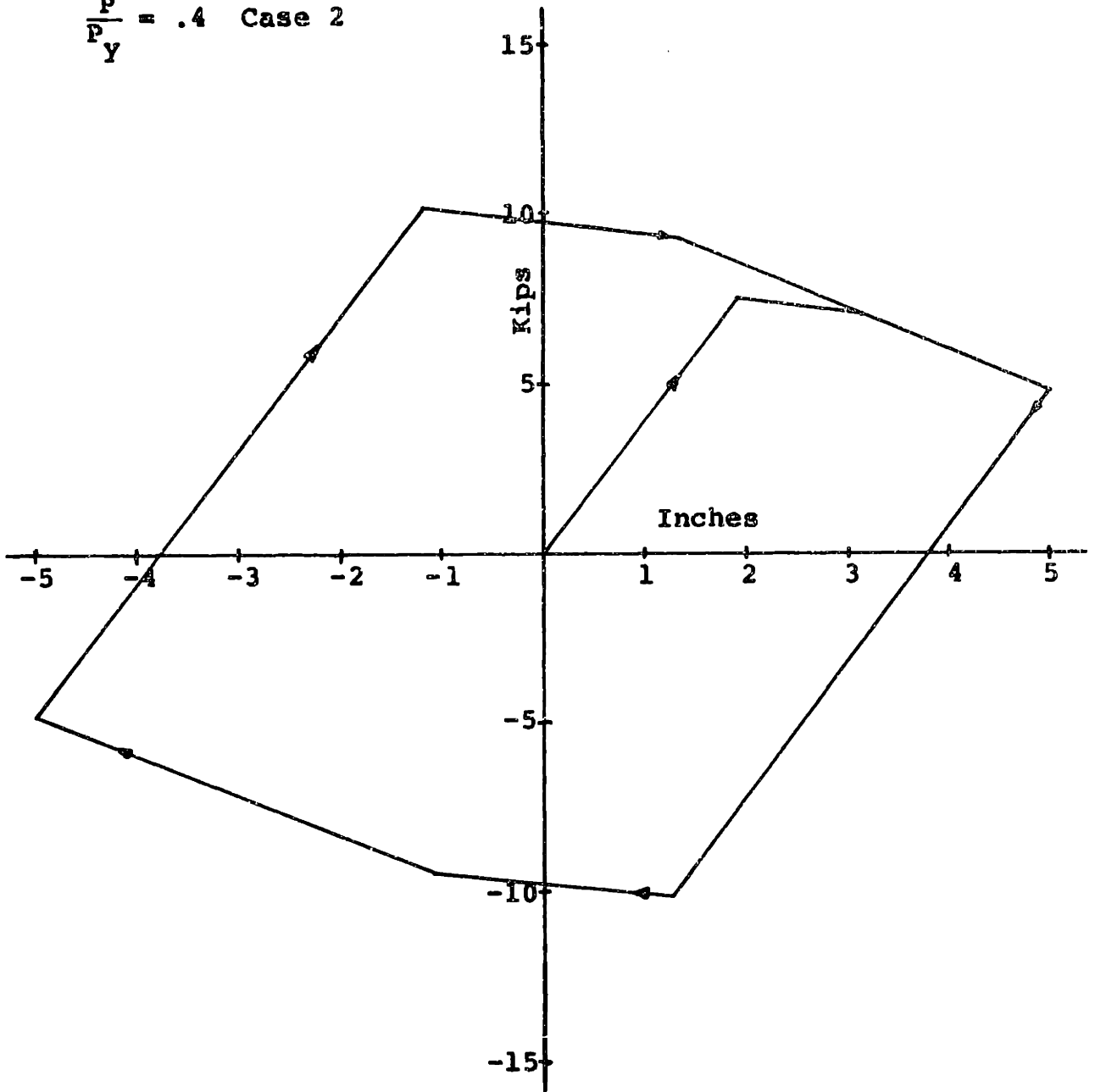


Figure 5-14. Graph of R vs Δ

Interaction Model

$$\frac{P}{P_y} = .4 \quad \text{Case 2}$$

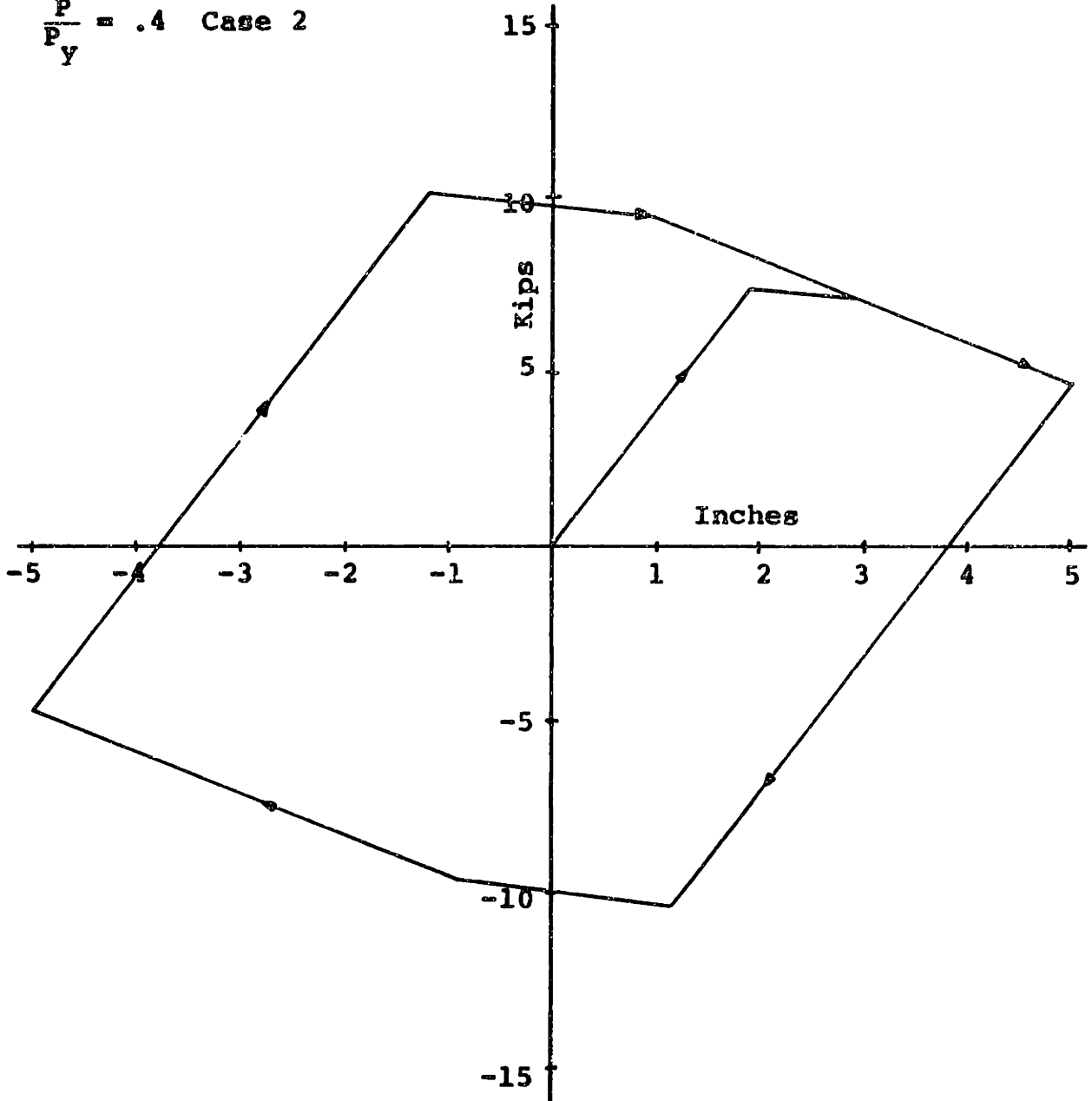


Figure 5-15. Graph of R vs Δ

Latona Model

$$\frac{P}{P_Y} = .4 \quad \text{Case 2}$$

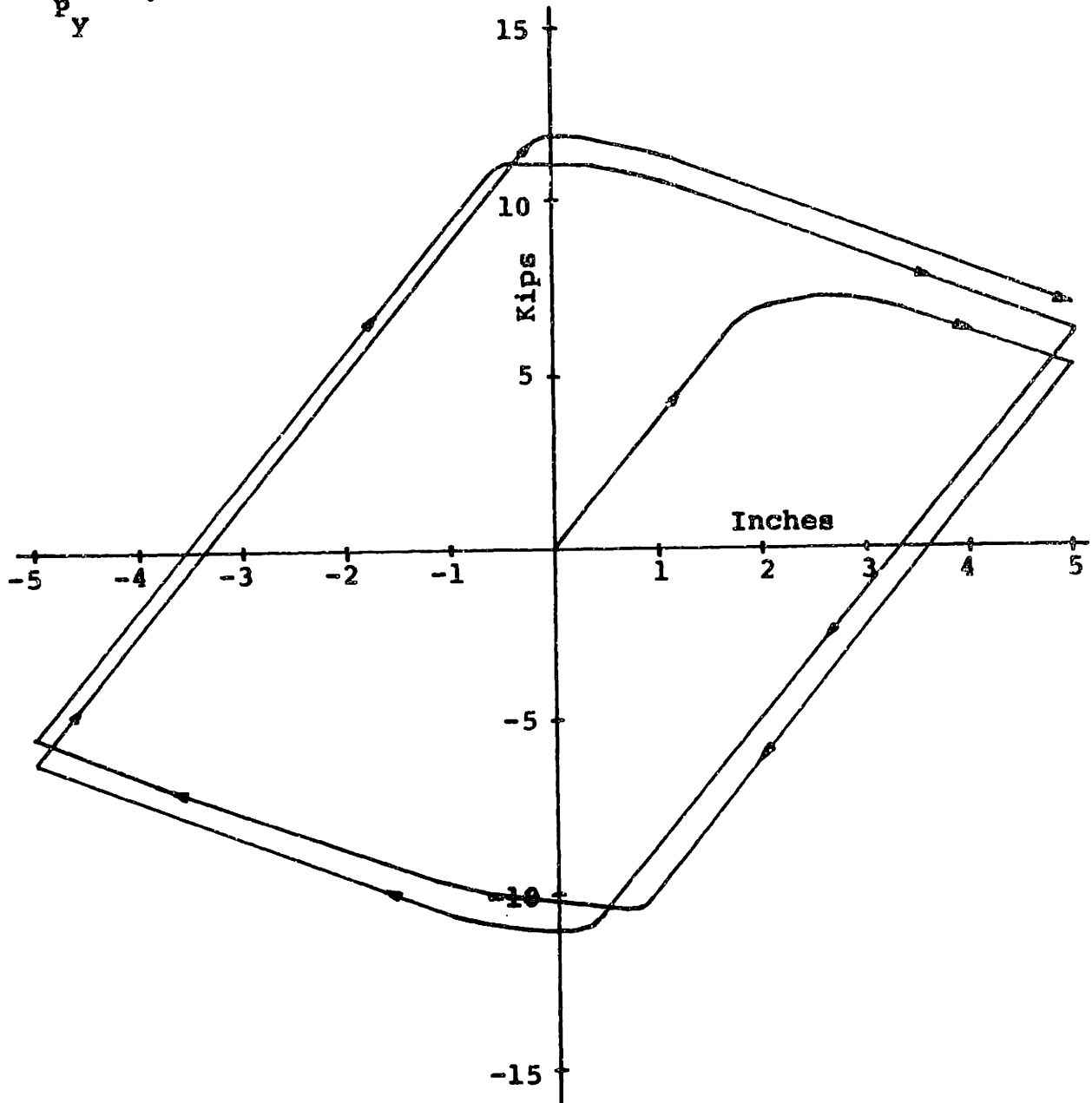
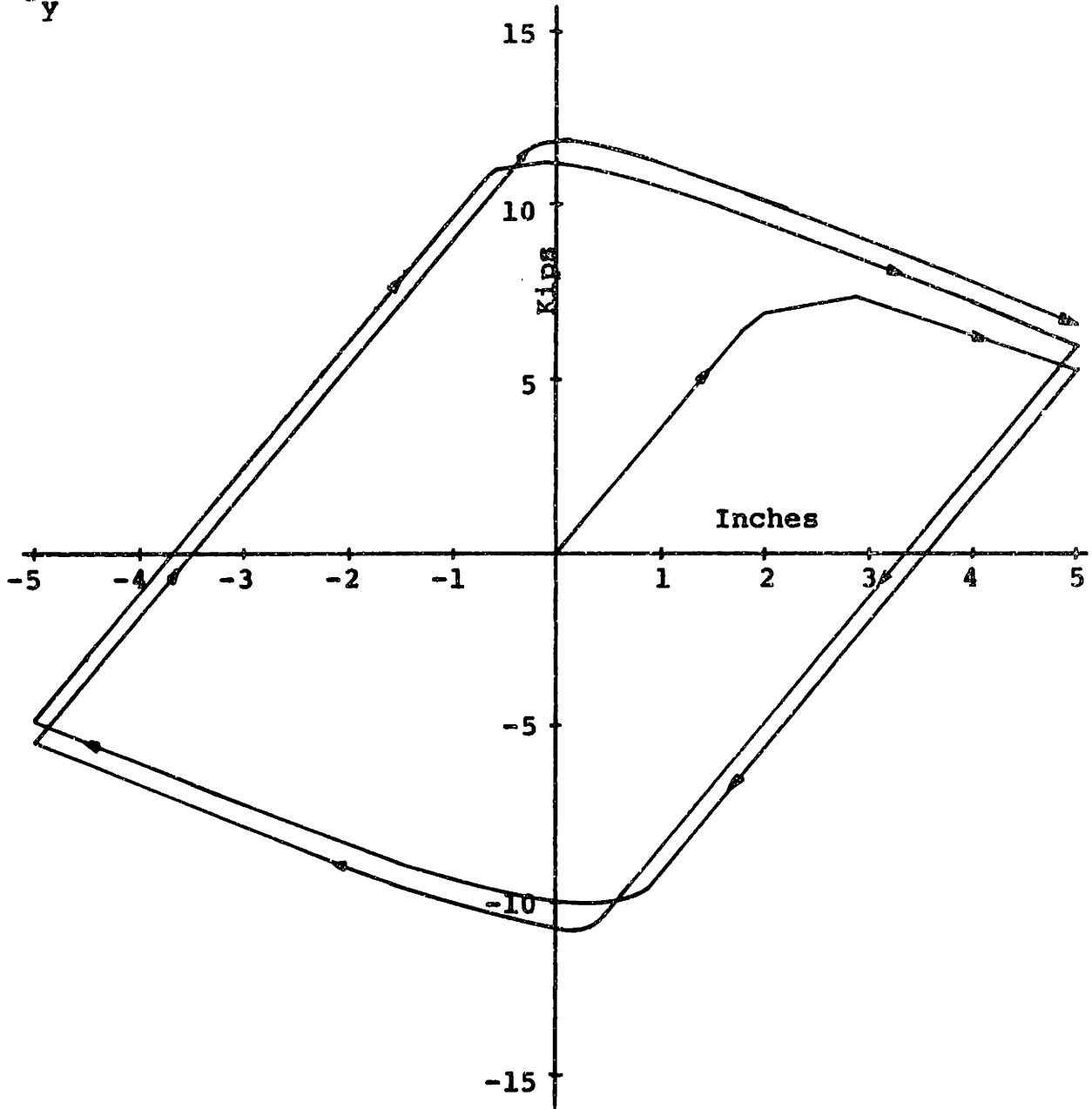


Figure 5-16. Graph of R vs Δ

Complex Model

$\frac{P}{P_Y} = .4$ Case 2



weaker, and hence plastic hinges will develop in the girder before failure occurs in either the top or bottom of the column. In fact, failure never occurs in the column, since the maximum displacement of five inches is not sufficient to cause yielding at the base of either column. The results for this case are shown in Figures 5-17 through 5-20 for $\frac{P}{P_Y} = .2$ and in Figures 5-21 through 5-24 for $\frac{P}{P_Y} = .4$. When the axial load is small, all the models give similar results. As usual, the Bending and Interaction Models show an abrupt transition when the girder fails, while the Latona and Complex Models show a more gradual transition, but in other respects the models are quite similar. At a large value of axial load, however, differences appear, although in all models the force displacement loops are stable, unlike the previous two cases. Since the first two cases involve substantial yielding in the column, and this case does not, it seems reasonable to assume that the increase in resistance observed in the first two cases is related to spreading of yielding in the column, and does not occur as long as the column remains elastic.

Because the column yield stress is so high in the third case, the column load corresponding to $\frac{P}{P_Y} = .4$ is about half the frame buckling load (assuming $K = 1$). This means that only the restraint offered by the stiff girder keeps the frame from buckling, and as soon as a hinge forms in the girder the frame becomes unstable. All the models reflect this failure by the downward slope of the R- Δ curve after a

Figure 5-17. Graph of R vs Δ

Bending Model

$$\frac{P}{P_y} = .2 \quad \text{Case 3}$$

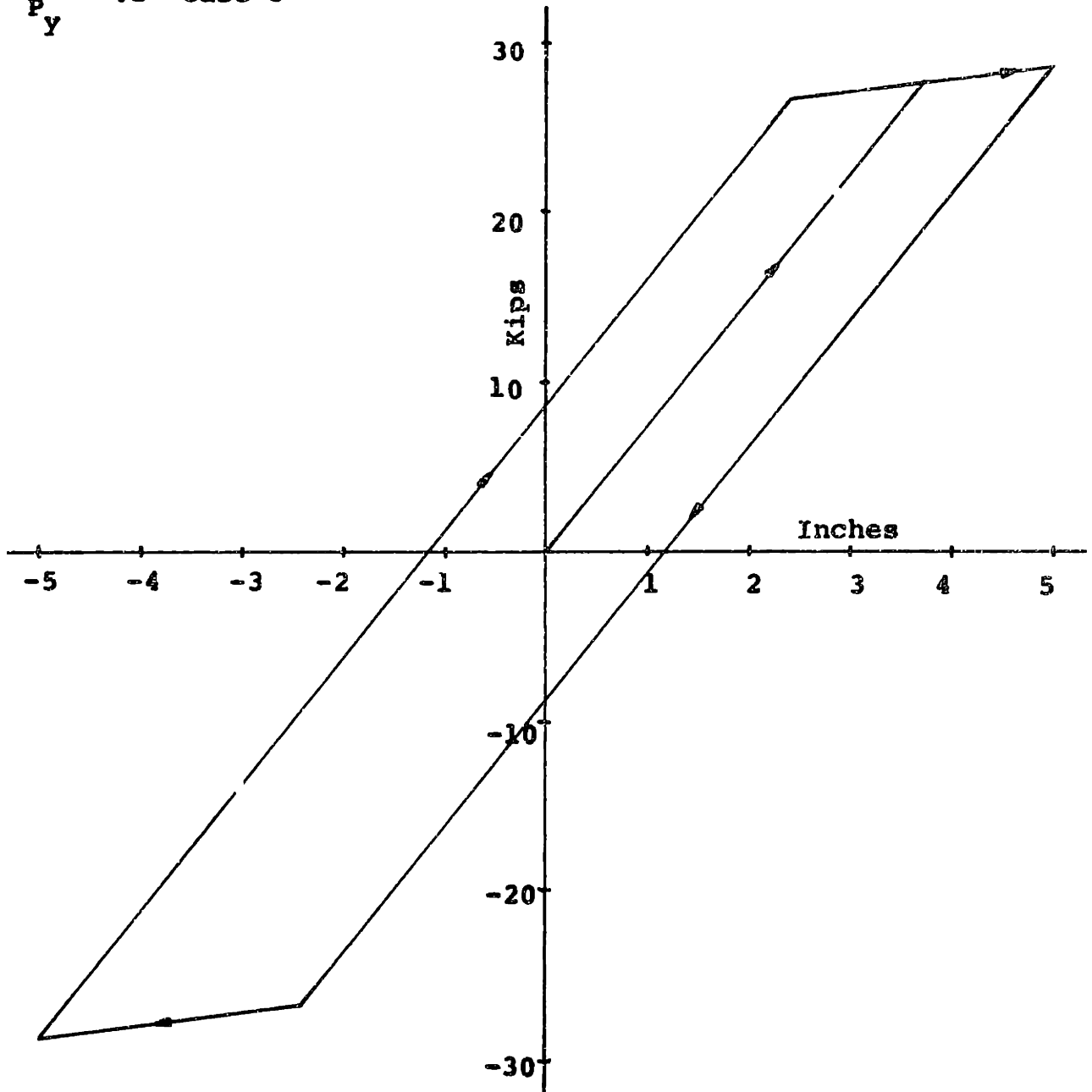


Figure 5-16. Graph of R vs Δ

Interaction Model

$$\frac{P}{F_y} = .2 \text{ Case 3}$$

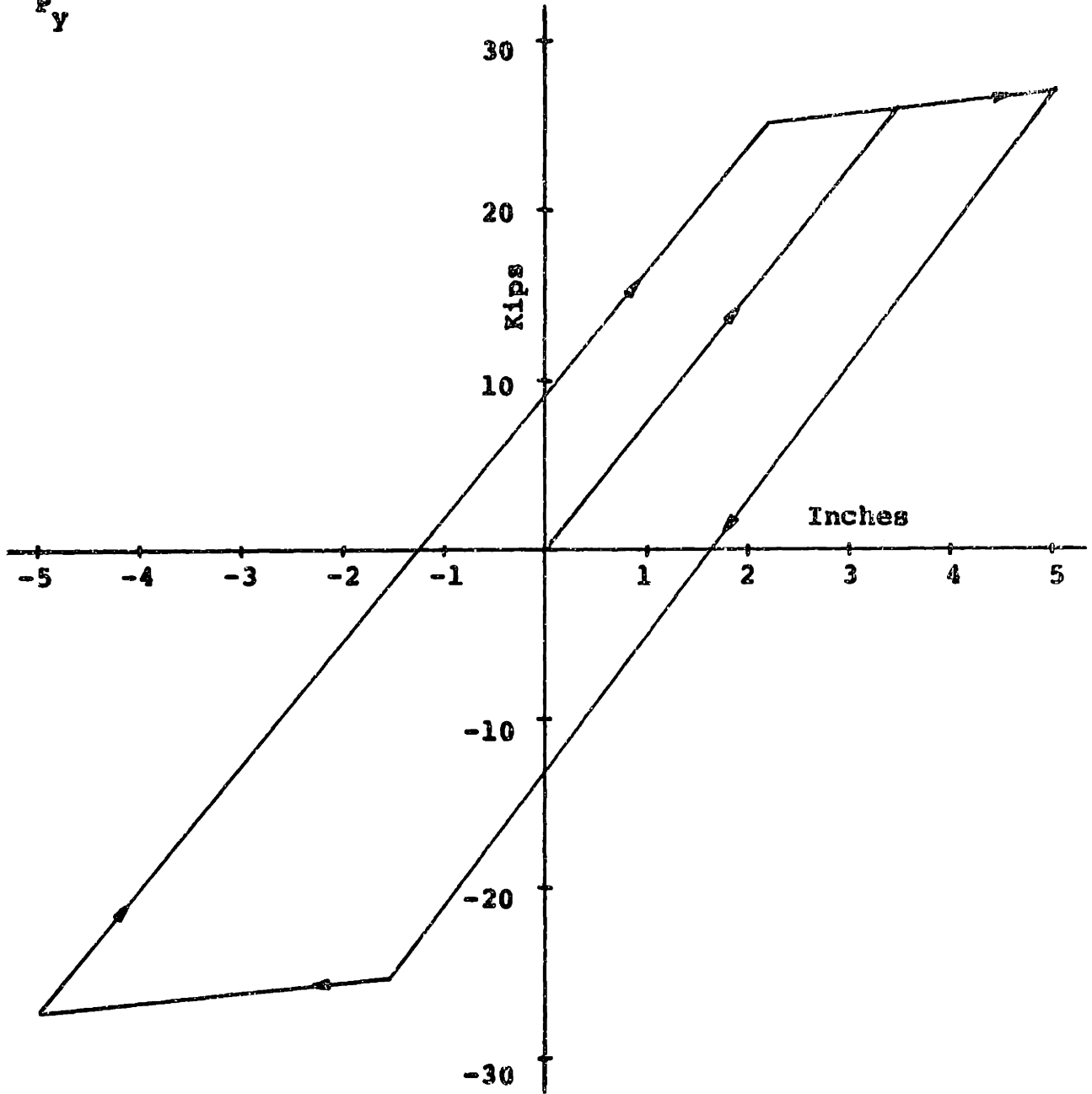


Figure 5-19. Graph of P vs Δ

Latona Model

$\frac{P}{P_y} = .2$ Case 3

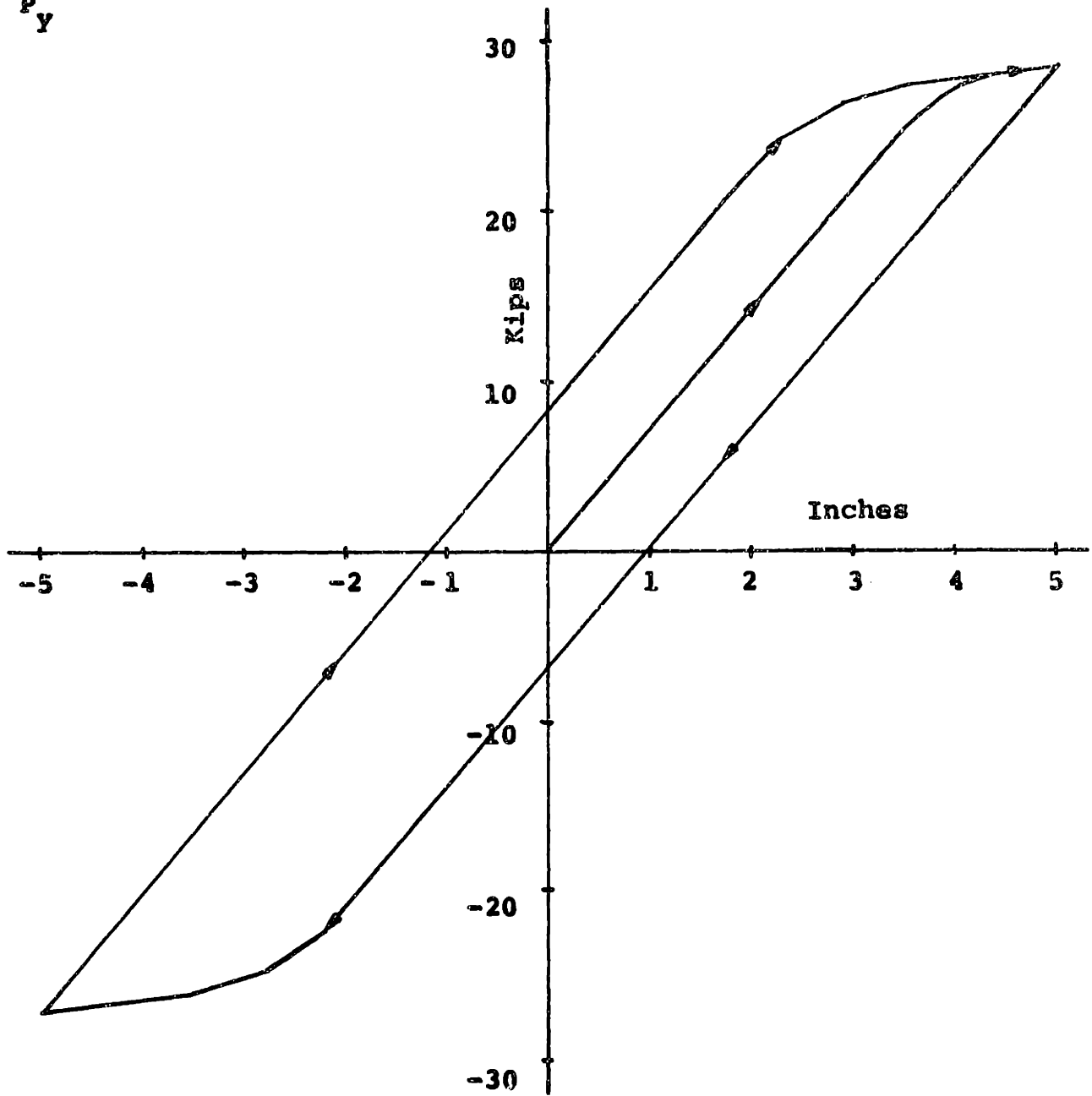


Figure 5-20. Graph of R vs Δ

Complex Model

$$\frac{P}{P_Y} = .2 \quad \text{Case 3}$$

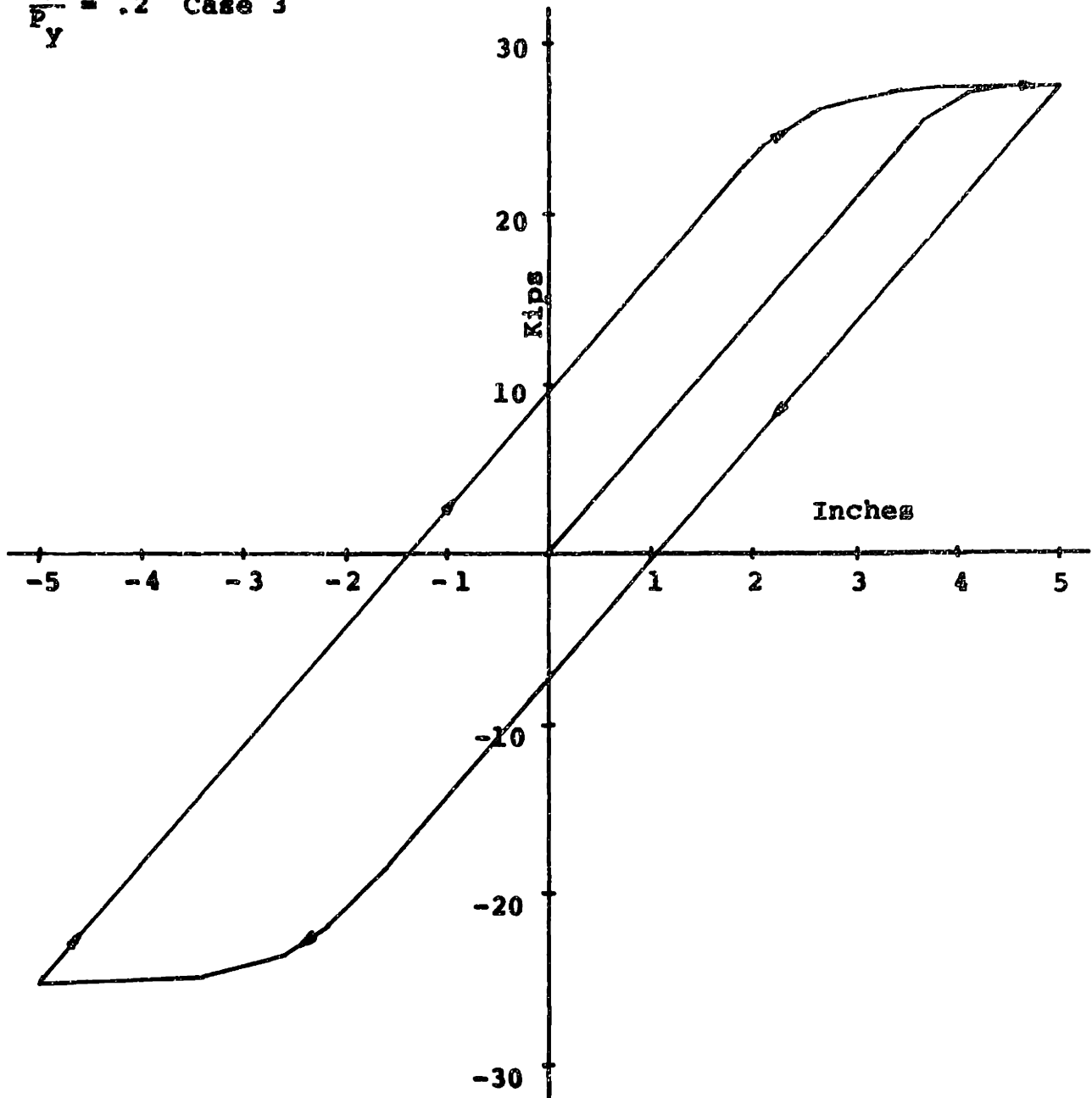


Figure 5-21. Graph of R vs A

Bending Model

$$\frac{P}{P_Y} = .4 \quad \text{Case 3}$$

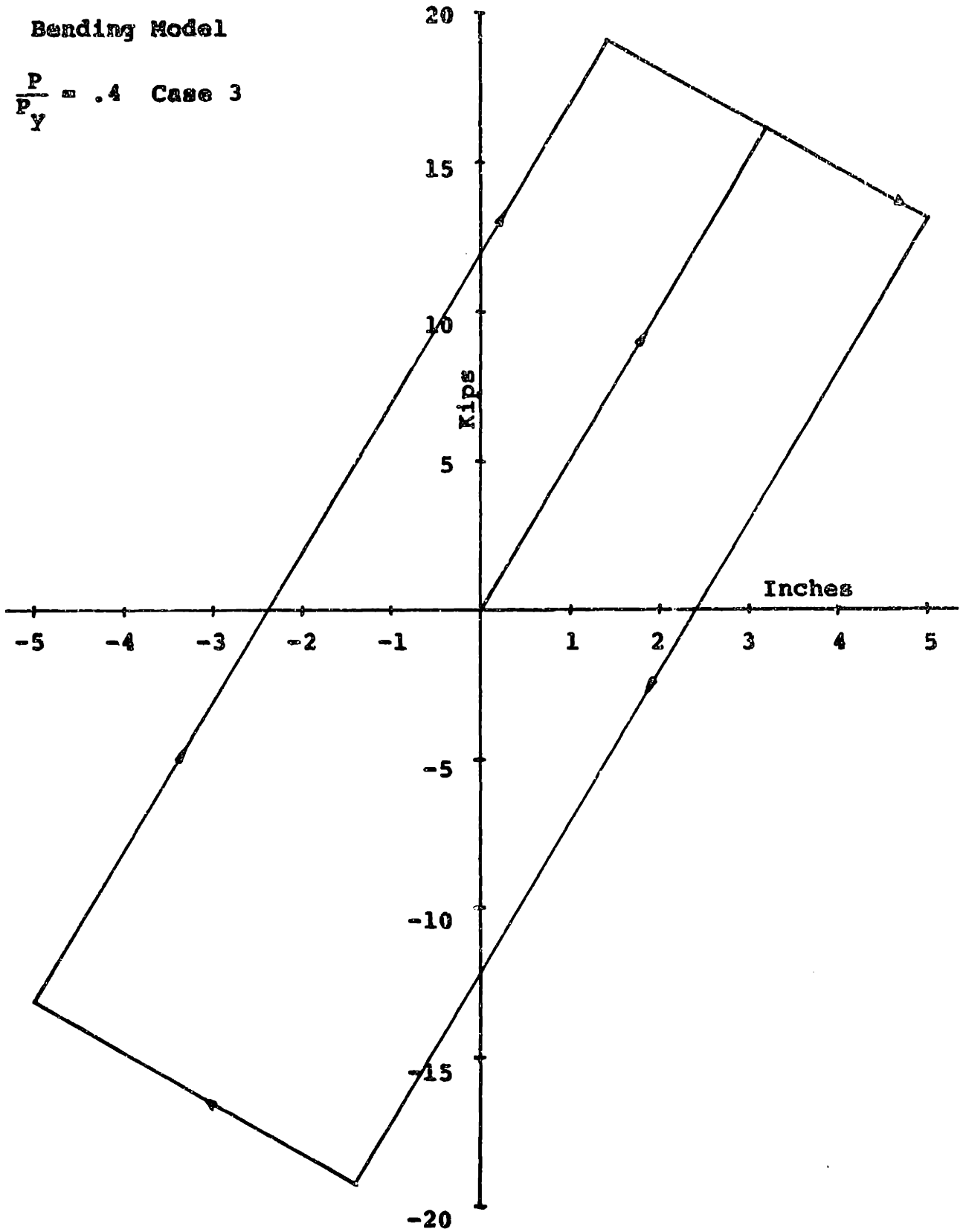


Figure 5-22. Graph of R vs Δ

Interaction Model

$$\frac{P}{P_y} = .4 \quad \text{Case 3}$$

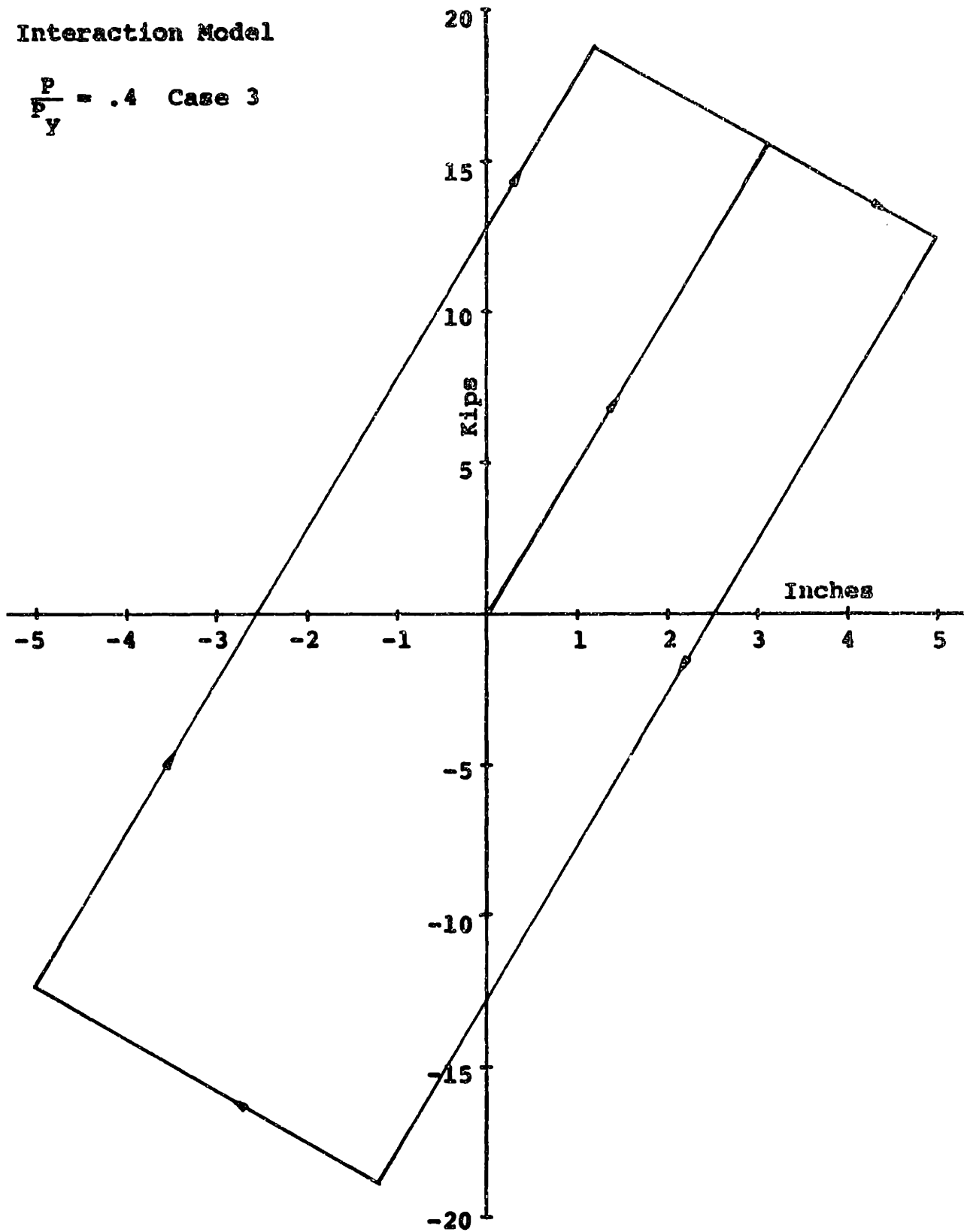


Figure 5-23. Graph of R vs Δ

Latona Model

$\frac{P}{P_Y} = .4$ Case 3

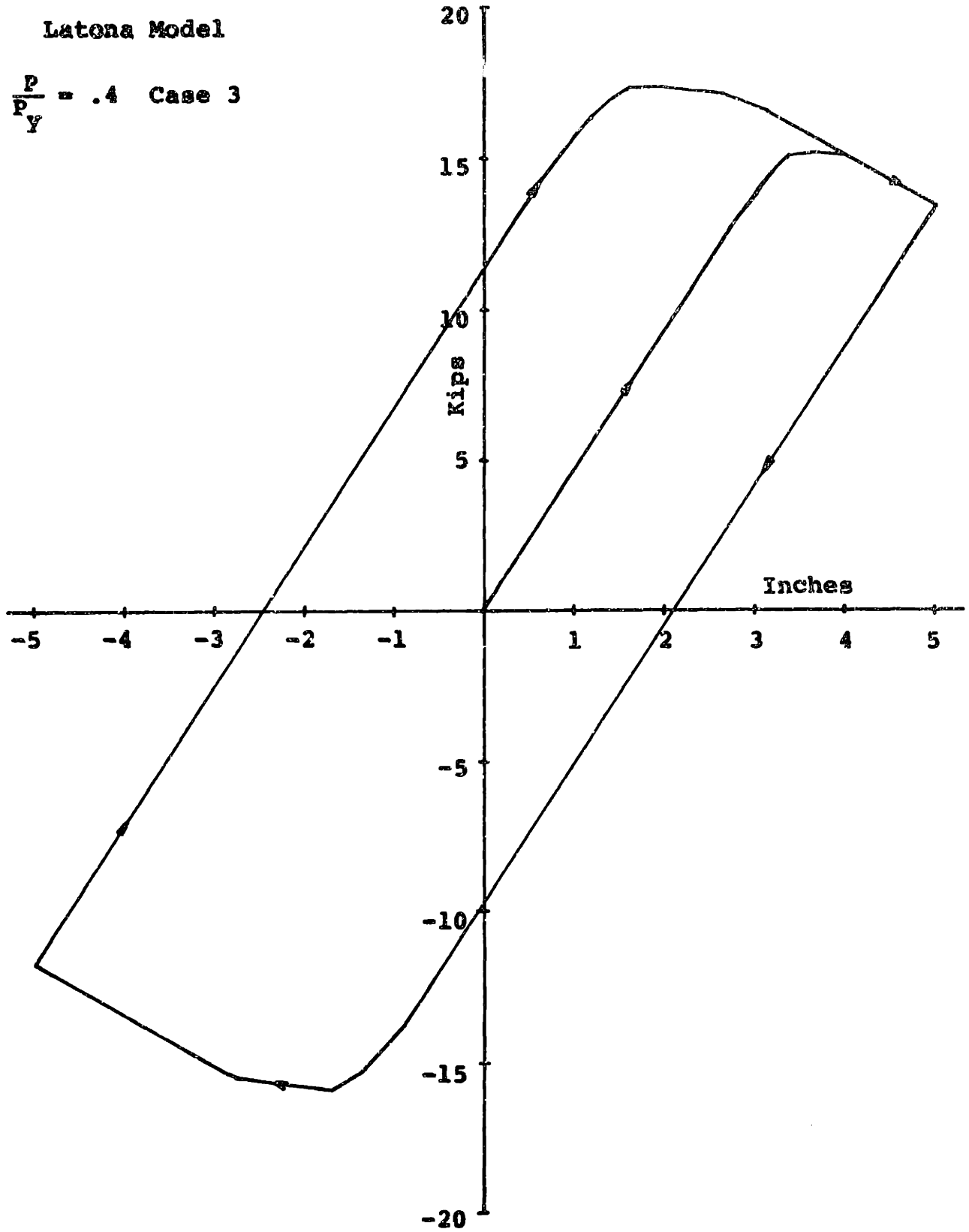
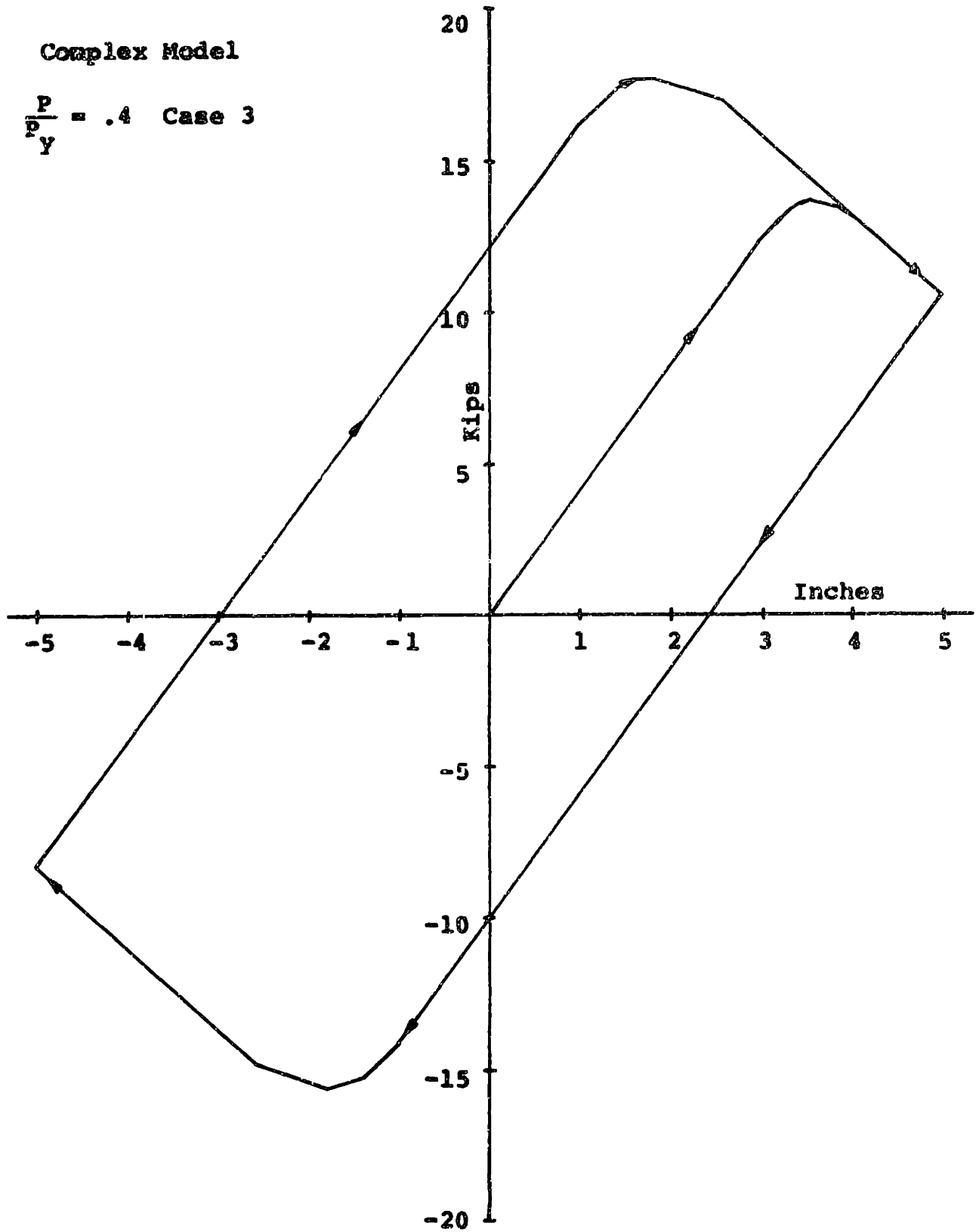


Figure 5-24. Graph of R vs Δ

Complex Model

$$\frac{P}{P_Y} = .4 \quad \text{Case 3}$$

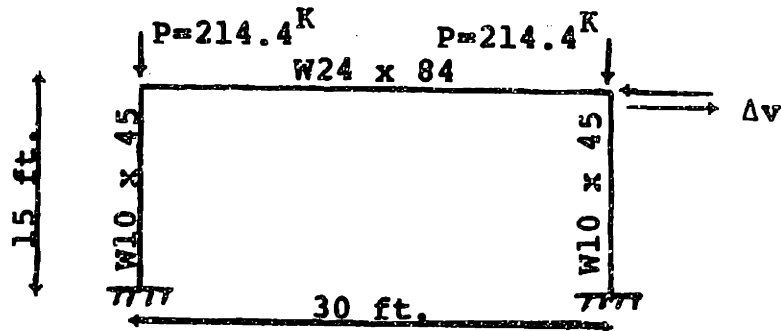


plastic hinge has formed in the girder, but this downward slope is much steeper in the Complex Model because of its ability to reproduce member deformations. The effect of member deformations on the initial failure load is also significant, the Complex Model giving a failure load about 10% lower than that of the Latona Model. It is interesting to note that in this case, as in the case of the slender beam column of Chapter 4, the softening effect caused by outer fibers yielding becomes important, and hence the Latona Model predicts a lower initial failure load than the simple models.

Thus the major difference between the models appears to occur when a column subjected to a large axial load yields. The presence of such a condition does not significantly change the behavior of the simple models, but in the Latona and Complex Models, the R- Δ curve becomes unsteady and the resistance of the frame appears to increase with each displacement cycle. There appears to be little difference between the Bending and Interaction Models, nor does there appear to be any major difference between the Latona and Complex Models. It is true that the Complex Model will give different results from the Latona Model when member deformations are important, but the predictions of the Latona Model are not greatly in error, even in this case, and in the other cases the agreement between the Complex and Latona Models is extremely good.

5.2 Latona Frame Study

One of the examples used by Latona in his thesis was a single bay single story frame with very large axial loads. Since column yielding in the presence of large axial loads appears to cause the major differences between the models, the predictions of the various models for Latona's frame will be examined in this section. The results given by the four models for a displacement increment of .1 in. are shown in Figures 5-25 through 5-28. Once again the simple models show a steady force displacement loop, while the complicated models predict one that is unsteady. The frame and its loading is shown below.



Because it has been shown in earlier chapters that the Latona and Complex Models are very sensitive to the size of the load increment, the same case was run again using the Complex Model and a displacement increment of .05 in. Figure 5-29 shows the results for this second run, and it can be seen that while there is a small decrease in the force values, the resistance still increases at each displacement cycle. A linear extrapolation from Figures 5-28 and 5-29 shows that the

Figure 5-25. Graph of R vs Δ

Bending Model

Latona Frame: 1 Bay, 1 Story

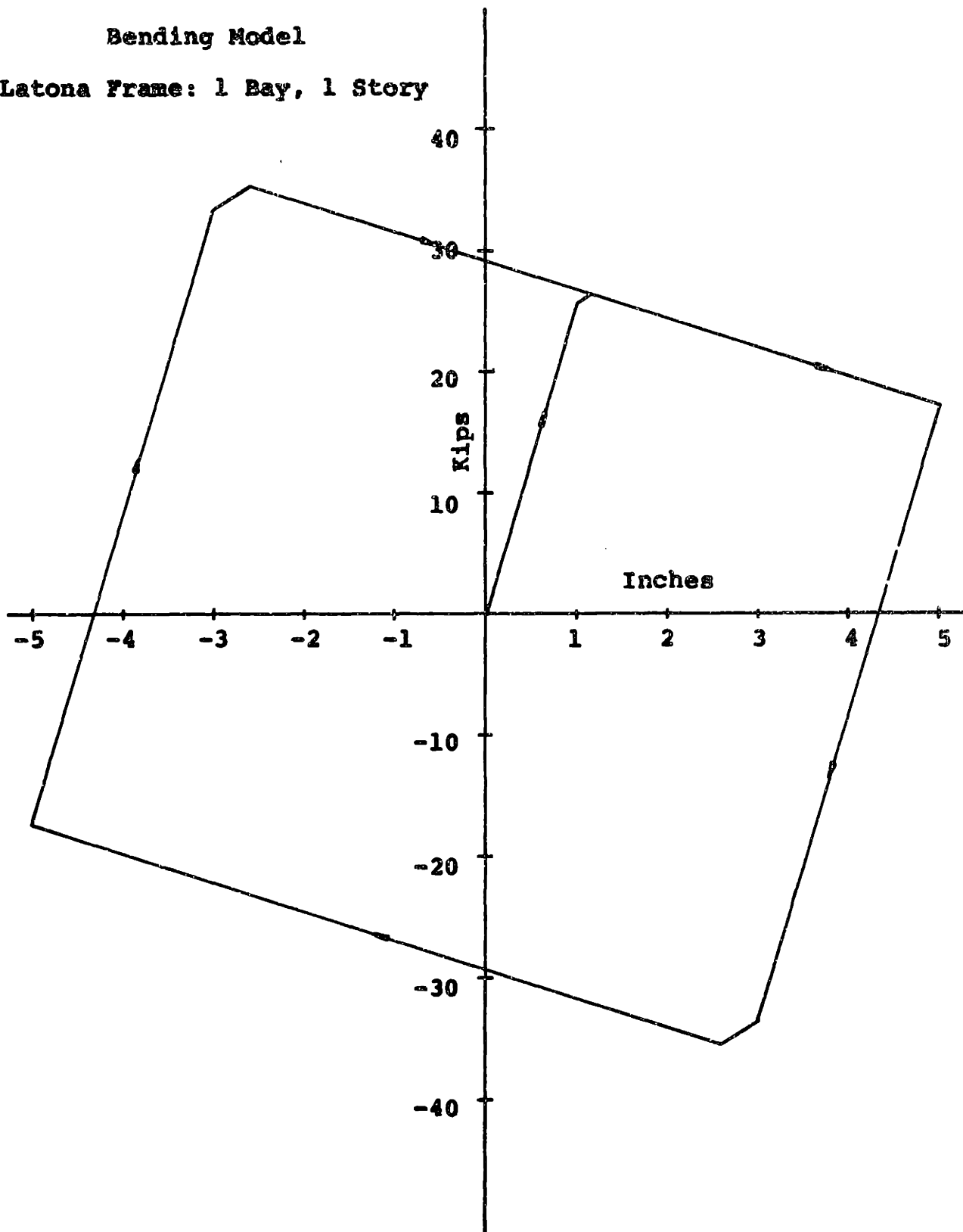


Figure 5-26. Graph of R vs Δ

Interaction Model
Latona Frame: 1 Bay, 1 Story

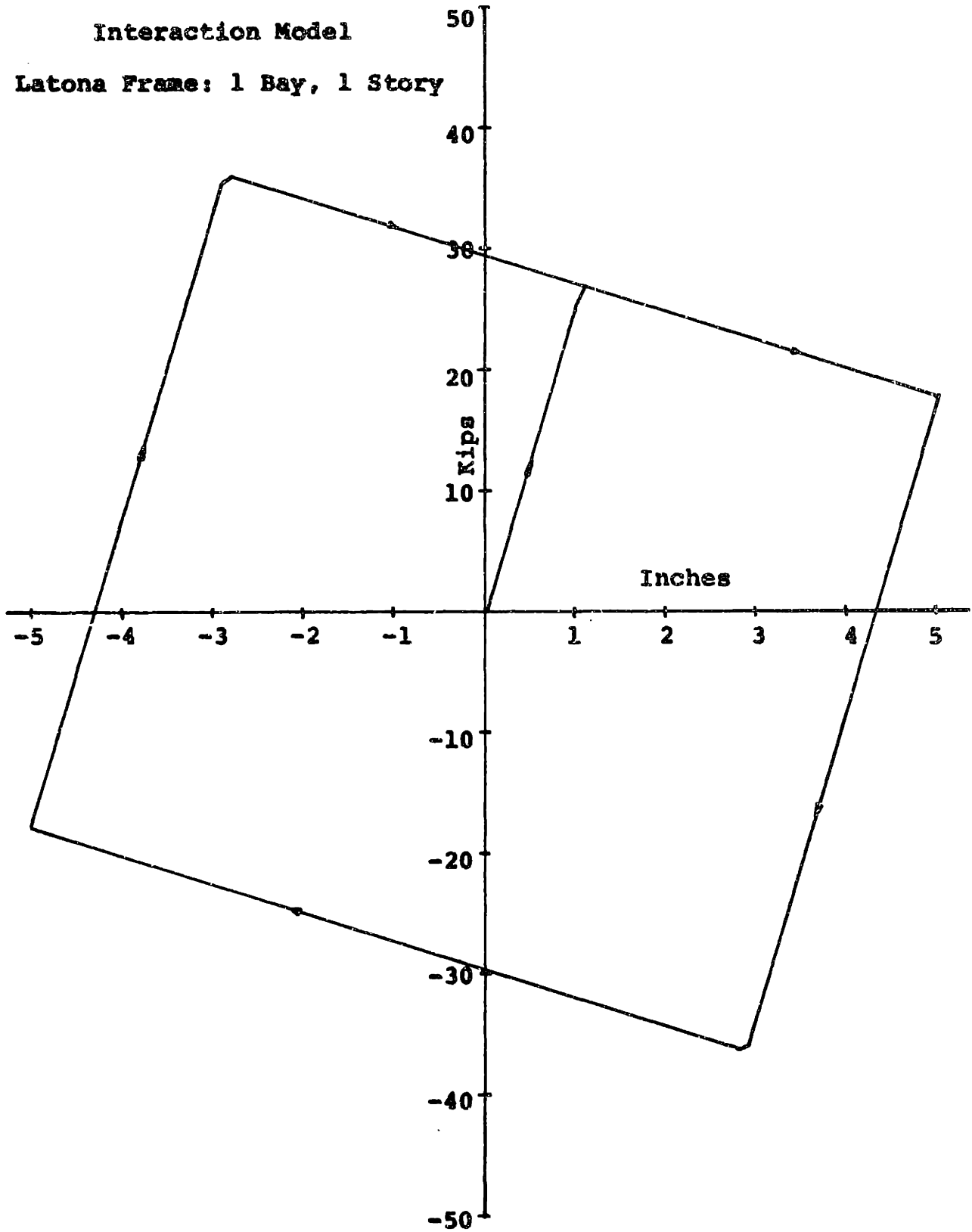


Figure 5-27. Graph of P vs Δ

Latona Model

Latona Frame:
1 Bay,
1 Story

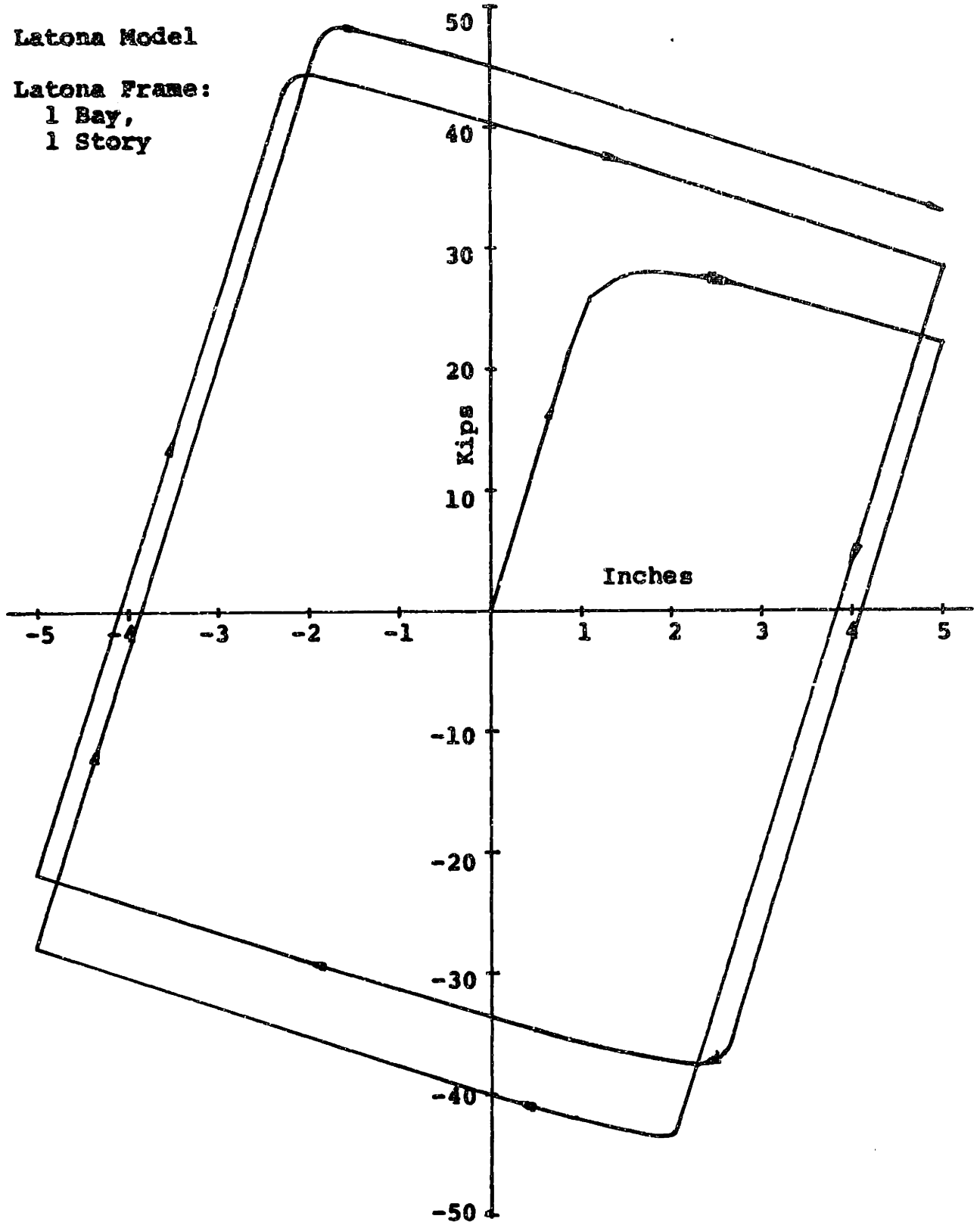


Figure 5-28. Graph of R vs Δ

Complex Model

Latona Frame:
1 Bay,
1 Story

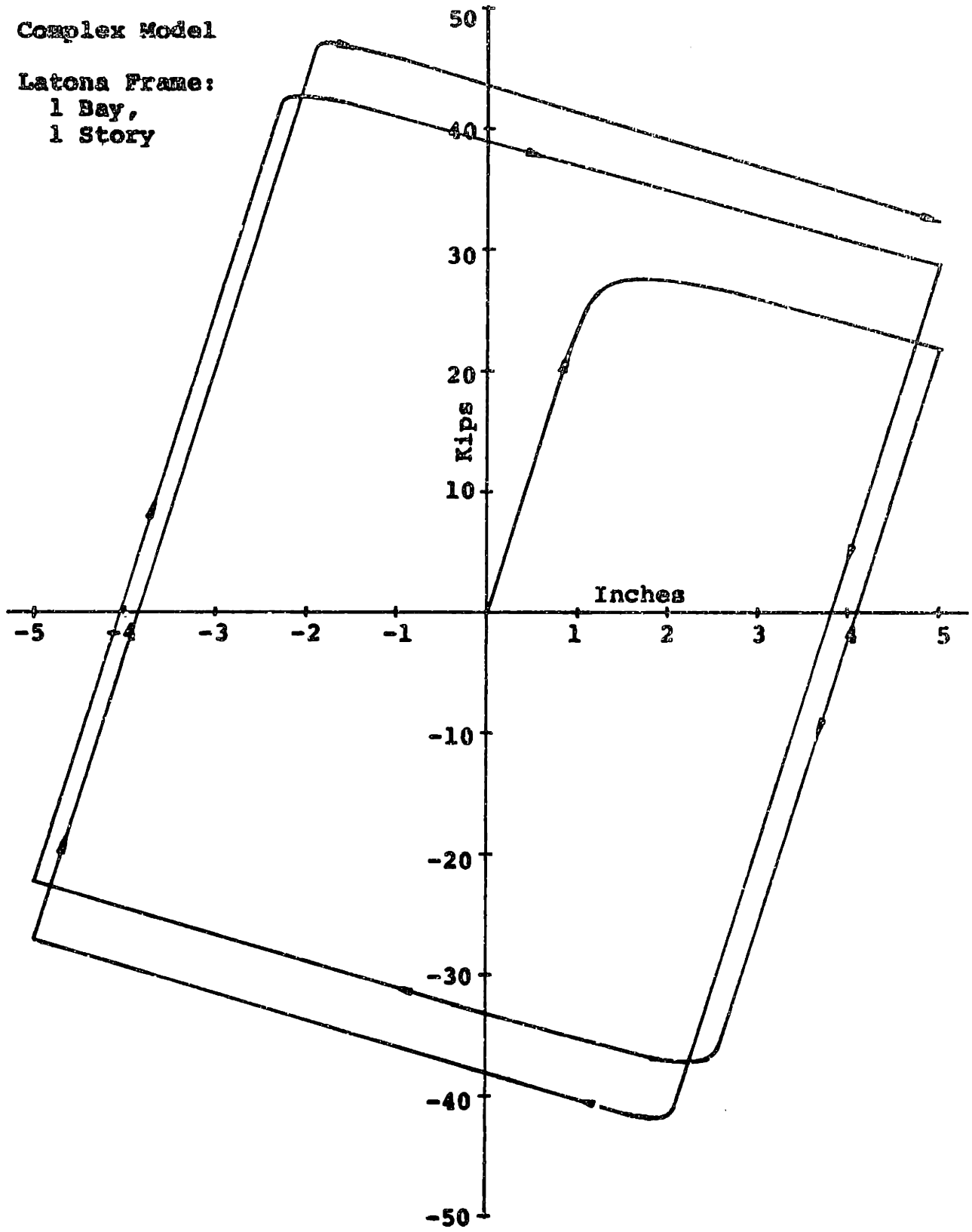
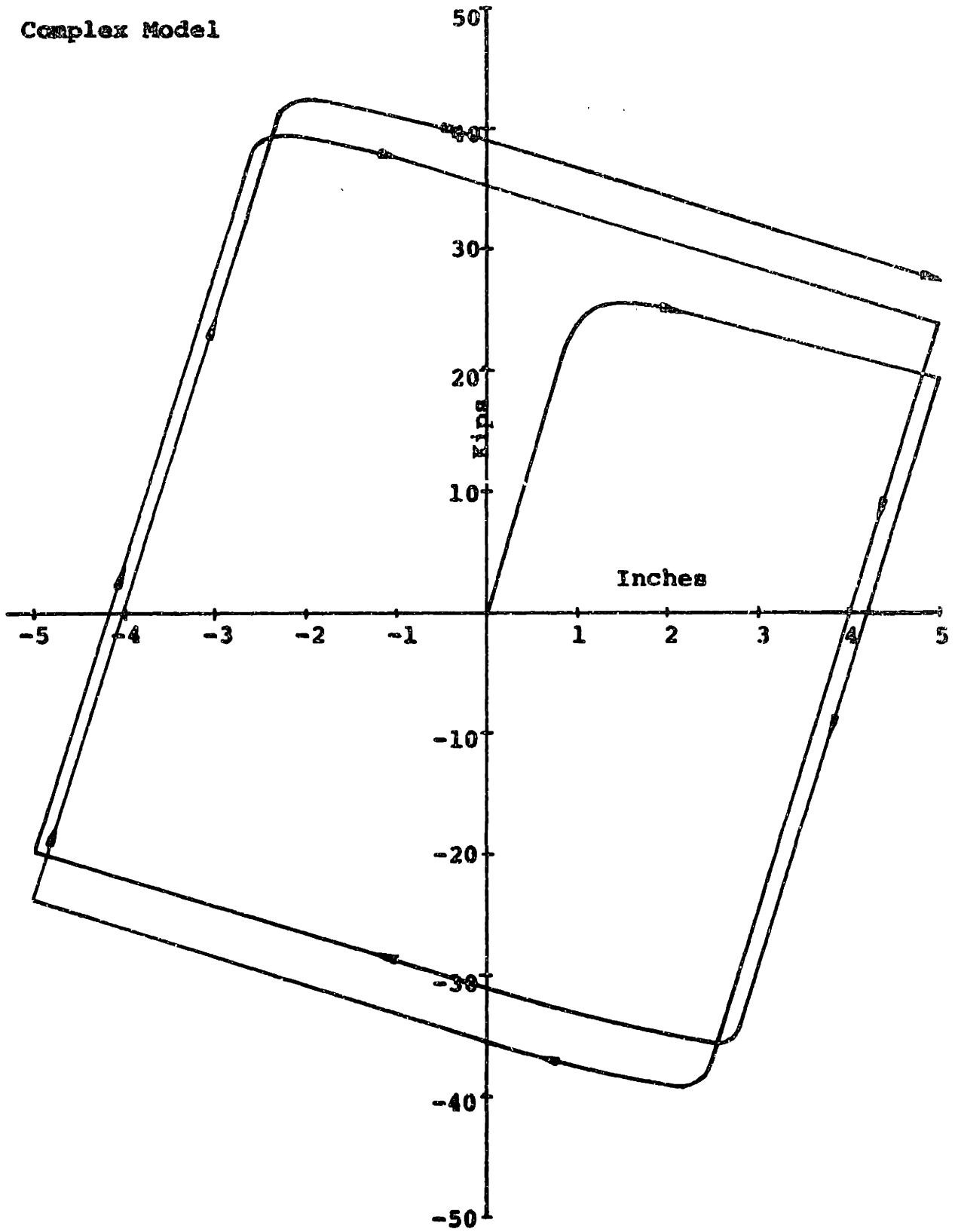


Figure 5-29. Graph of R vs Δ : $\Delta = .05$

Complex Model



increase in resistance will not vanish as the increment size goes to zero, and hence this increase represents the real behavior of the mathematical model, and not the result of an overlarge displacement increment.

Figures 5-28 and 5-29 both show that the increase in resistance for the third cycle is smaller than that for the second, and it appears that the force deformation loop may stabilize after several cycles. Figure 5-30 shows that this does, in fact, happen, and that there is very little increase in resistance between the third and fourth cycles. It should also be noted that the elastic loading and unloading portions of the loop become slightly stiffer at each cycle, the change in stiffness is slight, but it is definitely present, and it seems to stabilize also. In order to see how the behavior of the loop is affected by the percent strain hardening, two other runs have been made with the Latona Model, one for 1.5% strain hardening and one for 3% strain hardening. Figures 5-31 and 5-32 show the results of these two runs, and it can be seen that the phenomenon of increase in resistance still occurs, but that it occurs in a very different way. In both cases, most of the increase occurs in the first cycle, and the force displacement loop stabilizes much faster than in the case of .1% strain hardening. A comparison of the three graphs also shows that the slope of the force deformation curve after failure increases as the strain hardening increases, and also becomes more highly

Figure 5-30. Graph of R vs A

Latona Model

Latona Frame:
.18 Strain
Hardening

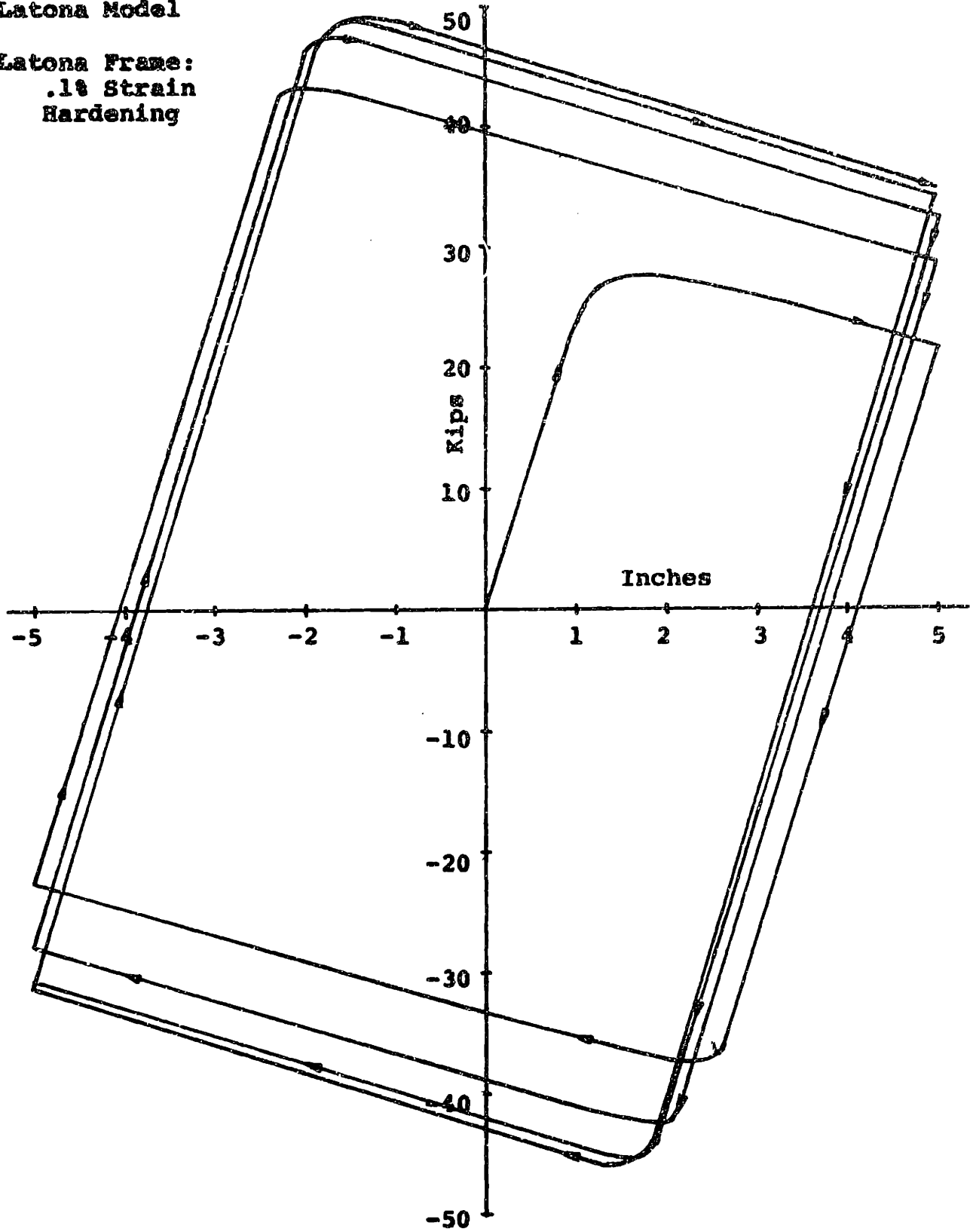


Figure 5-31. Graph of R vs Δ

Latona Model

Latona Frame:
1.5% Strain
Hardening

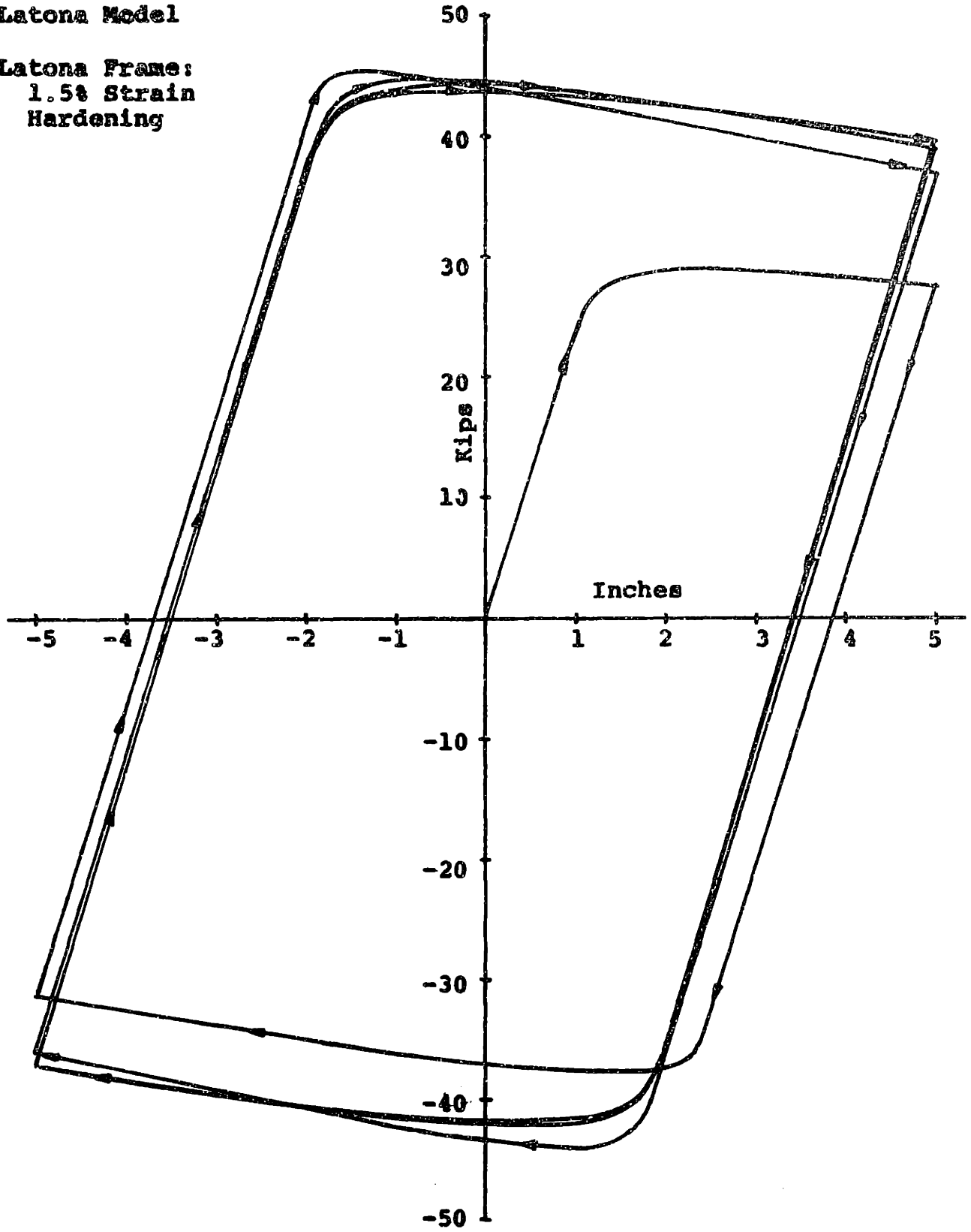
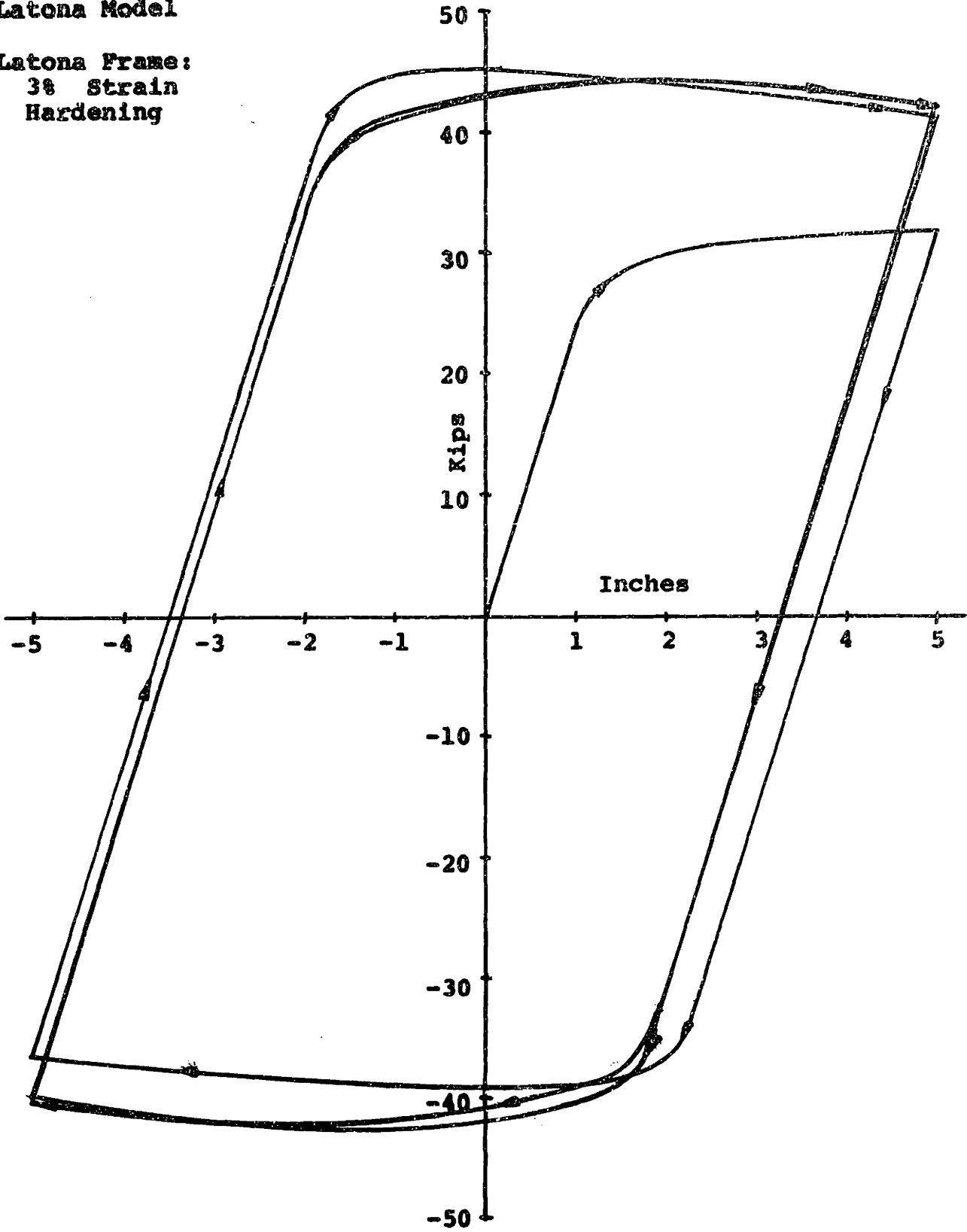


Figure 5-32. Graph of R vs Δ

Latona Model

Latona Frame:
3% Strain
Hardening



non-linear. This behavior is very similar to that of the beam column studied in Chapter 4, and shows that a small change in percent strain hardening may have a very significant effect on the formation of the failure mechanism, and the behavior of the frame after the mechanism has formed.

Since the major difference between the Latona Model and the simple models is the ability of the Latona Model to monitor the strain history of each member, the relationship between the axial displacement and the prescribed horizontal displacement needs to be examined. This relationship is shown in Figures 5-33 through 5-35 for each value of strain hardening. In each case, the axial displacement increases with each displacement cycle, and each increase is progressively smaller. This type of behavior does not occur in the simple models, as the axial displacement returns to its initial value after each cycle. Such recovery does not occur in the Latona Model, however, and the axial displacement grows with each displacement reversal. A similar effect was noted by Latona in his thesis, where he found that a beam subjected to cyclic rotation and constant axial load had an increasing axial strain.

Comparison of the three curves shows that in each case the axial displacement decreases during the period when the frame has not failed, and increases as soon as a failure mechanism starts to form. The rate of increase of axial displacement changes, however, becoming progressively stiffer at each reversal. This results in a smaller increase in axial

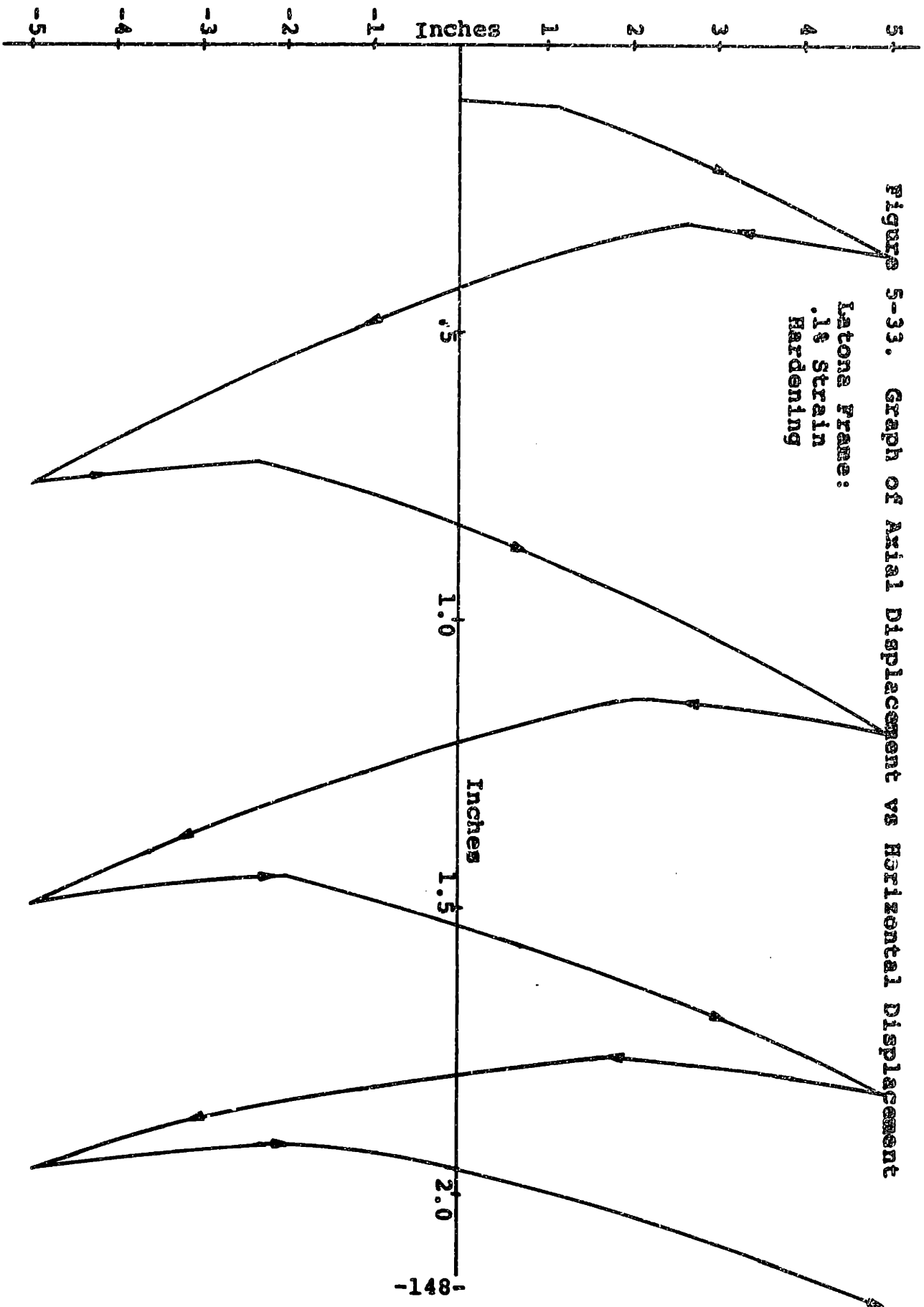
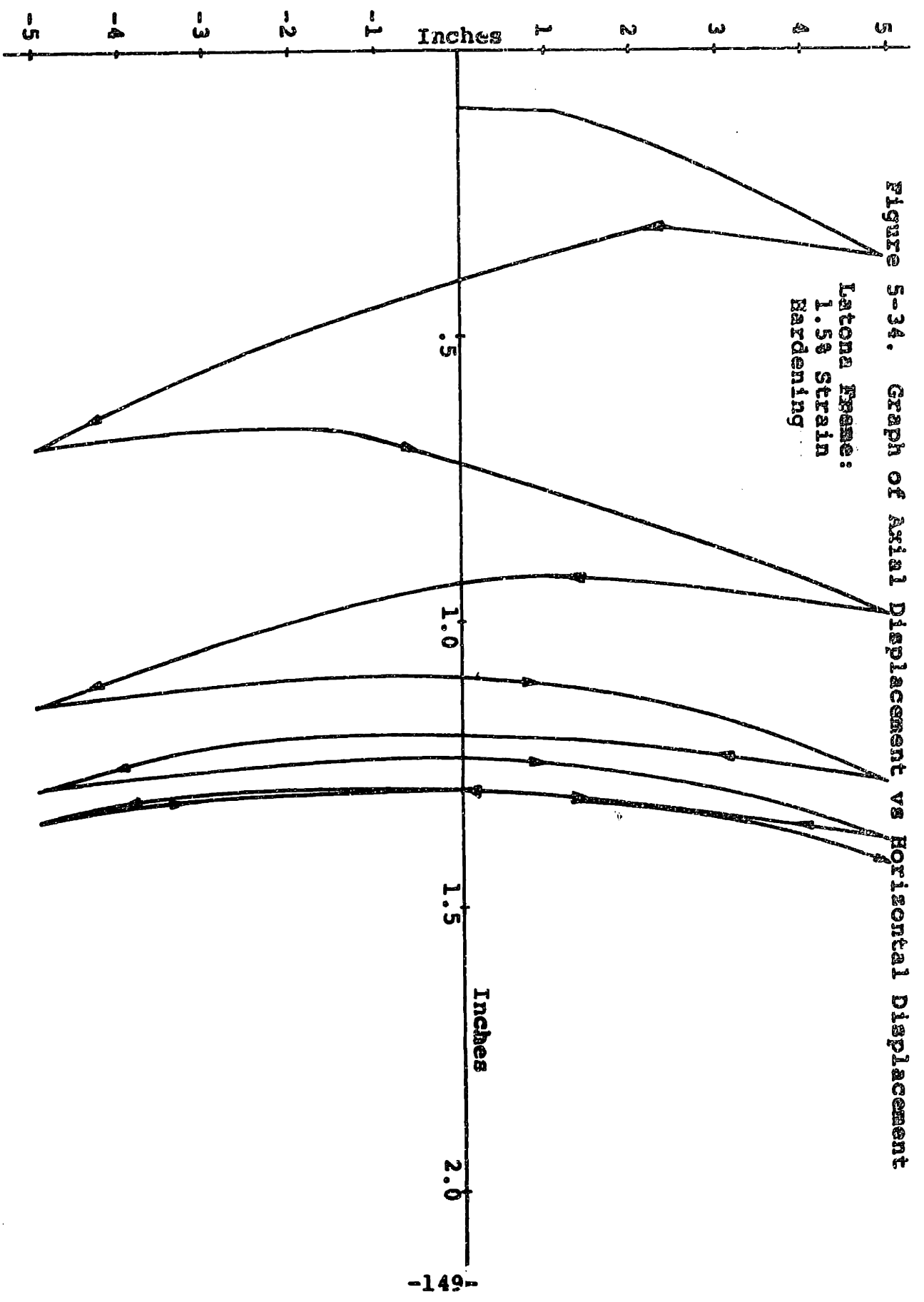


Figure 5-34. Graph of Axial Displacement vs Horizontal Displacement
Latona Frame:
1.5% Strain
Bardening



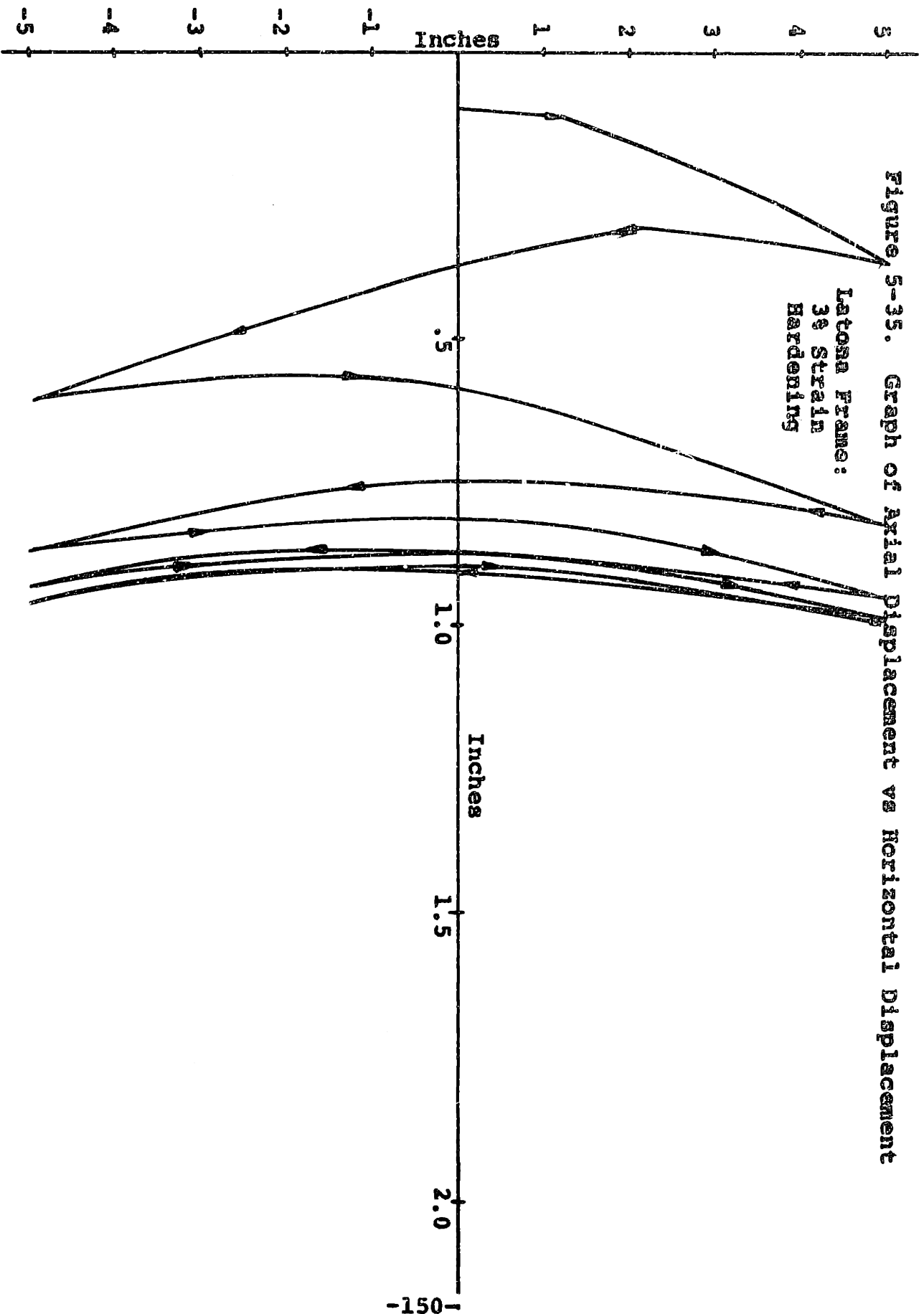


Figure 5-35. Graph of Axial Displacement vs Horizontal Displacement

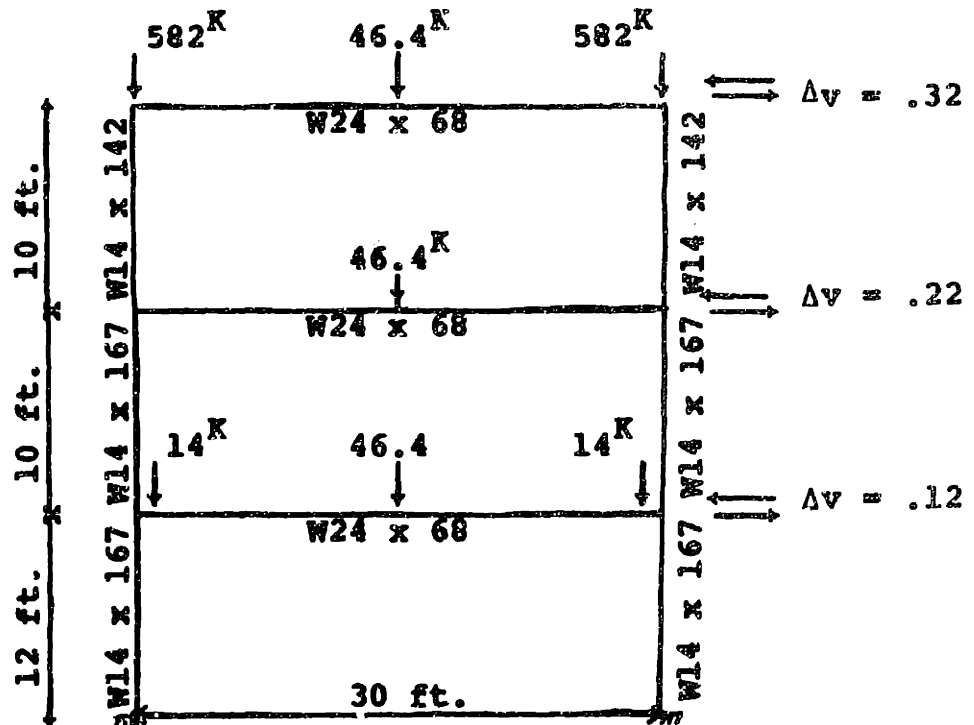
Latona Frames:
3% Strain
Hardening

displacement at each cycle, until eventually the situation stabilizes, and the relationship between axial displacement and horizontal displacement becomes very similar to that for the simple models. Figures 5-33 through 5-35 clearly show that the number of cycles necessary to reach a stable condition is a function of the percent strain hardening. In the case of 3% strain hardening, the curve is essentially stable after four displacement cycles, the 1.5% curve is nearly stable, and the .1% curve will clearly require several more cycles before it becomes stable. Although the results shown are for the Latona Model, they apply equally well to the Complex Model, and while the axial displacement shown in Figures 5-33 through 5-35 is the axial displacement of the right hand column in the frame, the left hand column displacement is essentially similar.

In summary, the increase in frame resistance when yielding of a column occurs under heavy axial load, appears to be related to the relationship between cyclic rotation and axial strain mentioned by Latona. Here, this relationship is quite complex, since in each displacement cycle the axial stiffness of the column appears to increase, and the rate of increase is affected by the percent strain hardening as well as by the number of cycles. A comparison of the models shows that the Latona Model represents this effect as well as the Complex Model, and that the simple models do not predict this

increase in axial displacement, because they do not keep track of the strain history of each member and cannot reproduce spreading of yielding and axial-bending coupling.

In addition to the single frame study, a run of the three story single bay frame in Latona's thesis was also made. The loading consisted of vertical loads and prescribed displacements, the latter being increased linearly at each story. The frame, the loads, and the displacement increments are shown below, and the results are shown in Figures 5-36 through 5-41 for the Interaction and Latona Models with .1% strain hardening.



The columns in this frame are quite heavily loaded, and it can be seen that the force deformation curves behave differently for the two models. The curves for the Interaction Model are

Figure 5-36. Graph of Rel. Shear vs Rel. Disp. - 1st Story

Interaction Model: Latona Frame: 1 Bay 3 Stories

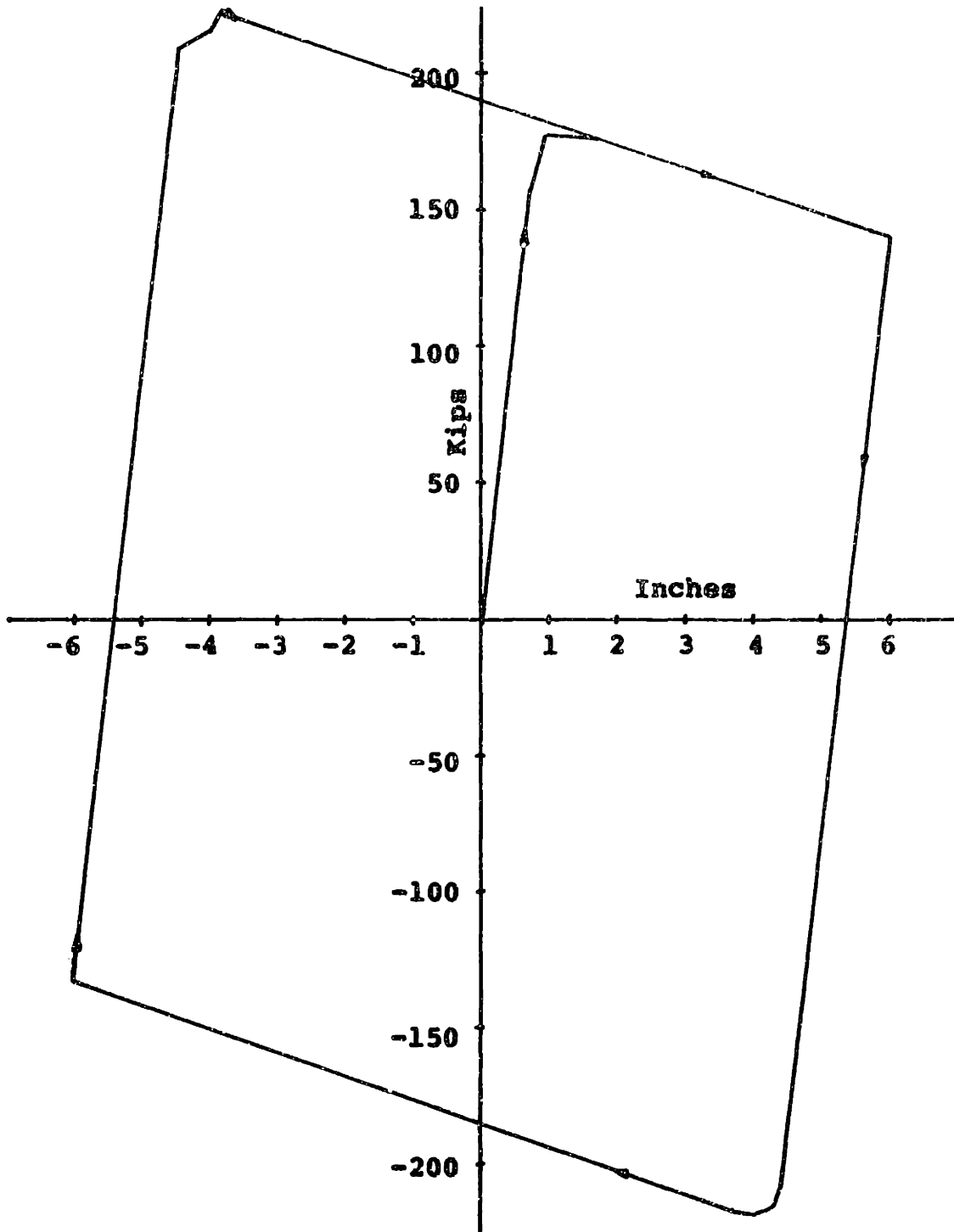


Figure 5-37. Graph of Rel. Shear vs Rel. Disp. - 1st Story
Latona Model: Latona Frame: 1 Bay, 3 Stories

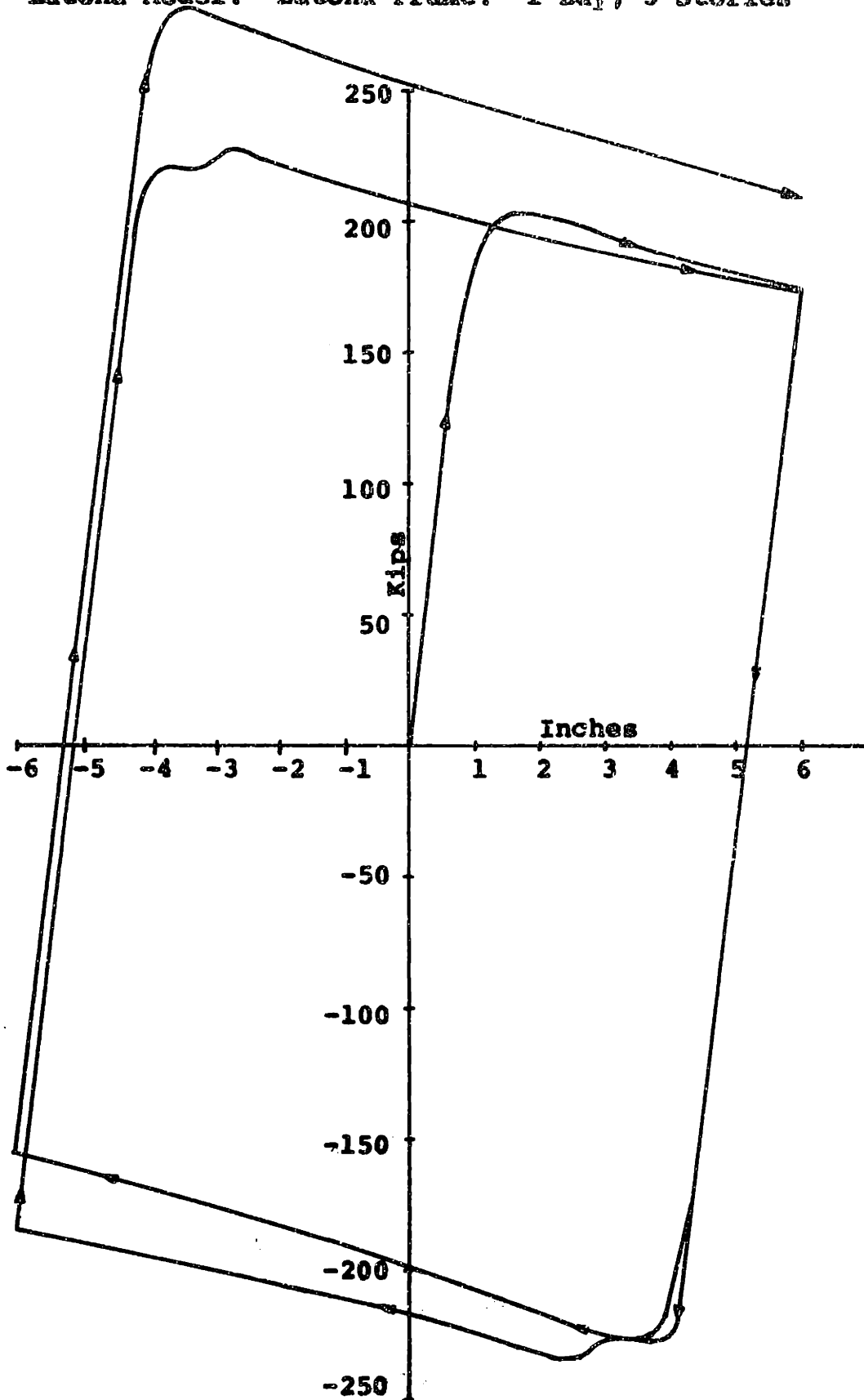


Figure 5-38. Graph of Rel. Shear vs Rel. Disp. - 2nd Story
Interaction Model

Latona Frame: 1 Bay, 3 Stories

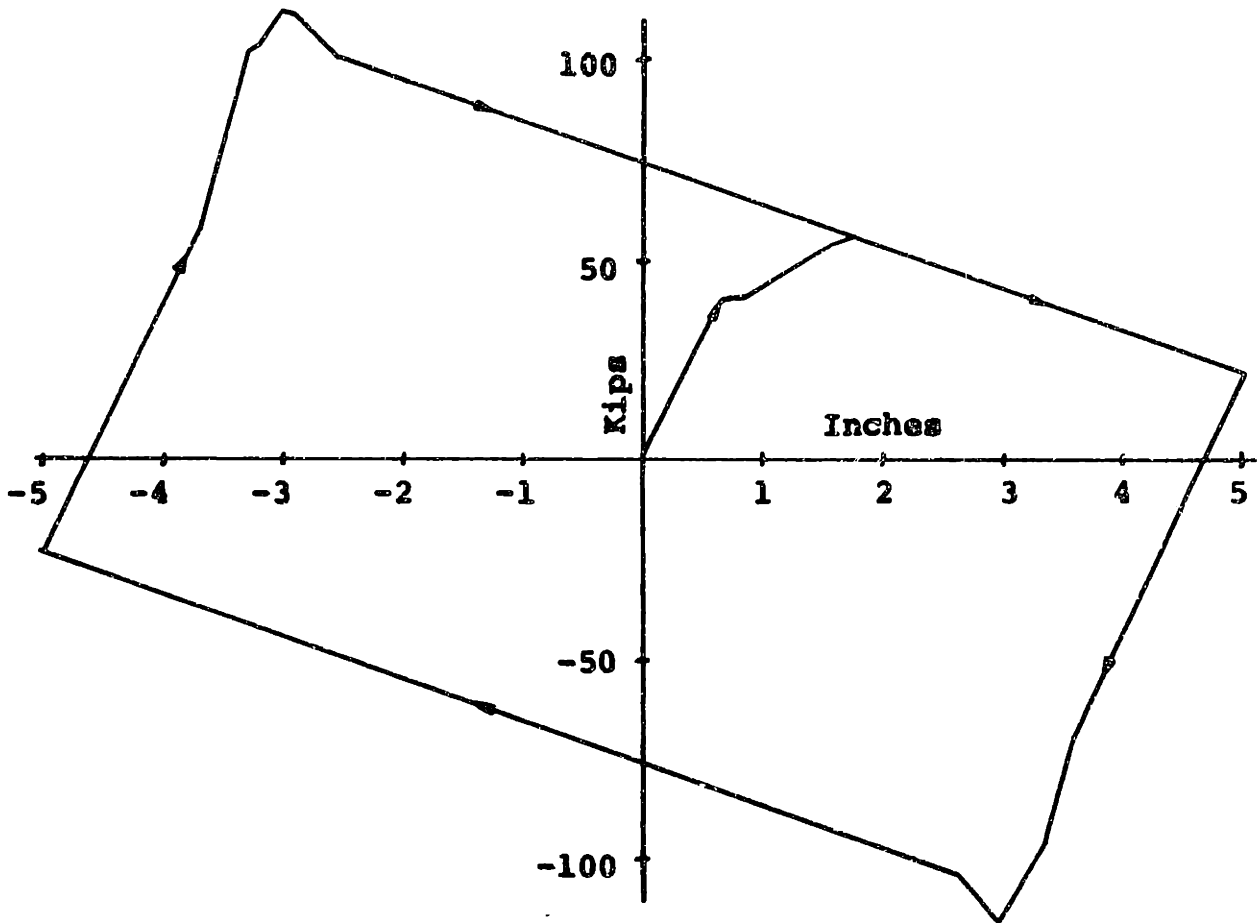


Figure 5-39. Graph of Rel. Shear vs Rel. Disp. - 2nd Story

Latona Model

Latona Frame: 1 Bay, 3 Stories

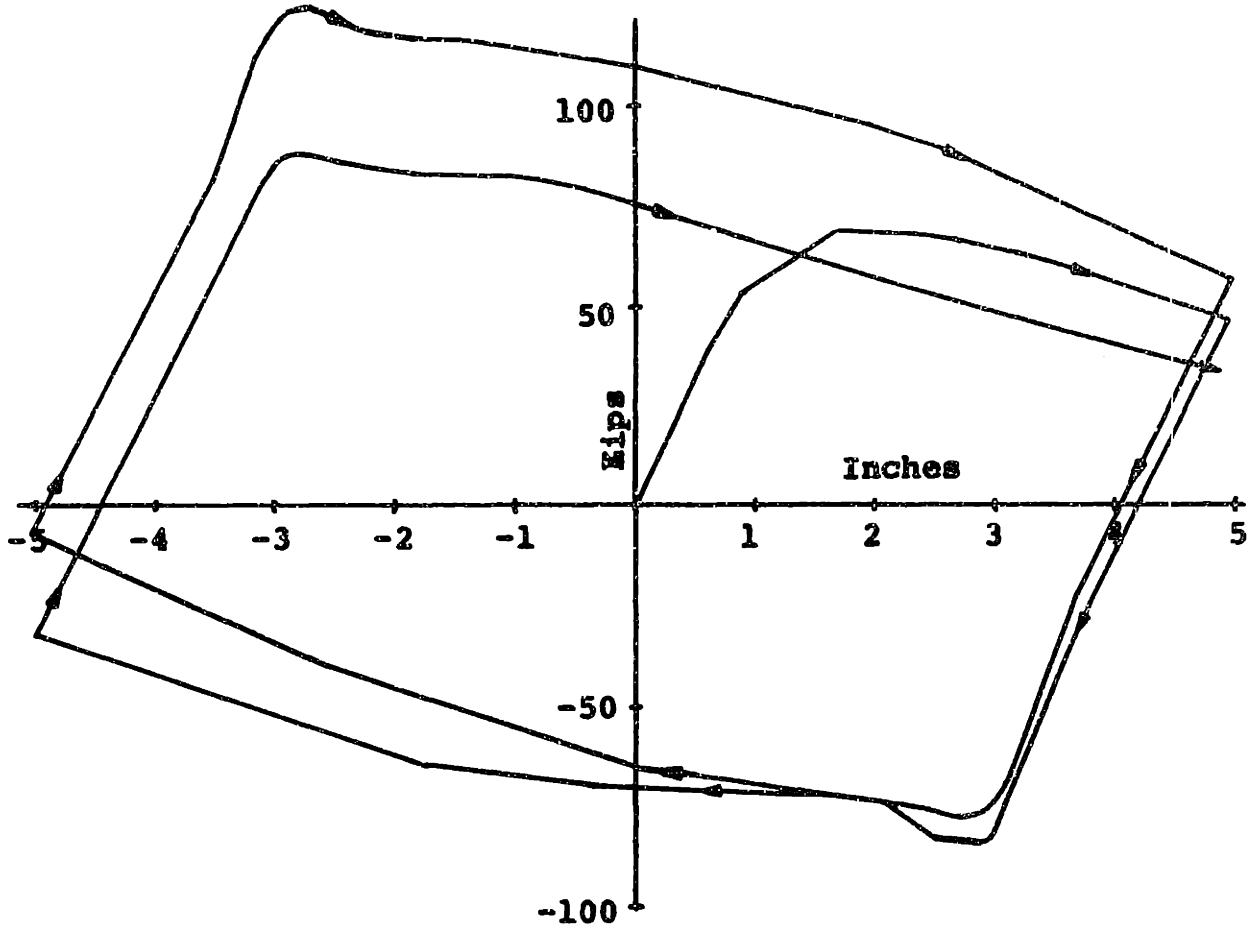


Figure 5-40. Graph of Rel. Shear vs Rel. Disp. 3rd Story

Interaction Model

Latona Frame: 1 Bay, 3 Stories

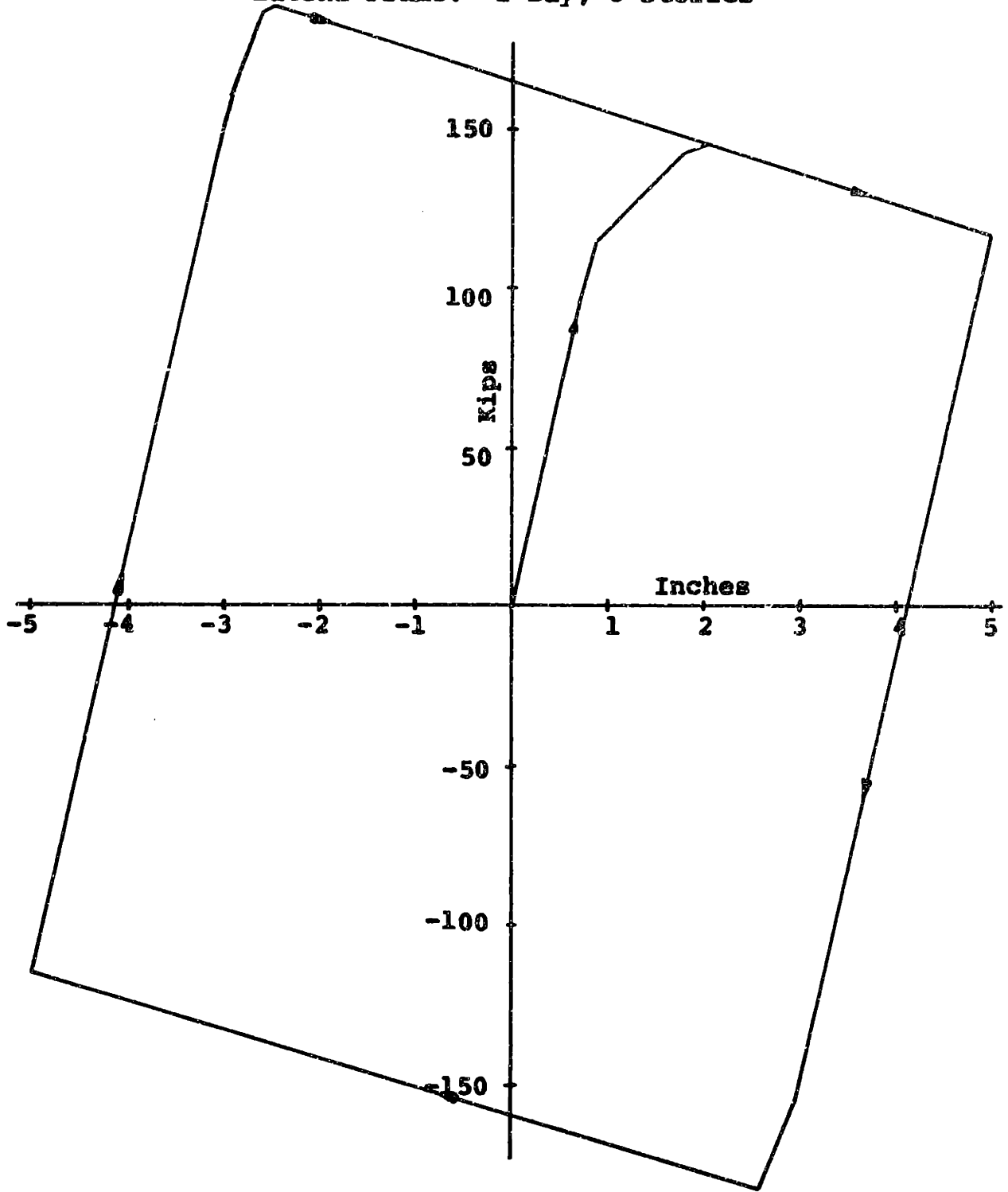
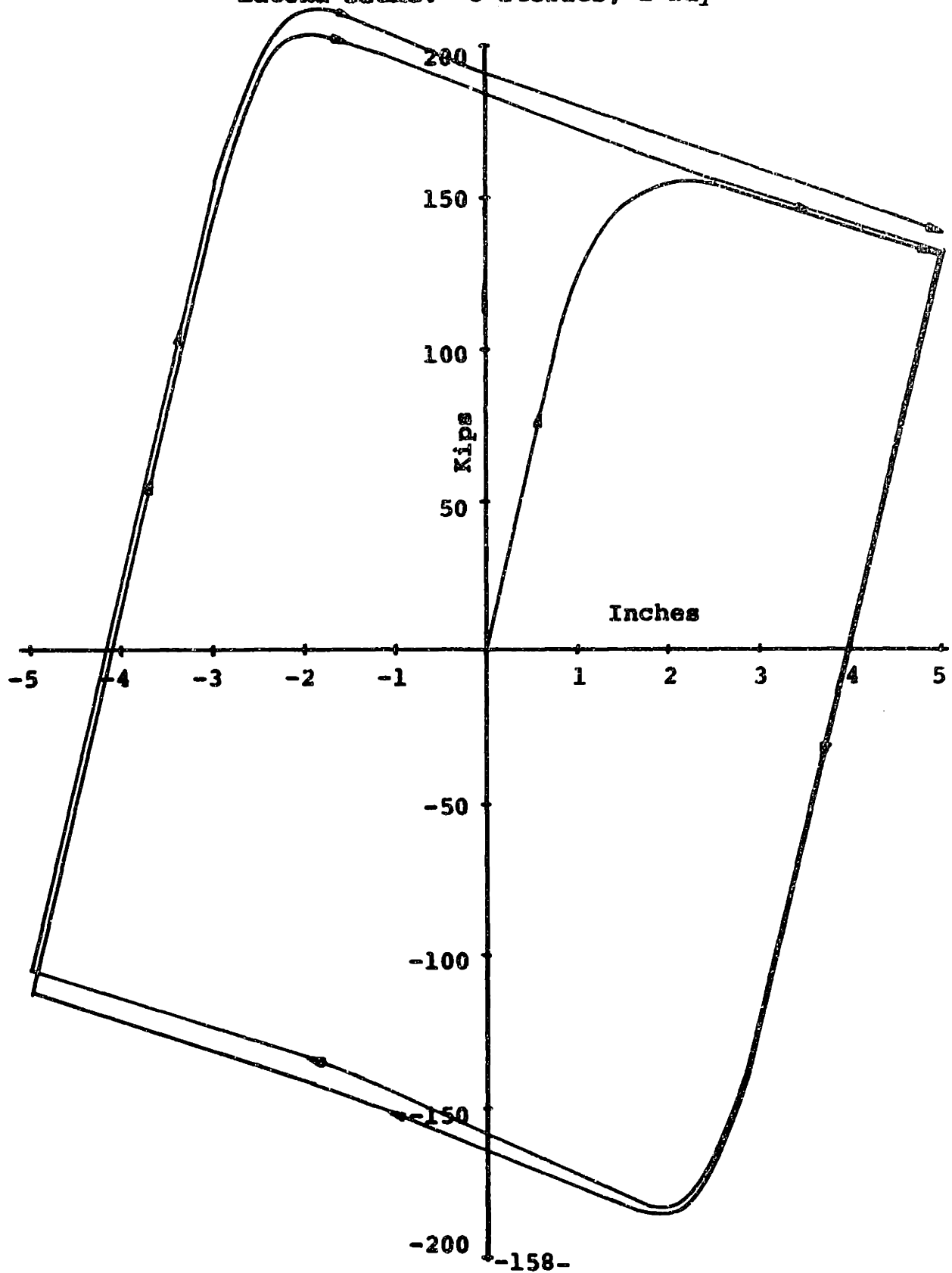


Figure 5-41. Graph of Rel. Shear vs Rel. Disp. - 3rd Story
Latona Model
Latona Frame: 3 Stories, 1 Bay



again steady, while those for the Latona Model show considerable unsteadiness. Because the forces and displacements are relative, and the frame is three stories, the curves are much more complicated than they were in the earlier cases. The basic difference between the simple and complicated models is still there, however, and it can be clearly seen that the two types of models give significantly different results in this case also. Further investigation will be required, however, before any definitive conclusions can be made about multistory frames.

6.0 CONCLUSION

The four mathematical models that have been examined in this thesis fall into two broad categories, simple models and complicated models. In the simple models, the member strains and stresses are not considered, and the criterion for failure is based on the member forces (point hinge model). In the complicated models, the criterion for failure is based on the member stresses, which are monitored at many points throughout the member. Although the two complicated models are theoretically substantially different, their predictions for the cases studied in this thesis are remarkably similar. The fact that the Complex Model takes the deformation of the member into consideration, while the Latona Model does not, appears to cause very little discrepancy in the results for practical cases. From this, it seems safe to conclude that member deformations are not very significant in a rigid frame, and they can be safely ignored unless a column is both very slender and very strong.

It is important to monitor the member stresses and strains for two reasons. The first reason is the unsteady force-deformation loop discussed in chapter five, which appears to occur whenever a column that is subjected to a large axial load yields. Such a failure appears to cause the axial strain to increase. Under cyclic rotation, the rate of increase being a function of the magnitude of the axial load and the percent strain hardening after yielding. The second

reason is that the softening of the member, due to the spreading of yielding, and the axial-bending coupling, may become more important than the effect of non-linear geometry in an individual member. This can be clearly seen in the case of the slender beam column of chapter four, where the failure load given by the Latona Model agrees very well with that predicted by the Complex Model, while the Interaction Model gives a load that is significantly higher.

In general, the simple models give very similar results, and usually predict failure loads that are lower than the failure loads for the complicated models. Since the complicated models are more sensitive to the size of the load increment than the simple models, much of this discrepancy can be eliminated by reducing the load increment, but this is, of course, expensive. In the case of slender members, the simple models cannot be relied upon to provide a lower bound for the failure load. In such a case, the reduction in member stiffness caused by the spreading of yielding may become very important, and the inability of the simple models to take this effect into account may lead to an overestimation of the critical load.

Clearly the major difference between the complicated and simple models is the increase in frame resistance when there is a heavy axial load in the columns. Because this increase in resistance appears to stabilize, and does so in a way that is dependent on the percent strain hardening and the

magnitude of the axial load, it may be possible to incorporate this effect into the simple models, if the precise nature of the relationship is further investigated. The role of this type of behavior under dynamic loading is hard to predict, but the variation of stiffness predicted by the simple models will not be accurate in these cases, and hence dynamic results may be expected to vary from the simple to the complicated models.

Thus the basic conclusions of this thesis are that the increased sophistication and expense of the Complex Model is only justified when unusually strong and slender structures are being investigated. In most practical cases, the Latona Model gives results that are virtually indistinguishable from those given by the Complex Model. There is a significant discrepancy between the Latona Model and the two simple models when yielding occurs in a column subjected to alternating rotation and a large axial load. It may be possible to eliminate this discrepancy between the models by including the increase in resistance in the simple models, but further study of the phenomenon is necessary before this can be done. It should also be noted that studies of multistory frames may reveal further differences between the models, and that these conclusions only apply to individual members and single story frames.

BIBLIOGRAPHY

1. Latona, Raymond W., "Non Linear Analysis of Building Frames for Earthquake Loading," Ph.D. Thesis, Massachusetts Institute of Technology, 1970.
2. Little, William A. and Samuel, Roger A., "Ultimate Strength Behavior of Small Scale Steel Frameworks Subjected to Reversed Loading," Research Report, Massachusetts Institute of Technology, 1966.
3. Korn, Alfred and Galambos, Theodore V., "Behavior of Elastic-Plastic Frames," Journal of the Structural Division, ASCE, Vol. 94, No. ST5, Proc. Paper 5942, May, 1968.
4. Kaldjian, Movses J., "Moment Curvature of Beams as Ramberg-Osgood Functions," Journal of the Structural Division, ASCE, Vol. 93, No. ST5, Proc. Paper 5488, October, 1967.
5. Bleich, Friedrich, "Buckling Strength of Metal Structures," McGraw Hill Book Co., New York, N.Y. 1952.
6. Morris, Glen A., and Fenves, Stephen J., "Elastic-Plastic Analysis of Frameworks," Journal of the Structural Division, ASCE, Vol. 96, No. ST5, Proc. Paper 7293, May, 1970.
7. Alvarez, Ronald J. and Birnstiel, Charles, "Inelastic Analysis of Multistory Multibay Frames," Journal of the Structural Division, ASCE, Vol. 95, No. ST11, Proc. Paper 6922, November, 1969.
8. Wright, E. Whitman and Gaylord, Edwin H., "Analysis of Unbraced Multistory Steel Rigid Frames," Journal of the Structural Division, ASCE, Vol. 94, No. ST5, Proc. Paper 5944, May, 1968.
9. Davies, J. Michael, "Frame Instability and Strain Hardening in Plastic Theory," Journal of the Structural Division, ASCE, Vol. 92, No. ST3, Proc. Paper 4836, June, 1966.

10. Newmark, Nathan M. and Rosenblueth, Emilio, "Fundamentals of Earthquake Engineering," Prentice Hall, Inc., Englewood Cliffs, N.J., 1971.
11. American Institute of Steel Construction, "Steel Construction Manual," AISC, Seventh Edition, 1970.
12. Lu, Lo-Wu, "Inelastic Buckling of Steel Frames," Journal of the Structural Division, ASCE, Vol. 91, No. ST6, Proc. Paper 4577, December, 1965.
13. Arnold, P., Adams, P.F., and Lu, L.-W., "Strength and Behavior of an Inelastic Hybrid Frame," Journal of the Structural Division, ASCE, Vol. 94, No. ST1, January, 1968.
14. Jennings, A. and Majid, K., "An Elastic Plastic Analysis by Computer for Framed Structures Loaded Up to Collapse," The Structural Engineer, Vol. 43, No. 12, December, 1965.
15. Popov, E.P., and McCarthy, R.E., "Deflection Stability of Frames Under Repeated Loads," Journal of the Engineering Mechanics Division, Vol. 86, No. EM1, January, 1960.

BIOGRAPHY

I was born on April 13, 1941, in Boston, and have lived in the town of Lincoln, Massachusetts, most of my life. I received my secondary education at Middlesex School in Concord, Massachusetts, obtained an A.B. in math from Harvard University in 1963, a B.S. in Civil Engineering from Tufts University in 1964, and an M.S. from the same university, in the same field, in 1966. During the summer of 1964 I worked as a rodman and later as a field engineer for The George A. Fuller Construction Company. That fall I worked as a research assistant in the Tufts University Computation Center, and the next summer as a programmer for I.B.M. In the fall of 1965 I became director of the Tufts University Computation Center, a job which ended when I received my degree in June, 1966. In June of 1970 I joined the firm of Neal Mitchell Assoc., and worked for them as a part time structural engineer until the firm failed in 1971. I am currently employed in the same capacity by the firm of Mitchell Systems.

APPENDIX A: LIST OF FIGURES

- 3-1 Graph of v vs P - Complex Model
- 3-2 Graph of P vs v - Complex Model
- 3-3 Graph of v vs P - Complex Model
- 3-4 Graph of v vs P - Complex Model
- 3-5 Graph of P vs v - Complex Model
- 3-6 Graph of P vs v - Complex Model
- 3-7 Graph of R vs v - Complex Model
- 3-8 Graph of R vs P - Complex Model
- 3-9 Graph of P vs v - Latona Model
- 3-10 Graph of P vs v - Latona Model
- 4-1 Graph of H vs v - Bending Model
- 4-2 Graph of H vs v - Interaction Model
- 4-3 Graph of H vs v - Latona Model
- 4-4 Graph of H vs v - Complex Model
- 4-5 Graph of H vs v - Bending Model
- 4-6 Graph of H vs v - Interaction Model
- 4-7 Graph of H vs v - Latona Model
- 4-8 Graph of H vs v - Complex Model
- 4-9 Graph of H vs v - Complex Model
- 4-10 Spreading of Yielding for Beam of Figure 4-9
- 4-11 Graph of P vs v - Interaction Model
- 4-12 Graph of P vs v - Latona Model
- 4-13 Graph of P vs v - Complex Model

- 4-14 Graph of P vs v - Interaction Model
- 4-15 Graph of P vs v - Latona Model
- 4-16 Graph of P vs v - Complex Model
- 4-17 Graph of R vs v - Interaction Model -
.1% Strain Hardening
- 4-18 Graph of R vs v - Latona Model - .1% Strain Hardening
- 4-19 Graph of R vs v - Complex Model - .1% Strain Hardening
- 4-20 Graph of R vs v - Interaction Model -
3% Strain Hardening
- 4-21 Graph of R vs v - Latona Model - 3% Strain Hardening
- 4-22 Graph of R vs Δ - Complex Model - 3% Strain Hardening
- 5-1 Graph of R vs Δ - Bending Model $\frac{P}{P_y} = .2$ Case 1
- 5-2 Graph of R vs Δ - Interaction Model - $\frac{P}{P_y} = .2$ Case 1
- 5-3 Graph of R vs Δ - Latona Model - $\frac{P}{P_y} = .2$ Case 1
- 5-4 Graph of R vs Δ - Complex Model - $\frac{P}{P_y} = .2$ Case 1
- 5-5 Graph of R vs Δ - Bending Model - $\frac{P}{P_y} = .4$ Case 1
- 5-6 Graph of R vs Δ - Interaction Model - $\frac{P}{P_y} = .4$ Case 1
- 5-7 Graph of H vs Δ - Latona Model - $\frac{P}{P_y} = .4$ Case 1
- 5-8 Graph of H vs Δ - Complex Model - $\frac{P}{P_y} = .4$ Case 1

- 5-9 Graph of R vs Δ - Bending Model - $\frac{P}{P_y} = .2$ Case 2
- 5-10 Graph of R vs Δ - Interaction Model - $\frac{P}{P_y} = .2$ Case 2
- 5-11 Graph of R vs Δ - Latona Model - $\frac{P}{P_y} = .2$ Case 2
- 5-12 Graph of R vs Δ - Complex Model - $\frac{P}{P_y} = .2$ Case 2
- 5-13 Graph of R vs Δ - Bending Model - $\frac{P}{P_y} = .4$ Case 2
- 5-14 Graph of R vs Δ - Interaction Model - $\frac{P}{P_y} = .4$ Case 2
- 5-15 Graph of R vs Δ - Latona Model - $\frac{P}{P_y} = .4$ Case 2
- 5-16 Graph of R vs Δ - Complex Model - $\frac{P}{P_y} = .4$ Case 2
- 5-17 Graph of R vs Δ - Bending Model - $\frac{P}{P_y} = .2$ Case 3
- 5-18 Graph of R vs Δ - Interaction Model - $\frac{P}{P_y} = .2$ Case 3
- 5-19 Graph of P vs Δ - Latona Model - $\frac{P}{P_y} = .2$ Case 3
- 5-20 Graph of R vs Δ - Complex Model - $\frac{P}{P_y} = .2$ Case 3
- 5-21 Graph of R vs Δ - Bending Model - $\frac{P}{P_y} = .4$ Case 3
- 5-22 Graph of R vs Δ - Interaction Model - $\frac{P}{P_y} = .4$ Case 3

- 5-23 Graph of R vs Δ - Latona Model - $\frac{P}{P_y} = .4$ Case 3
- 5-24 Graph of R vs Δ - Complex Model - $\frac{P}{P_y} = .4$ Case 3
- 5-25 Graph of R vs Δ - Bending Model -
Latona Frame: 1 Bay, 1 Story
- 5-26 Graph of R vs Δ - Interaction Model -
Latona Frame: 1 Bay, 1 Story
- 5-27 Graph of P vs Δ - Latona Model -
Latona Frame: 1 Bay, 1 Story
- 5-28 Graph of R vs Δ - Complex Model -
Latona Frame: 1 Bay, 1 Story
- 5-29 Graph of R vs Δ : $\Delta = .05$ - Complex Model
- 5-30 Graph of R vs Δ - Latona Model -
Latona Frame: 1% Strain Hardening
- 5-31 Graph of R vs Δ - Latona Model -
Latona Frame: 1.5% Strain Hardening
- 5-32 Graph of R vs Δ - Latona Model -
Latona Frame: 3% Strain Hardening
- 5-33 Graph of Axial Displacement vs Horizontal Displacement
Latona Frame: .1% Strain Hardening
- 5-34 Graph of Axial Displacement vs Horizontal Displacement
Latona Frame: 1.5% Strain Hardening
- 5-35 Graph of Axial Displacement vs Horizontal Displacement
Latona Frame: 3% Strain Hardening

- 5-36 Graph of Rel. Shear vs Rel. Disp. - 1st Story
Interaction Model - Latona Frame: 1 Bay, 3 Stories
- 5-37 Graph of Rel. Shear vs Rel. Disp. - 1st Story
Latona Model - Latona Frame: 1 Bay, 3 Stories
- 5-38 Graph of Rel. Shear vs. Rel. Disp. - 2nd Story
Interaction Model - Latona Frame: 1 Bay, 3 Stories
- 5-39 Graph of Rel. Shear vs. Rel. Disp. - 2nd Story
Latona Model - Latona Frame: 1 Bay, 1 Story
- 5-40 Graph of Rel. Shear vs Rel. Disp. - 3rd Story
Interaction Model - Latona Frame: 1 Bay, 3 Stories
- 5-41 Graph of Rel. Shear vs. Rel. Disp. - 3rd Story
Latona Model - Latona Frame: 1 Bay, 3 Stories